Summer 2006

Investigation of Ultracold Rubidium Atoms in a Pulsed Far off Resonance Trap

Minarni Minarni
Old Dominion University

INVESTIGATION OF ULTRACOLD RB ATOMS IN A PULSED FAR OFF RESONANCE TRAP

by

Minarni Minarni
B.S. October 1989, Riau University
M.S. August 1994, Hampton University
M.S. May 2005, Old Dominion University

A Dissertation Submitted to the Faculty of
Old Dominion University in Partial Fulfillment of the
Requirement for the Degree of

DOCTOR OF PHILOSOPHY

PHYSICS

OLD DOMINION UNIVERSITY
August 2006

Approved by:

Charles I. Sukenik (Director)

Anatoly Radyushkin

Gail Dodge

Mark Havey

Sacharia Albin

ABSTRACT

INVESTIGATION OF ULTRACOLD RB ATOMS IN A PULSED FAR OFF RESONANCE TRAP

Minarni Minarni
Old Dominion University, 2006
Director: Dr. Charles I. Sukenik

This dissertation reports on the design, construction, and investigation of a pulsed optical dipole force trap which uses laser light to confine ultracold rubidium (Rb) atoms. Because the laser frequency is detuned far from the atomic resonance frequency, the optical dipole force trap is also called a "far-off-resonance trap" (FORT). The use of pulsed laser light to create an optical trap may find application in expanding the number of atomic species which can be confined. The experiments reported here are principally aimed, however, at understanding the physics of pulsed FORT dynamics in anticipation of using the free electron laser (FEL) at Jefferson Lab (Jlab) to construct a FORT. The Jlab FEL will provide a tunable, high power laser light source enabling the realization of spatially large and/or energetically deep traps which are not presently accessible with table-top laser sources. Here, a mode-locked Nd:YAG laser is used as a pulsed laser source. Since the conservative optical dipole force trap does not cool Rb atoms, ultracold atoms must be loaded into the FORT. The optical dipole force trap is formed at the focus of a Gaussian, 1.06 μm Nd:YAG laser beam which is located at the center of a high vacuum chamber and superimposed onto the center of a pre-cooled Rb atom cloud that has been previously accumulated in a magneto-optic trap (MOT). The performance of the pulsed FORT is compared to a continuous wave mode (cw) FORT which is built using the same laser beam; the operation of the two kinds of FORTs can be switched easily without disturbing the experimental alignment. The dependencies of FORT loading efficiency to FORT and MOT parameters such as FORT laser power, loading time, storage/holding time, detuning of the primary MOT laser frequency, and repump laser intensity are investigated. There are about 1.5×10^7 ultracold rubidium atoms in the MOT. At 7 Watts FORT laser power, about 8% of the atoms are loaded successfully into the cw FORT and about 5% into the pulsed FORT under similar, but not identical, conditions. In most respects both the cw and pulsed FORTs show

comparable behavior. The behavior of both FORTs depends strongly on FORT laser power. As expected, at higher power, more atoms can be loaded into the FORT. Both FORTs also depend on the loading time and holding time. The highest loading efficiency is obtained at 100 ms loading time while the average lifetime of both FORTs is 1 s and set primarily by background gas pressure. The maximum loading efficiency for both FORTs is reached at 13.2 $\mu W/cm^2$ repump laser intensity. The dependence of FORT loading efficiency on the MOT primary laser intensity during the loading stage has also been investigated. Both FORTs show similar behavior on this parameter. Important differences in FORT dynamics have been observed also. Detuning of the MOT laser frequency from resonance and reduction of the repump laser intensity during the loading stage are key steps to obtaining high loading efficiency. The maximum loading for both FORTs is obtained at -8Γ detuning where Γ is the natural linewidth of the ^{85}Rb transition used for laser cooling (5.9 MHz). However, there is a difference between both FORTs performance at smaller detuning. The pulsed FORT does not work very well at smaller detuning. Analysis of the loading and loss rates during FORT loading indicates that at smaller detuning the pulsed FORT loading rate is lower while the loss rate is slightly higher, as compared to the cw case. The observed divergence of behavior is consistent with a reduction of the cooling of atoms as they are loaded into the pulsed FORT, suggesting that the pulsed light interferes with atomic cooling when the MOT light is closer to resonance. Spectroscopy of atoms confined in the FORT also supports the notion that the MOT light-atom interaction is different in cw and pulsed FORTs.

ACKNOWLEDGMENTS

First of all, I would like to thank my adviser, Dr. Charles Sukenik, for letting me work in his lab and for giving me a lot of freedom to plan and run the experiment. His sense of humor, his advice and his knowledge on every aspect of laser cooling and trapping make me consider myself lucky to be working in his lab. Working in Dr. Sukenik's lab for several years has also been a great experience for me. I also thank Dr. Mark Havey, Dr. Donghyun Cho, and Dr. Bob Jones for all of their input on the experiment.

There are many fellow students who have given their talent and enthusiasm to help make this pulsed FORT project successful. My thanks go to S.L. Frierson who built the magneto-optical trap (MOT) used on this project, to Chang Yong Park and Ji Young Kim who traveled far from Seoul, Korea and worked very hard to build the first data acquisition components and write the first LabVIEW codes for the experiment. Additional thanks goes to Chris Lucas who spent two years helping to build and troubleshoot the diode laser systems, optimize the Nd:YAG laser, and build some of the electronics. I also thank Mike Shaffer, who is working on another project in the same lab, for sharing thoughts, jokes, and lab equipment. Thanks to Eman Ahmed, who is now in charge of continuing this project for her help in finishing my data taking process.

My thanks go to Mr. Walt Hooks, Ms. Annette Vialet and Ms. Delicia Malin for their welcomeness every time I went to the Main Office. Thanks also to Mr. Bob Evans and Mr. Bobby Powell for the technical help in the machine shop and physics shop. Thanks to Rocio Olave and Salim Balik, Marija Raskovic, Jan Drake, Sharon Careccia and many others that I can not mention one by one here for their friendship.

I would also like to thank the other members of my committee, Dr. Sacharia Albin from Engineering, Dr. Anatoly Radyushkin who teaches Mathematical Physics with fun, and Dr. Mark Havey for teaching atomic physics with fun and opening my eyes to the atomic physics world. My thanks also go to Dr. Gail Dodge and Dr. Lepsha Vuskovic who are always ready to help everyone and especially female graduate students. They served many very fine meals at the "women in physics dinner." They are such a role model for woman physicists.

Finally I would like to dedicate this dissertation to my husband, and my son and daughter for their patience and encouragement while I was pursuing my degree.

TABLE OF CONTENTS

LIST OF TABLES

LIST OF FIGURES

CHAPTER I

INTRODUCTION

The tremendous progress in laser cooling and trapping techniques for ions and neutral atoms has brought very significant advances in atomic, molecular, and optical physics and other subfields of physics. Over the decades since it was first proposed, trapping and cooling of ions and neutral atoms has become routine for more than 150 research labs around the world [1]. While most early experiments in the laser cooling and trapping field have used alkali metals as samples of atoms, it is not uncommon nowadays for alkaline-earth metals or noble gases to be studied as well. In addition, not only have stable ions and neutral atoms been cooled and trapped but radioactive elements also are being used as research samples [2, 3]. The developments include the discovery and application of a variety of cooling mechanisms in addition to the Doppler cooling scheme such as evaporative cooling and sub-Doppler cooling [4, 5]. Applications of confined and cooled samples of atoms that are widely promising include precision measurements, atom optics [6, 7, 8], quantum computing, Bose-Einstein Condensation (BEC) [9, 10] and ultracold molecules [11].

The early theoretical and experimental work in manipulating neutral atoms using laser light was done by Letokhov and Ashkin in the 1970's as proposed theoretically by Askar'yan in 1962 [12, 13]. Cooling neutral atoms using a pair of counter propagating laser beams, whose frequency are tuned slightly below the atomic frequency resonance, was first proposed in 1975 by Hansch and Schawlow [14], at the same time as the proposal to trap ions in ion traps by Wineland and Dehmelt [15]. This technique is known as Doppler cooling because the cooling mechanism is based on the Doppler effect. Several attempts were made in the 1980's to produce a slowed beam of atoms. These attempts included compensating for the change in the Doppler shift as the atoms were slowed. Phillips and Metcalf were able to decelerate a thermal beam of sodium atoms using a laser beam and a varying magnetic field to provide a changing Zeeman shift in order to counteract the Doppler shift as the atoms decelerated [16]. Chu *et al.* in 1984–85 used the frequency chirping technique to slow a beam of sodium atoms and to send it to the intersection of three pairs of counter propagating laser beams [17]. Since the motion of atoms in the intersection region

This dissertation follows the style of *The Physical Review A*.

is similar to the motion of a particle in a viscous medium, it was called "optical molasses." Chu then improved the scheme by using a weak magnetic field and circularly polarized laser light upon the suggestion of Dalibard. The scheme is known today as a magneto-optical trap (MOT) [18]. Cohen-Tannoudji and co-workers also contributed to the early development of laser cooling and trapping techniques and with Phillips explained the cooling mechanism in the sub-Doppler limit [19]. For the development of the field of laser cooling and trapping, the Nobel Prize in Physics was awarded to S. Chu, W. Phillips, and C. Cohen-Tannoudji in 1997.

Besides the MOT, there are a number of other traps that have been built to confine ions or neutral atoms. These traps use different types of forces. A MOT uses radiation pressure to cool and trap atoms. Magnetic traps confine atoms by exerting a force on the atomic magnetic dipole moments while ion traps use an inhomogeneous magnetic field (Penning Trap) or an oscillating electric field (Paul Trap) to trap ions. There is also a gravitational trap which uses the force of gravity to confine atoms [20]. The optical dipole force is used to build what is known as an optical dipole force trap. The force arises from the interaction of a spatially inhomogeneous laser field with the induced atomic electric dipole moment.

Recently, a growing number of experiments in laser cooling and trapping have used an optical dipole force trap rather than a MOT or a magnetic trap because it provides a high density sample of atoms, low scattering rate, and does not require a complicated magnetic system. The first optical dipole force trap was built by Chu *et al.* [21] to trap pre-cooled sodium atoms from an optical molasses using a single, strongly focused, continuous-wave Gaussian laser beam tuned several hundred gigahertz below the D1 resonance transition of sodium. About 500 atoms were captured in the optical trap in a volume of about 10^3 μm^3 resulting in a density of 10^{11}–10^{12} cm^{-3}. A technique that loads the pre-cooled atoms from the MOT to an optical dipole force trap has improved the number of atoms confined in the trap [22] and become a standard procedure to make an optical dipole force trap.

Many treatments have been applied to the optical trap to get a high density of atoms and a low scattering rate [23, 24, 25, 26, 27, 28]. The first optical dipole force traps used a trap laser with frequency detuned slightly below atomic resonance (red detuning) and a power on the order of a few mW. Now, because of the advances in laser production such as the high power CO_2 lasers and the family of Nd:YAG lasers, one can build an optical dipole force trap detuned far from resonance (far off

resonance trap–FORT) and much further from resonance (quasi electrostatic trap–QUEST) as well as detuned above atomic resonance (blue detuning) with laser power on the order of many tens of Watts [29, 30, 31]. Optical dipole force traps also have been used to create a BEC and quantum degenerate Fermi gases. Early experiments on BEC used a MOT to collect cooled atoms and cooled them further using sub-Doppler laser cooling. The atoms were then transferred to a magnetic bottle and cooled to below the condensation temperature by evaporation [9, 10]. Trapping a BEC using an optical dipole force trap is done by cooling the atoms with the sub-Doppler cooling mechanism and transferring them to a quasi electrostatic dipole trap followed by evaporatively cooling to the BEC transition by lowering the power of the trapping beam [32, 33]. A degenerate Fermi gas of ^{6}Li atoms also has been confined in a CO_2 optical dipole force trap by forced evaporation [34].

Trapping atoms using short pulses of light from a mode-locked laser has been proposed by some research groups [35, 36, 37]. The idea is to irradiate the atomic samples by counter-propagating short pulses with time duration of picoseconds. Within the region where the two pulses overlap, the atoms experience a restoring force toward the center of the overlap region. The proposals included the idea of using the scheme to reflect neutral atoms and molecules, acting as a mirror, and also suggested that the pulses can be used to control particles in a far-off resonant interaction. The first experiment on a cw mode-locked (pulsed) optical dipole force trap was reported by Clarke *et al.* in 2000 [38]. They used two lasers: a Ti:Sapphire and a YV:YVO_4 laser which can be switched from continuous mode to mode-locked operation in the experiment. They reported that the performance for both types of optical dipole force traps are comparable.

In this dissertation, we report on an experiment to build a mode-locked optical dipole force trap (pulsed FORT) and a continuous-wave optical dipole force trap (cw FORT) using light from a Nd:YAG laser to confine ^{85}Rb atoms [39]. The pulsed FORT uses the Nd:YAG laser beam operated while mode-locked. A mode-locked laser beam contains a train of laser pulses whose instantaneous power output is not constant. This kind of laser sometimes is called a continuous (cw) mode-locked laser, to differentiate it from single pulse lasers. The cw FORT uses the Nd:YAG laser beam operated in continuous mode; the power output of the laser is continuous/constant over time.

The motivation for this experiment, in addition to exploiting some of the advantages of using pulsed laser light to trap ultracold atoms, is the availability of the free electron laser (FEL) at Jefferson Lab (Jlab), which provides tunable, high power pulsed laser light which will enable us to build a spatially large (the FORT size is as large as the MOT) and energetically deep optical dipole force trap. The goal of this project is to understand the physics of pulsed FORT operation. Understanding the dynamics of a pulsed FORT is critical for successful realization of a FORT using the FEL. The Jlab FEL operates in the Infra Red (IR) regime with wavelength range from 1.0–10 μm and will be extended to the Ultra Violet (UV) regime in the future. In the IR regime, the FEL has an average laser power up to 10 kW and repetition rate in continuous pulse (mode locked) operation from 4.7–75 MHz. The Nd:YAG laser we used has an average laser power up to 10 Watts with wavelength 1.06 μm and repetition rate 82 MHz which is comparable to the upper range of the FEL's rate [40].

Since the optical dipole force trap uses a conservative force, it does not cool atoms. It also has a shallower potential compared to a magneto-optical trap (MOT), so ultracold atoms have to be loaded into the optical dipole force trap. The MOT provides a convenient source of ultracold atoms, but the physics of loading from a MOT to a FORT is non-trivial. The dynamics of the loading processes from a MOT to a FORT, which used a cw mode Ti:Sapphire laser was investigated thoroughly by Kuppen *et al.* and Corwin [41, 42] for ^{85}Rb atoms, and using a CO_2 laser to confine ^{6}Li atoms by O'Hara *et al.* [43] but no detailed investigation using a cw mode-locked Nd:YAG laser (FORT Laser) for ^{85}Rb atoms has been done. Principal findings of previous experiments were that lower hyperfine repump laser intensity and larger MOT trapping laser detuning during loading are among the critical parameters needed for efficient loading from a MOT to a cw FORT. In this experiment, the loading rates and loss rates of atoms in the FORT are studied over a range of important trap parameters which include varying the power of the FORT laser beam or the well depth of the FORT, detuning of the MOT trapping laser, hyperfine repump laser intensity, and MOT trapping laser intensity. Both the cw and pulsed FORT were built by focusing the FORT laser to a calculated 16 μm waist with an average power up to 8 Watts after being shifted by an acousto-optical modulator (AOM) which was used as an optical switch. The focal spot of the FORT beam is superimposed onto a Rb atom cloud at the center of a high vacuum chamber where the magnetic field from

the anti-Helmholtz coils for the MOT is set to zero.

This dissertation is divided into 6 chapters. The theoretical background of the experimental aspects such as the principles of atom cooling using laser light, trapping using dipole forces, the characteristics of mode-locked laser pulses, and the heating and loss rates that affect the loading processes from MOT to FORT will be derived in Chapter II. The layout of the apparatus, lasers, and the electronics used will be presented in Chapter III. Controlling the experiment using the computer system and detection of the number of atoms trapped in the FORT is very crucial to get accurate data; this will be explained in Chapter IV. The results of the experiments based on the parameters that contribute to loading efficiencies and the details of the spectroscopy experiment performed on atoms in the cw and pulsed FORT will be presented in Chapter V. Finally in Chapter VI, the conclusions and the possible future directions of pulsed FORT experiments will be discussed.

CHAPTER II

THEORETICAL CONCEPTS

In this chapter, the fundamental theory of laser cooling and trapping techniques will be presented. The information on the physical characteristics of the rubidium atom will be presented in Sec. II.1 and the theory of laser cooling is derived in Sec. II.2 along with the basic principle of a magneto-optical trap (MOT). The principle of the optical dipole force trap will be discussed in Sec. II.3 while the characteristics of a mode-locked laser beam will be explained in Sec. II.4. The physics of pulsed FORT operation is discussed in Sec. II.5. Finally, the heating and loss in the optical dipole force trap will be discussed in Sec. II.6

II.1 RUBIDIUM

Theoretically, almost every atom can be cooled and trapped as long as there is an interaction between laser light and the atom. In practice, there are many criteria that have to be fulfilled to make a laser cooling and trapping experiment successful [44]. First, the atom needs to have a cooling transition which is accessible by an available laser with enough power and suitable frequency. Second, one needs to be able to scatter photons on the chosen transition so that the spontaneous emission out of the excited state should go entirely to the ground state or metastable state from which it was excited (cycling transition). The feasibility of producing an atomic beam or vapor which can be sent to the observation chamber and cooled by a laser beam is also one of the requirements for a successful laser cooling experiment. So far, there are mainly three types of atoms that have been successfully cooled and trapped; alkali-metal atoms, metastable noble gas atoms, and alkaline-earth atoms. However, some other elements in the periodic table have also been used in laser cooling and trapping experiments such as silver, erbium, and ytterbium. Alkali metals were the first elements used in laser cooling and trapping experiments for several reasons. The first reason is because most of their cooling transition frequencies are in the visible region or near-IR and easily accessible by commercial lasers such as diode lasers, dye lasers, and Ti:Sapphire lasers. Second, they can be vaporized easily without a complicated oven. Alkali-metal atoms also have a single electron outside of a closed shell hence they have a relatively simple hydrogen-like structure of energy levels and

only the valence electron contributes to the orbital angular momentum of the atom. This is very important for having a cycling transition.

The most common neutral alkali-metal atoms used in laser cooling and trapping experiments are rubidium and cesium since the cooling transitions are accessible by commercial diode lasers, followed by sodium whose cooling transition is accessible by a dye laser. Lithium is of interest in quantum degeneracy experiments since it can provide a bosonic as well as fermionic stable isotope [34] while potassium is harder to cool since it has an unusual hyperfine structure. Hydrogen atoms are very difficult to cool because their transition has to be excited by far-ultraviolet frequency light, a laser in this frequency range is not easily feasible at present. However Bose-Einstein Condensation has been achieved using atomic hydrogen [45]. Finally, since francium is a radioactive element, a francium beam is hard to produce, though francium has also been confined in a MOT. Most of the laser cooling and trapping experiments using francium and other short-lived radioactive atoms have a goal to create a large sample of heavy atoms in order to be used for testing the Standard Model including atomic parity non-conservation (PNC), searches for a permanent electric dipole moment (EDM), and β decay [46].

II.1.1 General Physical Properties

Rubidium is an alkali-metal whose name comes from Latin word *rubidius* meaning dark red, and was discovered by Robert Bunsen and Gustav Kirchhoff in 1861 in the mineral lepidolite (a form of mica) through the use of a spectroscope. Rubidium can be liquid at room temperature and has a melting point at about 40°C and boiling point at 686 °C. It is a soft, silvery-white metallic element which ignites spontaneously in air and reacts violently with water [47].

Natural rubidium is a mixture of two isotopes; ^{85}Rb and ^{87}Rb. The isotopes have different nuclear spins and abundance. ^{85}Rb is the only stable isotope of rubidium and has 72.2 % abundance while ^{87}Rb is a radioactive isotope with a half-life of 48.8 $\times$ 10^9 years and 27.8 % abundance. Both isotopes have been widely used in laser cooling and trapping experiments.

II.1.2 Spectral Properties

With atomic number 37, rubidium has an electron configuration in the ground state of $1s^2\ 2s^2p^6\ 3s^2p^6d^{10}\ 4s^2p^6\ 5s^1$. From this configuration, it is clear that the ground state

of a rubidium atom has a closed shell with one valence electron. Since the core is a closed shell, it does not contribute to the orbital angular momentum of the rubidium atom, only the valence electron does. Using Russell-Saunders notation, S and P refer to the total orbital angular momentum with value 0 and 1 respectively, the ground state of the atom can be written as $5^2S_{1/2}$ with total orbital angular momentum L = 0 and total angular momentum J = 1/2. Due to the spin-orbit interaction (LS-Coupling), the excited state 5P is split into two fine-structure components with J = 1 ± 1/2. These 5S – 5P transitions which are known as the D-doublet of alkalis are very important in laser cooling experiments. The transition from $5^2S_{1/2}$ – $5^2P_{1/2}$ is known as the D1 line with a transition wavelength of 795.0 nm and the transition from $5^2S_{1/2}$ – $5^2P_{3/2}$ is known as the D2 line with a wavelength of 780.1 nm.

Besides the spin-orbit interaction, there is also an interaction of the nuclear magnetic moment with the total angular momentum of the electron. This is described in term of the total angular momentum $\mathbf{F} = \mathbf{I} + \mathbf{J}$ where **I** is the nuclear spin of the atom which has magnitude I = 5/2 for ^{85}Rb and I = 3/2 for ^{87}Rb and **J** is the total angular momentum of the electron. This interaction splits the ground state and the excited states into what is called hyperfine structure. Here, the ground state splits into two $5^2S_{1/2}$ states with quantum number F = 2, F = 3 for ^{85}Rb, and F = 1, F = 2 for ^{87}Rb. The excited states split into two and four lines for $5^2P_{1/2}$ and for $5^2P_{3/2}$ respectively. The complete fine structure and hyperfine structure of ^{85}Rb and ^{87}Rb atoms can be seen in Fig. 1. For ^{85}Rb, the transition from F = 3 to F′ = 4 is used for the cooling/trapping transition because it is a closed transition and has the highest transition strength. This transition can be excited by a laser with wavelength 780.1 nm. For ^{85}Rb, the lifetime of the excited states is 26.63 ns and the linewidth is $\sim$ 6 MHz. Some atoms can make an off resonant transition from F = 3 to F′ = 3 for ^{85}Rb and then decay into F = 3 or F = 2. If the atoms go into F = 2, the trapping laser light can no longer excite the atoms and a second laser (repump laser) is needed to pump the atoms back to the excited states (from which they will subsequently decay) to keep the population of atoms in the upper hyperfine level of the ground state.

In a weak magnetic field (Zeeman effect), each hyperfine state F splits into the states m_F = −F, ...,F. The energy splitting is $\Delta E_{m_F} = m_F\, g_F\, \mu_B \times B$, where μ_B is Bohr's magneton, B is the magnetic field flux density and g_F is the g-factor for each state in F. The transition between these states and excited states can be made using

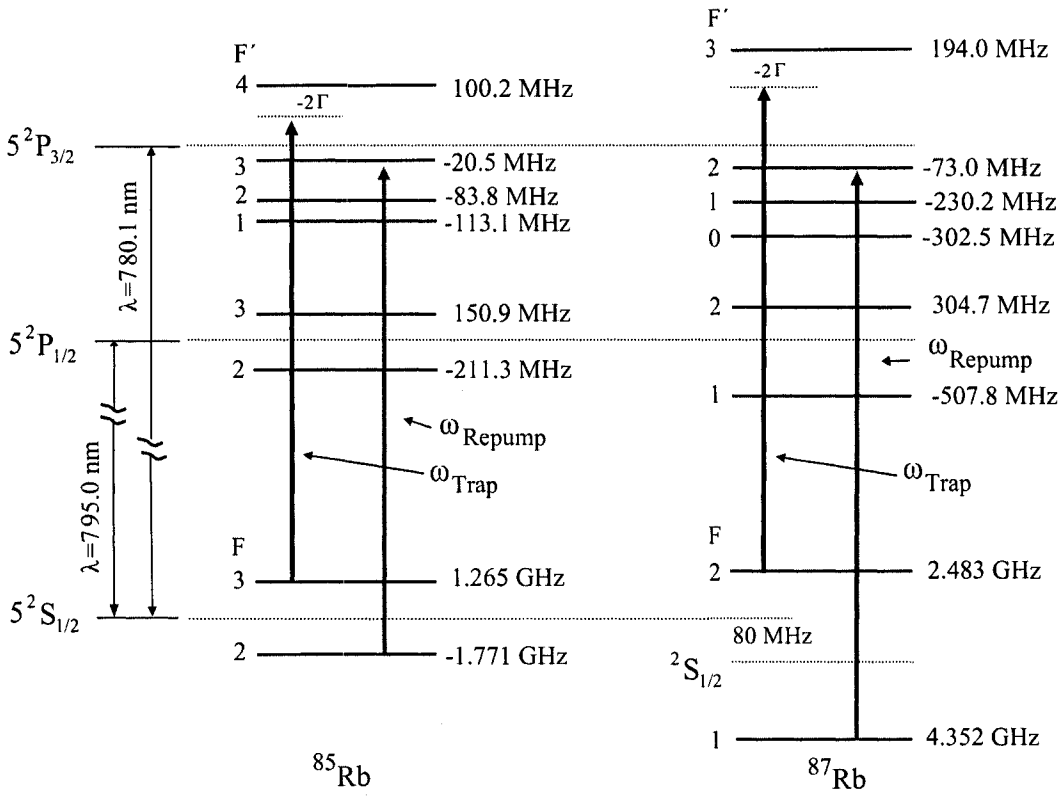

FIG. 1: Energy level diagram of 5S–5P transition of ^{85}Rb and ^{87}Rb.

linear and circular polarized laser light. The effect of the weak magnetic field will be discussed further in the section describing the magneto-optical trap (MOT).

II.2 LASER COOLING

Laser cooling and trapping relies on the interaction between laser light and an atom to exert a controllable force on the atom [44]. There are two kinds of light forces acting on the atom; dissipative and dispersive. The dissipative forces (radiation pressure or scattering force) are velocity dependent and hence can be used for laser cooling. Purely dispersive forces (reactive forces) are conservative and can be used for trapping. Cooling is then associated with the reduction of the atomic velocity spread around a given value and trapping is related to the control of the position of the atoms in space [48].

The basic scheme to understand the cooling process is to consider the process of absorption and emission of photons by an atom. As seen in Fig. 2, when an atom of

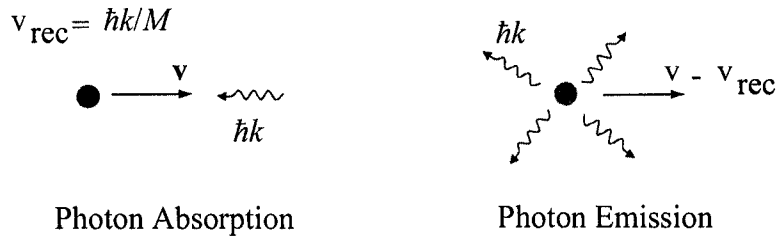

FIG. 2: The photon absorption and photon emission by an atom involves transferring photon momentum $\hbar\mathbf{k}$ and changing the atom's velocity in the amount of the recoil velocity.

mass M absorbs a photon from the laser light with wave vector $\mathbf{k}$, the atom becomes excited. The atom's net momentum decreases by $\hbar\mathbf{k}$ which is related to a recoil velocity $v_{rec} = \hbar k/M$ and the atom slows down. After a time $\tau = 1/\Gamma$, the excited atom releases a photon spontaneously to the ground state in a random direction. In this emission process, the momentum of the atom changes in the amount of $-\hbar\mathbf{k}'$. The emission process can be portrayed as a random walk of the atom in momentum space with step size of $\hbar\mathbf{k}'$. This process is observed as a momentum diffusion or heating of the atom. So, the net change in the momentum of the atom due to a single absorption-emission event is $\Delta\mathbf{p} = \hbar(\mathbf{k}-\mathbf{k}') = \hbar(\Delta\mathbf{k})$. The mean contribution of $\hbar\mathbf{k}'$ is zero because spontaneous emission occurs with the same probability in two opposite directions, making $\Delta\mathbf{p} = \hbar(\mathbf{k})$. The atoms are being slowed down in one direction which is the direction of the laser beam, but at the same time experience a diffusive heating due to the random walk in momentum space.

The net force $\mathbf{F}$ on the atom as a result of its interaction with laser light or the force from absorption followed by spontaneous emission is

$$\mathbf{F} = \hbar\mathbf{k}\ \gamma_p. \tag{1}$$

The first term is the amount of momentum being transferred for each photon. The second term γ_p is the scattering rate which is given by a Lorentzian[1]

$$\gamma_p = \frac{\Gamma}{2}\frac{s}{1+s+(\frac{2(\Delta+\omega_D)}{\Gamma})^2}, \tag{2}$$

here

$s = I/I_{sat}$, the normalized intensity,

[1]It means the Lorentzian-shaped emission line.

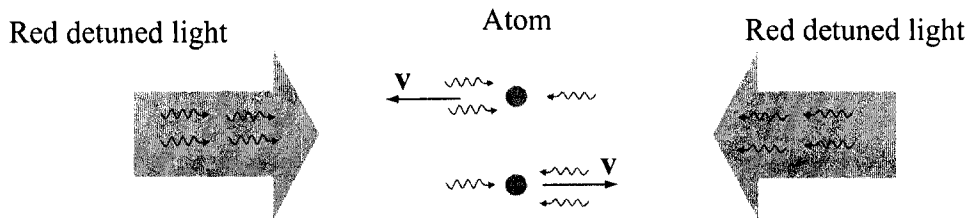

FIG. 3: A one-dimensional optical molasses. An atom moving to the left scatters more light coming from the left, an atom moving to the right scatters more light coming from the right.

$I_{sat} \equiv \pi hc\Gamma/3\lambda^3$, saturation intensity,
Δ = detuning from the atom's resonance frequency,
$\omega_D = -\mathbf{k}.\mathbf{v}$= the Doppler shift.

In Eq. (2), Γ is the natural linewidth of the excited state which is equal to the inverse of the natural life time of the excited state. For the resonance transition of ^{85}Rb, with $\Gamma/2\pi$ = 6 MHz, the maximum acceleration due to the light force is 0.1×10^6 m/s^2 or equals 10^4g for a single photon recoil. By substituting Eq. (2) into Eq. (1), the net scattering force can be rewritten as

$$\mathbf{F}(\mathbf{v}) = \hbar\mathbf{k}\frac{\Gamma}{2}\frac{s}{1+s+(\frac{2(\Delta-\mathbf{k}.\mathbf{v})}{\Gamma})^2}. \tag{3}$$

II.2.1 Doppler Cooling

To cool neutral atoms using a pair of counter propagating laser light whose frequency is tuned slightly below the atomic frequency resonance was first proposed in 1975 by Hansch and Schawlow [14]. Since the Doppler effect plays a central role in this scheme, the cooling process is often called "Doppler cooling."

A schematic Doppler cooling process is shown in Fig. 3. Consider an atom with a cooling transition; a ground state and an excited state. The resonance frequency of the transition is ω_0 and the excited state can emit photons with a decay rate Γ. The atom which is moving with velocity $\mathbf{v}$ is illuminated by two counter-propagating laser beams whose frequency is ω. Because of the Doppler effect, the atom moving toward the incoming laser beam sees the laser frequency shifted higher (blue shifted) by an amount $\omega_D = \mathbf{k}.\mathbf{v} = \omega_0(\mathrm{v/c})$. So by detuning the laser frequency lower (red detuned), the atom is more likely to scatter photons from this laser beam. The

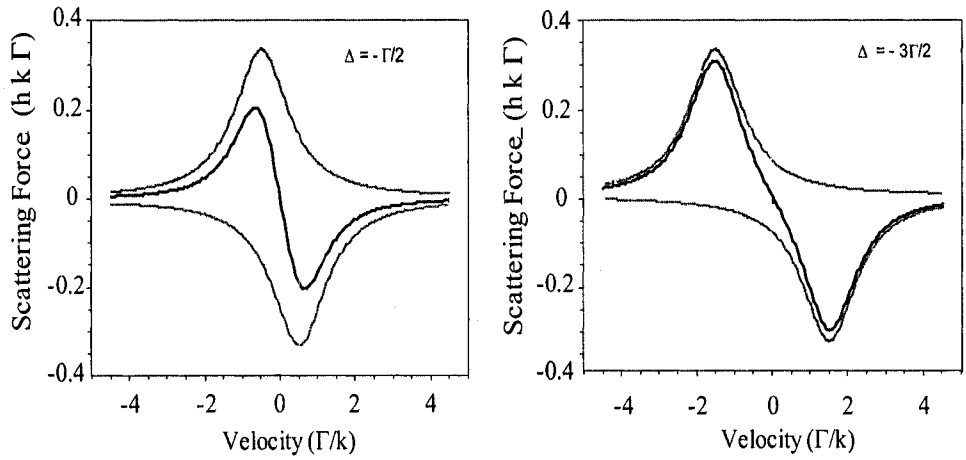

FIG. 4: Each of the counter-propagating beams exerts a scattering force with a Lorentzian velocity dependence (gray line). The average force exerted on the atoms is the sum of these forces (solid line).

atom which is moving to the left sees the frequency of the laser beam moving to the right closer to resonance resulting in increased photon scattering while it sees the frequency of the laser beam moving to the left shifted out of resonance and hence it is less likely to scatter photons from this beam. The opposite happens to the atoms moving to the right. This scheme is called one-dimensional molasses.

The average force for the one-dimensional molasses, as shown in Fig. 3, is the sum of the forces due to the two counter-propagating laser beams $\mathbf{F}_{\rm av} = \mathbf{F}_+ + \mathbf{F}_-$ [44],

$$\mathbf{F}_\pm = \pm\frac{\hbar\mathbf{k}\Gamma}{2}\frac{s}{1+s+(\frac{2(\Delta\mp|\mathbf{k}.\mathbf{v}|)}{\Gamma})^2}, \tag{4}$$

$$\mathbf{F}_{\rm av} \cong \frac{4\hbar k^2 s}{[1+s+(\frac{2\Delta}{\Gamma})^2]^2}\frac{2\Delta}{\Gamma}\mathbf{v} = -\kappa_1\,\mathbf{v}. \tag{5}$$

For $\Delta < 0$, the one-dimensional molasses with two counter-propagating beams indeed reduces the velocity of the atoms with a damping coefficient κ_1. As shown in Fig. 4 for detuning $\Delta = -\Gamma/2$ and $\Delta = -3\Gamma/2$, both at $s = 2$, the net force from the two beams displays the viscous damping around v = 0. For low intensity approximation ($s \ll 1$) and low velocity (kv $\ll \Gamma$), Eq. (5) becomes

$$\mathbf{F}_{\rm av} \cong \frac{4\hbar k^2 s}{[1+(2\Delta/\Gamma)^2]^2}\frac{2\Delta}{\Gamma}\mathbf{v} = -\kappa_1\,\mathbf{v}. \tag{6}$$

The nature of the absorption and emission processes sets a limit on the temperature that can be achieved by this cooling process. The fluctuations of the scattering force due to random kicks from spontaneous emission and the random nature of the absorption events results in diffusion in momentum or heating [44, 49, 50]. There are a number of ways to derive the cooling limit given by the Doppler cooling process. One of the ways is by setting the sum of the heating and cooling rates to zero (steady-state condition). As mentioned earlier, in a given absorption/emission cycle or a scattering process, the atoms receives two random kicks of magnitude $\hbar\mathbf{k}$. The scattering rate at which the atoms get the kicks from both plane waves is derived from Eq. (2) and given by[2]

$$\gamma_p = \Gamma \frac{s}{1 + (\frac{2\Delta}{\Gamma})^2}. \tag{7}$$

A momentum diffusion coefficient D_p is defined as

$$D_p \equiv \langle \dot{p}^2 \rangle / 2 = \gamma_p \, \hbar^2 \, k^2. \tag{8}$$

such that D_p/M is the heating rate $\dot{E}$ due to the randomness, which can be written as

$$\frac{\partial E}{\partial t}|_{heat} = D_p/M = \gamma_p \, (\hbar k)^2/M. \tag{9}$$

Here p is the average momentum imparted to the atoms, M is the atomic mass.

The cooling rate due to the cooling force as derived in Eq. (6) is

$$\frac{\partial E}{\partial t}|_{cool} = \mathbf{F}.\mathbf{v} = -\kappa_1 \mathrm{v}^2 \tag{10}$$

where κ_1 equals to

$$\kappa_1 = \frac{4\hbar \, k^2 \, s}{[1 + (2\Delta/\Gamma)^2]^2} \frac{2\Delta}{\Gamma}. \tag{11}$$

In steady state,

$$\frac{\partial E}{\partial t}|_{heat} + \frac{\partial E}{\partial t}|_{cool} = 0 \tag{12}$$

then using Eq. (9) and Eq. (10),

$$D_p/\kappa_1 = M \, \mathrm{v}^2 = M \, \langle \mathrm{v}^2 \rangle = k_B T. \tag{13}$$

Here, k_B is the Boltzmann constant, v^2 becomes $\langle \mathrm{v}^2 \rangle$ if $\hbar k^2/M \ll \Gamma$ which is well satisfied for the strong dipole transition of rubidium and most other atoms used in

[2]This is for s $\ll$ 1 (low saturation) and kv $\ll \Gamma$ (small velocity).

laser cooling [50]. The last term of Eq. (13) comes from the equipartition theorem in one degree of freedom. Using Eq. (8) and Eq. (11),

$$k_B T = \frac{\hbar\Gamma}{4}\frac{1+(2\Delta/\Gamma)^2}{2\Delta/\Gamma}. \tag{14}$$

The Doppler limit or the minimum temperature is obtained for detuning $\Delta = -\Gamma/2$. From Eq. (14), the Doppler temperature or Doppler limit at low saturation and small velocity is obtained as

$$T_D = \frac{\hbar\Gamma}{2k_B}. \tag{15}$$

II.2.2 Sub-Doppler Cooling

The theory of Doppler cooling assumes an atom with a simple two-level state structure, however many real atoms have hyperfine structure and Zeeman sublevels which gives rise to a new cooling mechanism. It was discovered after an accurate temperature measurement of the optical molasses was developed. The measurement resulted in a surprising temperature of optical molasses which was actually below the Doppler limit T_D. The cooling mechanisms rely on multilevel atoms, light shifts, polarization gradients, and optical pumping [5, 51]. For this reason, this cooling mechanism is known as "polarization gradient cooling." It is also called sub-Doppler cooling since lower temperatures can be achieved using this mechanism.

The interaction between nearly resonant light and atoms can drive transitions between atomic energy levels due to the scattering process which is a velocity-dependent mechanism. The interaction also can shift the atomic energy levels (Zeeman sublevels) due to the Stark shift, this mechanism depends on the spatial varying light field. The spatial varying light field can be obtained using two counter-propagating light beams with the same intensity and wavelength but orthogonal polarization, the superposition of these beams produces a standing wave whose polarization varies in space. The total electric field of two counter-propagating beams which propagate in the z-direction with wavelength ω can be written as

$$\mathbf{E}(\mathbf{z},t) = \mathbf{E}(\mathbf{z})e^{-i\omega t} + \mathbf{E}^*(\mathbf{z})e^{+i\omega t}, \tag{16}$$

where the field vector is given by

$$\mathbf{E}(\mathbf{z}) = E_0(\mathbf{e}_x e^{ikz} + \mathbf{e}_y e^{-ikz}) = \sqrt{2}E_0 e^{ikz}\mathbf{e}(z). \tag{17}$$

Here $\mathbf{e}(z) = \frac{1}{\sqrt{2}}(\mathbf{e}_x + \mathbf{e}_y\, e^{-2ikz})$. It is clear that the polarization $\mathbf{e}(z)$ of the light field varies in space.

In the low intensity limit (the optical coherences and any mechanisms in the excited states can be ignored), the light shifts ΔE_g of the ground magnetic substates due to the light field are given by [44]

$$\Delta E_g = \frac{\hbar\,\Delta\, s\, C_{ge}^2}{1 + (2\Delta/\Gamma)^2}, \tag{18}$$

where s is the normalized intensity, Δ is the detuning from the atom's resonance frequency, C_{ge} is the Clebsch-Gordon coefficient that describes the coupling between the atom and the light field which depends on the polarization of the light field and the magnetic quantum number. The values of C_{ge} of each transition are different and can be found in [44].

There are two different configurations used to realize sub-Doppler cooling, which are related to the two distinct configurations of polarization gradients. The first is illustrated by two orthogonal, linearly polarized counter-propagating laser beams which have the same intensity and wavelength (lin $\perp$ lin configuration). The second is by using two orthogonal, counter-propagating laser beams having circular polarization (σ^+- σ^- configuration). The mechanism involving two orthogonal, linearly polarized, counter propagating beams is shown in Fig. 5. Using Eq. (17), it is shown that the polarization varies from linear to circular with a period of $\lambda/2$ where $k = 2\pi/\lambda$. There are four alternating linear to circular polarization changes for each period $\lambda/2$, the polarization state everywhere can be expressed as a superposition of two circular polarization states with vectors $(\mathbf{e}_x \pm \mathbf{e}_y)/\sqrt{2}$. In contrast, for σ^+- σ^- configuration, the resulting light field has a constant magnitude and is linearly polarized everywhere but the direction rotates through an angle 2π every λ. In this case, the light shift is independent of position because the polarization is linear everywhere and the optical pumping mechanism is different than in the lin $\perp$ lin configuration.

Optical pumping is the transfer of population between atomic magnetic (Zeeman) sublevels. The optical pumping mechanism for the lin $\perp$ lin configuration is described in Fig. 6 for a J = 1/2 $\leftrightarrow$ J = 3/2 transition. The Zeeman effect splits the ground state J = 1/2 to the m = 1/2 and m = $-1/2$ states, while the excited state is split to states with m = $-3/2$, $-1/2$, 1/2, and 3/2. Consider a point where the field is σ^+ circularly polarized. In such a field, atoms in a ground state m = 1/2 can only be coupled to the m = 3/2 excited state and decay back to the same ground state.

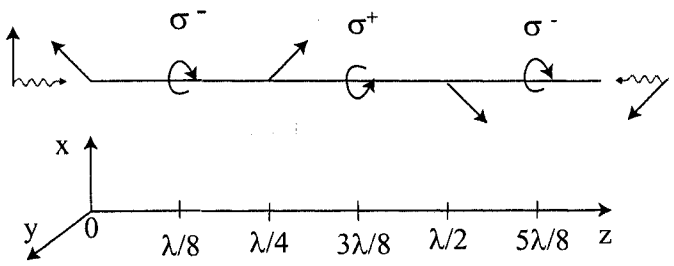

FIG. 5: Superposition of two orthogonal, linearly polarized, counter-propagating laser beams. The polarization of the light field changes four times in a period of $\lambda/2$.

Atoms with a ground state m $= -1/2$ can be coupled by the light field to m $= 1/2$ and decay back to either the m $= 1/2$ or m $= -1/2$ ground state. The Clebsch-Gordon coefficient for a transition from a ground state m $= 1/2$ to m $= 1/2$ is bigger than from a ground state m $= -1/2$ to m $= 1/2$, the atoms at m $= 1/2$ excited state are more likely to decay spontaneously to a ground state m $= 1/2$. The net result of the cycles of absorption and spontaneous emission in σ^+ circularly polarized light is the optical pumping of atoms from the m $= -1/2$ ground state to the m $= 1/2$ ground state which has lower energy.[3]

As atoms move through a polarization-changing light field, the atoms must increase their potential energy (climb a hill) to overcome the polarization change. The ground state m $= 1/2$ becomes less strongly coupled to the light field until the atom reaches the region where the light field has σ^- circular polarization and the atom is optically pumped to m $= -1/2$.[4] In other words, as an atom reaches the top of the hill and is about to start gliding down, optical pumping transfers the atom to another lowest energy ground state, the previously gained potential energy carried away by the spontaneously emitted photon, again the atoms are at the bottom of hill, and start to climb until they reach the next different polarized light field. This

[3]In σ^+ circularly polarized field, the ground state m $= -1/2$ has higher energy than the ground state m $= 1/2$.

[4]The optical pumping due to σ^- circularly polarized light works on the same principle as σ^+ circularly polarized light in the opposite sense; atoms from ground state m $= 1/2$ are pumped into m $= -1/2$ which has a lower energy.

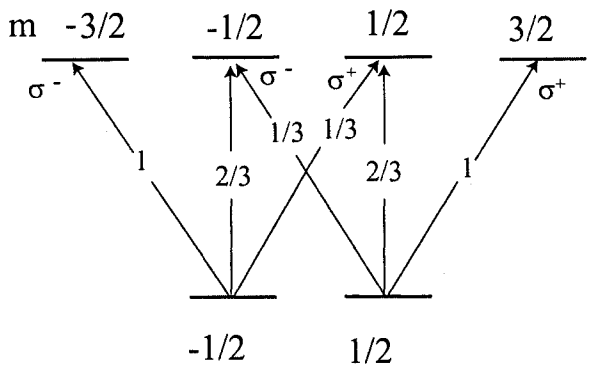

FIG. 6: Optical pumping in a J = 1/2 ↔ J = 3/2 transition by σ^+, σ^-, and linearly polarized light. The Clebsch-Gordon coefficients for each allowable transition are shown.

cooling mechanism reminded Dalibard and Cohen-Tannoudji of the Greek myth Sisyphus who was punished to keep pushing a heavy rock up hill hence they named the technique "Sisyphus cooling."

In a low intensity field and with large detuning, redistribution between these ground states due to optical pumping can be slow compared to the change of light polarization, the process is not adiabatic. Since the optical pumping takes out the energy of atoms (energy loss) as the atoms move, the efficiency of this cooling mechanism depends on the velocity of the atoms. Sisyphus cooling works best for optimum velocity $v_s \approx \lambda/4\tau_p$ or when the atoms undergo one optical pumping process while traveling over a distance $\lambda/4$ [44, 48]. Atoms which are moving too fast do not respond to the optical pumping hence they do not lose energy, while atoms which are moving too slowly will be pumped to other sublevels before reaching the hill and hence lose less energy. The damping force $F = -\beta$ v for this mechanism can be estimated from the distance dependence of the energy loss. Using relations $\tau_p \equiv 1/\gamma_p$ and $v_s \cong \gamma_p/k$, the force at the optimum velocity can be written as

$$F = \Delta W/\Delta z \cong \Delta E\ k \equiv -\beta v_s. \tag{19}$$

Here τ_p is the pumping time, γ_p is the pumping rate which is related to the scattering rate, β is the friction coefficient or the damping rate that needs to be estimated, and ΔE is the energy shift. At detuning $|\Delta| \gg \Gamma$ the pumping rate becomes $\gamma_p =$

$s\Gamma^3/4\Delta^2$. By choosing $C_{ge}^2 = 1$, the damping rate and the energy shift can be written as

$$\beta/M = \hbar k^2 \Delta/2M\Gamma, \quad \Delta E = \frac{\hbar\Gamma^2 s}{4\Delta}. \tag{20}$$

It can be shown that by comparing the damping coefficient of Doppler cooling from Eq. (5), the damping rate of sub-Doppler cooling is larger by a factor of $(2|\Delta|/\Gamma)$ and it does not depend on the laser intensity while the energy shift and the pumping rate depend on the intensity. The damping force is smaller compared to the damping force due to Doppler cooling, however the damping coefficient becomes larger when the pumping rate becomes smaller, because the optimum velocity becomes smaller also.

Loading the ultracold atoms from a MOT (as will be explained in the next chapter) to an optical dipole trap (FORT) needs an efficient method of cooling during the loading process. Once the atoms are trapped, further cooling can be applied to achieve high phase-space density and lower temperature if needed for further applications. Doppler cooling has been used frequently to cool the atoms during loading while sub-Doppler cooling has also been used for improving the loading efficiency and to cool the trapped atoms. A MOT can provide a temperature down to $10T_{rec}$ when its operation is optimized by sub-Doppler cooling. Other cooling techniques that are most commonly used for cooling the trapped atoms in a FORT are Raman cooling, sideband cooling, evaporative cooling, and adiabatic cooling [52].

II.2.3 MOT

Doppler cooling in a one-dimensional molasses can be extended into three dimensions by using six laser beams. However, the molasses does not trap atoms, the atoms simply perform a spatially diffusive random walk and there is no confinement in space. The scattering force, which is velocity-dependent, however, can be made position-dependent. The position-dependent force is created by adding an inhomogeneous magnetic field to an optical molasses which is built using circularly polarized laser beams. The configuration is known as a magneto-optical trap (MOT) which was originally conceived by Chu *et al.* upon suggestion by Dalibard [18]. A complete study of the MOT including the development of the external cavity diode laser system used as the MOT laser beams was demonstrated by Wieman and co-workers [54, 55] and has become a standard procedure to produce ultracold atoms.

Details of the dynamics of a MOT in three dimensions are rather complex to

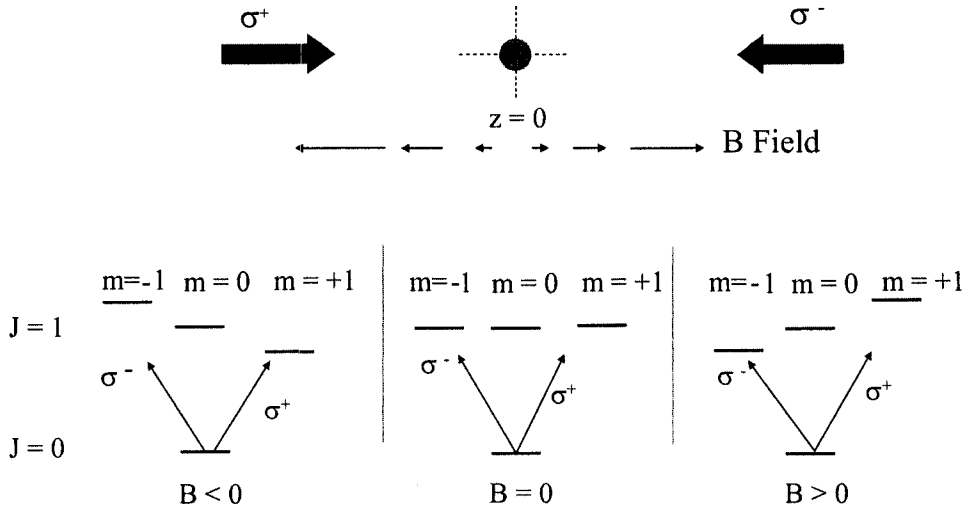

FIG. 7: The magneto-optical trap (MOT) in one dimension. The top part of the diagram shows a one-dimensional MOT with a pair of circularly-polarized counter-propagating beams and a gradient magnetic field which is zero at the center and increases linearly from the center. The bottom of the diagram shows schematically the Zeeman shifting of a J = 0 to J = 1 transition with allowable transition related to the circular polarized laser light.

illustrate, therefore, here the simple case (one dimension) will be used to explain the basic principle of the MOT. As in Fig. 7, consider an atom with a J = 0 ground state and a J = 1 excited state in one dimension (z-axis). The atom is illuminated by circularly-polarized counter-propagating laser beams with frequency ω in the z-direction and immersed in a gradient magnetic field. The excited state (J = 1) is split into 3 Zeeman sublevels with $m_J = -1, 0, 1$, respectively. Because of its polarization orientation, the beam from the left can only excite transitions to the m=+1 state while the beam from the right can only excite transitions to the m = −1 state. The magnetic field is zero at the origin z = 0 and varies along the z axis. At z > 0, the magnetic field perturbs the energy level so that the $\Delta m = -1$ transition shifts to lower frequency while the $\Delta m = +1$ transitions shifts to higher frequency. Since the laser frequency ω is detuned below all of the atomic transition frequencies, the σ^- laser light is closer to resonance than the σ^+ laser light. An atom at z = 0 sees no net radiation pressure because of the two counter propagating beams and hence remains in its position, the atom which moves to the right (z > 0) will scatter many photons by absorbing the σ^- laser light and thereby get pushed back towards z = 0.

The opposite happens for z < 0, the magnetic field shifts the energy levels such that the $\Delta m = +1$ transition shifts to lower frequency while the $\Delta m = -1$ transitions shifts to higher frequency. When the atom moves to the left, it will absorb the σ^+ laser light and get pushed back towards z = 0. So, in any direction the atom goes, it gets pushed back towards z = 0.

In this configuration, the damping force or the scattering force in Eq. (5) which is due to the optical molasses gets a position dependence resulting in a trapping force or a restoring force which is proportional to position z,

$$\mathbf{F}_{\mathrm{av}} = -\kappa_1 \mathbf{v} - \kappa_2 \mathbf{z}. \tag{21}$$

Here κ_1 is the damping coefficient as defined in Eq. (5), κ_2 is the spring constant of the restoring force which depends on the magnetic moment for the transitions used and the magnetic field strength (Zeeman shifts) [44]. Equation (21) is an equation of a damped harmonic oscillator. So the atoms in the MOT undergo a damped harmonic motion with the damping rate given by $\Gamma_{\mathrm{mot}} = \kappa_1/M$ and the oscillation frequency $\omega_{\mathrm{mot}} = \sqrt{\kappa_2/M}$.

The three-dimensional MOT is illustrated in Fig. 8a. The MOT is built using three sets of counter-propagating laser beams with opposite circular polarizations and a pair of anti-Helmholtz coils with opposite electric current to create a gradient magnetic field. In Fig. 8(b), a MOT cloud at the center of a vacuum chamber is shown.

II.3 OPTICAL DIPOLE FORCE TRAPS

This section introduces optical dipole force traps from two different physical points of view. In the first point of view, we consider the atom as a simple classical or quantum-mechanical oscillator. In the second, we consider the atom as a multilevel system. The derivations in this section are mainly taken from [52].

When a polarizable atom is placed into a laser light source, the electric field $\mathbf{E}$ of the light induces an atomic dipole moment $\mathbf{d}$ that oscillates at the laser frequency ω. The dipole moment is proportional to the electric field and given by:

$$\mathbf{d} = \alpha(\omega)\,\mathbf{E}. \tag{22}$$

Here, $\alpha(\omega)$ is the complex polarizability which depends on the field frequency ω. The interaction potential of the induced dipole moment $\mathbf{d}$ in the driving field $\mathbf{E}$ is given

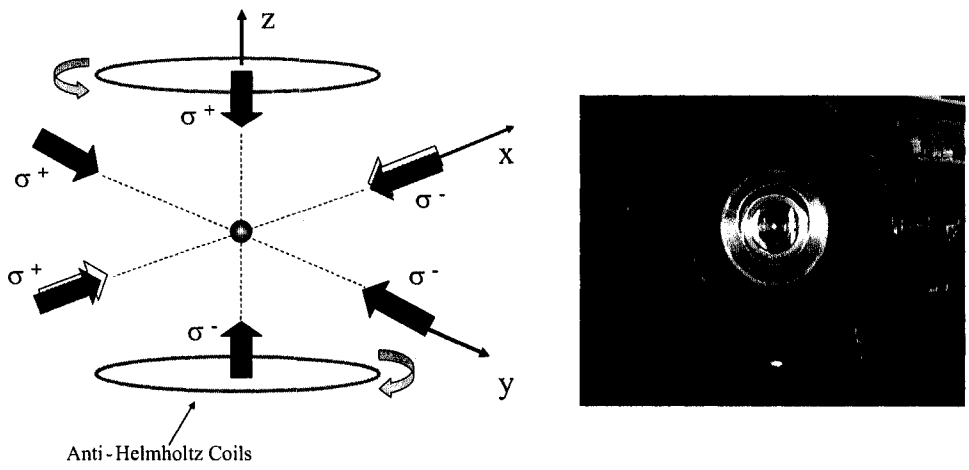

(a) (b)

FIG. 8: The magneto-optical trap (MOT) in three dimensions is comprised of 3 sets of counter-propagating beams (solid black arrow) with two opposite circular polarizations and a pair of anti-Helmholtz coils to create a gradient magnetic field, with zero at the center (a). There is also a pair of repump beams (white arrow) which optically pumps atoms that decay to different ground states by off resonance transitions. The MOT cloud is seen at the center of a vacuum chamber (b).

by

$$U_{dip}(r) = -\langle d\,\mathbf{E}\rangle = -\frac{1}{2\varepsilon_o c}\,\mathrm{Re}(\alpha)\,I, \qquad I = \frac{\varepsilon_o c}{2}|E|^2. \tag{23}$$

In Eq. (23), the angular brackets denote the time average over the rapidly oscillating terms. Note that the dipole moment is not a permanent one, but is induced. The optical dipole force arises from the dispersive interaction of the dipole moment with the intensity gradient of the light field which is given as the gradient of U_{dip}

$$\mathbf{F}_{dip}(r) = -\nabla U_{dip}(r) = \frac{1}{2\varepsilon_o c}\,\mathrm{Re}(\alpha)\,\nabla I(\mathbf{r}). \tag{24}$$

So the optical dipole force is a conservative force which is proportional to the gradient of the field intensity. It acts in the direction of the gradient of the laser intensity while the dissipative force for laser cooling (radiation pressure or scattering force) acts in the direction of laser propagation.

The power absorbed by the oscillator from the driving field (and re-emitted) as dipole radiation is given by

$$P_{abs} = \langle \dot{\mathbf{d}}\,\mathbf{E}\rangle = 2\omega\,\varepsilon_o c\,\mathrm{Im}(\tilde{p}\,\tilde{E}^*) = \frac{\omega}{\varepsilon_o c}\,\mathrm{Im}\,(\alpha)\;I. \tag{25}$$

The absorption results from the imaginary part of the polarizability, which describes the out-of-phase component of the dipole oscillation. By considering the light as a stream of photons with photon energy $\hbar\omega$, the absorption can be interpreted in term of photon scattering in cycles of absorption and subsequent spontaneous reemission process. The scattering rate can be defined as

$$\Gamma_{sc} = \frac{P_{abs}}{\hbar\omega} = \frac{1}{\hbar\varepsilon_o c} \operatorname{Im}(\alpha)\, I. \tag{26}$$

The interaction potential in Eq. (23) and the scattering rate in Eq. (26) are the two main parameters that are always considered in the discussion of optical dipole force traps. Creating a deep interaction potential well while having a low scattering rate is the main goal in building an optical dipole force trap.

In order to come up with applicable expressions for both parameters, the frequency dependent polarizability $\alpha(\omega)$ is derived. The derivation starts by considering the atoms as a *Lorentzian atom*, which consists of an electron elastically bound to a core with an eigenfrequency ω_0 corresponding to the optical transition frequency. In the oscillating light field, the atom (electron) behaves as a driven oscillator whose oscillation is driven by the light field. The polarizability is obtained by solving the equation of motion for the driven oscillation of the electron,

$$\ddot{x} + \Gamma_\omega \dot{x} + \omega_0^2 x = -eE(t)/m_e, \tag{27}$$

with the result being

$$\alpha = \frac{e^2}{m_e} \frac{1}{\omega_0^2 - \omega^2 - i\omega\Gamma_\omega}. \tag{28}$$

Here, Γ_ω is the classical damping rate due to the radiative energy loss, it is given by

$$\Gamma_\omega = \frac{e^2\omega^2}{6\pi\varepsilon_0 m_e c^3}. \tag{29}$$

By extracting e^2/m_e from Eq. (29), introducing $\Gamma \equiv \Gamma_{\omega_0} = (\omega_0/\omega)^2\, \Gamma_\omega$ and substituting into Eq. (28), the classical polarizability is written as

$$\alpha = 6\pi\varepsilon_0 c^3 \frac{\Gamma/\omega_0^2}{\omega_0^2 - \omega^2 - i(\omega^3/\omega_0^2)\Gamma}. \tag{30}$$

The polarizability can also be calculated using a semiclassical approach by considering the atom as a multilevel quantum system interacting with the classical radiation field. The damping rate for the semiclassical approach, which corresponds to the spontaneous decay rate of the excited level, is calculated using the dipole matrix

element between the ground state and the excited states. One finds that when saturation effects can be neglected which is true in our experiment (the far detuned case, very low saturation), the semiclassical result is similar to the classical calculation above. Therefore it can be used in deriving the dipole potential and the scattering rate in the case of large detuning and low scattering rate. So using Eq. (30), the dipole potential in Eq. (23) is written as

$$U_{dip}(r) = -\frac{3\pi c^2}{2\omega_o^3}[\frac{\Gamma}{\omega_o - \omega} + \frac{\Gamma}{\omega_o + \omega}]I(r), \tag{31}$$

and the scattering rate in Eq. (26) is given by

$$\Gamma_{sc}(r) = \frac{3\pi c^2}{2\hbar\omega_o^3}(\frac{\omega}{\omega_o})^3[\frac{\Gamma}{\omega_o - \omega} + \frac{\Gamma}{\omega_o + \omega}]^2 I(r). \tag{32}$$

Equation (31) and (32) shows two resonant contributions at $\omega = \omega_0$ and $\omega = -\omega_0$. In most experiments, the laser is tuned relatively close to the resonance ω_0 such that $\Delta \equiv \omega - \omega_0 \ll \omega_0$, in this case the second term in the equations above can be neglected and this approximation is known as the *rotating wave approximation* (RWA), hence the equation can be simplified to

$$U_{dip}(r) = \frac{3\pi c^2}{2\omega_o^3}\frac{\Gamma}{\Delta}I(r), \tag{33}$$

and the scattering rate in Eq. (26) is given by

$$\Gamma_{sc}(r) = \frac{3\pi c^2}{2\hbar\omega_o^3}\left(\frac{\Gamma}{\Delta}\right)^2 I(r). \tag{34}$$

Equation (33) and (34) can also be derived from a quantum mechanical point of view where the interaction of atoms with the light radiation field is represented by a time-dependent Schrodinger equation. The Hamiltonian for the interaction with the radiation field $\mathbf{E}(\mathbf{r},t)$ is given by [44, 52]

$$H_1(t) = -\mu E(r,t)\,,\ \mu = -e\mathbf{r}. \tag{35}$$

Here μ is the electric dipole operator. The solution of the total Hamiltonian leads to an energy shift of the ith unperturbed energy ε_i which can be written as

$$\Delta E_i = \sum \frac{|\langle j|H_1|i\rangle|^2}{\varepsilon_i - \varepsilon_j}. \tag{36}$$

For a two-level atom, using the "dressed state" picture, Eq. (36) simplifies to

$$\Delta E_i = \pm\frac{|\langle e|H_1|g\rangle|^2}{\Delta}|E|^2 = \pm\frac{3\pi c^2}{2\omega_0^3}\frac{\Gamma}{\Delta}I. \tag{37}$$

Here $I = 2\varepsilon_0 c|E|^2$ has been used. This perturbative result for the energy shifts reveals a very important fact that the ground state of the atoms gets shifted by the amount in Eq. (37) while the excited state get shifted in the opposite direction.[5] This equation gives the same result as Eq. (33).

For the red detuned case, the detuning Δ is less than zero since the laser frequency is tuned below atomic resonance, the dipole potential is negative and atoms are attracted into the light field. The minimum of the potential is found at the position where the intensity is maximum. In relation to Eq. (37), for the low saturation case, the atoms spend most of their time in the ground state, the light-shifted ground state can be interpreted as the relevant potential for the motion of the atoms. This red detuned trap is easily built using a single focused Gaussian laser beam where the atoms are trapped at the focus. For the blue detuned case, the detuning is larger than zero, the dipole interaction repels atoms out of the field and the potential is minima at the minima intensity. This kind of trap is likely hard to build since the laser beam used needs to have a minimum at the center (box-like potentials with hard repulsive wall).

Equation (33) and (34) are also valid for far off resonance (optical dipole force) traps. In contrast, if the laser frequencies are much lower than the atomic resonance frequency, the polarizability is considered to be well approximated by its zero frequency (DC) value. The trap using this laser light is known as a quasi-electrostatic trap (QUEST). This trap does not rely on a specific transition, therefore it can trap all internal states of an atom simultaneously, as well as different atomic or molecular species. For the FORT, as in Eq. (33) and (34), the dipole potential scales as I/Δ and the scattering rate scales as I/Δ^2. The relation between the dipole potential and the scattering rate can be written as

$$\hbar\Gamma_{sc} = \frac{\Gamma}{\Delta} U_{dip}. \tag{38}$$

To have an optical dipole force trap with a very low scattering rate at a given potential depth, it is desirable to use laser light with high intensity and very large detuning.

For multi level atoms that have fine structures such as in alkali-metal atoms, the potential in Eq. (33) is modified to include the effect of two D lines in the fine structure,

$$U_{dip} = \frac{\pi c^2 \Gamma}{2\omega_o^3}\left(\frac{1}{\Delta_{D_1}} + \frac{2}{\Delta_{D_2}}\right) I, \tag{39}$$

[5] it is known as AC Stark shift.

and the scattering rate in Eq. (34) is given by

$$\Gamma_{sc} = \frac{\pi c^2 \Gamma^2}{2\hbar\omega_o^3}\Big(\frac{1}{\Delta_{D_1}^2} + \frac{2}{\Delta_{D_2}^2}\Big) I. \tag{40}$$

Here Δ_{D_1} and Δ_{D_2} are detunings from the D1 and D2 lines respectively. These formula are valid for the case of detuning large compared to the excited state hyperfine splitting and the excited state linewidth and for linearly polarized laser light. For ^{85}Rb with transition line $5^2S_{1/2} - 5^2P_{1/2}$ for the D1 line and the transition from $5^2S_{1/2} - 5^2P_{3/2}$ for the D2 line, and with $I_{sat} = 2\pi^2\hbar c\Gamma/3\lambda^3$ as the saturation intensity, Eq. (39) and (40) can be rewritten as

$$U_{dip} = \frac{\hbar\Gamma^2 I}{24 I_{sat}}\Big(\frac{1}{\Delta_{1/2}} + \frac{2}{\Delta_{3/2}}\Big), \tag{41}$$

and the scattering rate in Eq. (26) is given by

$$\Gamma_{sc} = \frac{\Gamma^3 I}{24 I_{sat}}\Big(\frac{1}{\Delta_{1/2}^2} + \frac{2}{\Delta_{3/2}^2}\Big). \tag{42}$$

As mentioned earlier, for the red detuned case, the minima of potential is found at the position where the intensity is maximum and thereby a trap can easily be built using a single focused Gaussian laser beam. The general equation for a focused Gaussian beam of peak intensity I_0 is written as [53]

$$I(z,r) = I_0 \frac{w_0^2}{w^2(z)} \exp^{-2r^2/w^2(z)}. \tag{43}$$

Here $I_0 = 2P/\pi w_0^2 =$ the intensity at the waist, w_0 is the minimum spot size (waist size), z and r are the axial and radial position respectively, and $w(z)$ is the $1/e^2$ radius at z and r,

$$w(z) = w_0\sqrt{1 + (\frac{z - z_0}{z_R})^2}, \tag{44}$$

where $r = \sqrt{x^2 + y^2}$, an $z_R = \pi w_0^2/\lambda$ is the Raleigh range. z_0 is the axial position at $w(z) = w_0$. The experimental form of the potential energy for a red detuned FORT then is given by

$$U(z,r) = -U_0 \frac{w_0}{w^2(z)} \exp^{-2r^2/w^2(z)}. \tag{45}$$

U_0 is the minimum potential (well depth) of the trap at $z = 0$ and $r = 0$ which is already given in equation (41). For radial shape ($z = 0$), Eq. (45) is rewritten as

$$U(r) = -U_0 \exp^{-2r^2/w_0^2}. \tag{46}$$

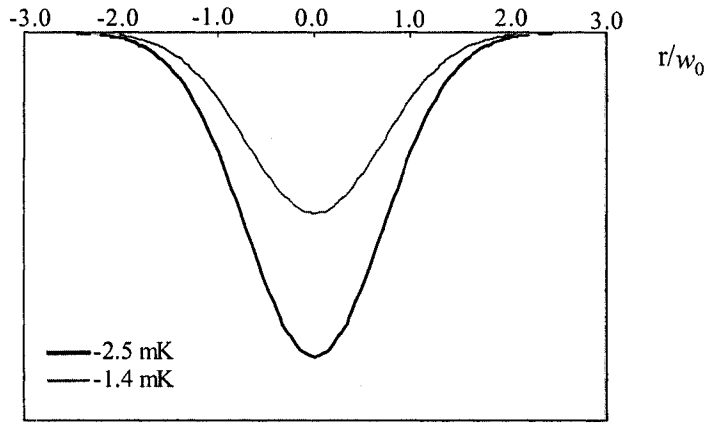

FIG. 9: The radial potential depths of a cw red detuned optical dipole trap (FORT) at the focus of a cw Gaussian laser beam as a function of the radial distance for two different laser powers, but the same waist size w_0.

The plot of radial potential well depth of a cw FORT for 7 Watts and 4 Watts of laser powers (as measured before entering the vacuum chamber) and the calculated waist $\sim$ 16 μm is shown in Fig. 9. 7 Watts of laser power creates a potential depth -2.5 mK and 4 Watts of laser power gives -1.4 mK potential depth. These potential depths are calculated using Eq. (31). The calculation of the potential depth using Eq. (39) gives only small difference, -2.2 mK for 7 Watts and -1.2 mK for 4 Watts. The values of laser power 7 Watts and 4 Watts are measured before the beam are sent to the chamber, we include 8% loss in the calculation due to the uncoated window where the beam enters the chamber.

II.4 MODE-LOCKED LASER

Lasers can be divided into two general categories; continuous wave (cw) and pulsed. A cw laser emits a steady beam for as long as the laser medium is excited. A Helium-Neon (He-Ne) laser is a good example of a cw laser. A pulsed laser emits light in individual pulses. An example of a pulsed laser is a Nd:YAG laser. However most Nd:YAG lasers can be operated in cw and pulsed modes. The pulsed laser can be divided further into categories such as single pulse, Q-switched, and mode-locked, according to the behavior of the standing wave in the laser cavity. All cw lasers may be pulsed, either mechanically using a shutter, electronic, or photonic components.

Characterization of the laser beam output can be described by two kinds of modes;

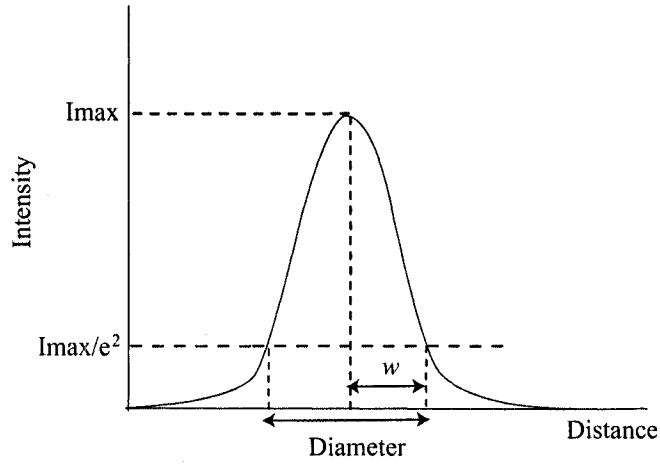

FIG. 10: Schematic diagram of a Gaussian laser beam. The size of the beam is the diameter of the beam at $1/e^2$ intensity.

longitudinal modes and transverse modes. The longitudinal modes depict the variations in the electromagnetic field along the optical axis of a laser cavity while the transverse electromagnetic (TEM) modes express the variations of the electromagnetic field in the direction perpendicular to the optical axis or perpendicular to the traveling wave. The behavior of pulsed lasers is easier to describe in term of the longitudinal modes. A discussion on the TEM modes is very important if a precise beam shape is needed. The longitudinal modes can be portrayed by waves traveling in a rope or a string while the TEM modes like vibrations of a drum surface.

A single mode TEM_{00} laser beam or Gaussian laser beam is the most widely used for laser cooling and trapping applications. Other TEM modes such as TEM_{01} laser beam or a Laguerre mode laser beam is used to make a blue detuned FORT. The size of the beam can be varied by varying the size of a small aperture mounted inside the cavity before the output coupler. Figure 10 shows the typical schematic of a Gaussian laser beam. The spot size w is the radial distance (radius) from the center point of maximum intensity to the $\frac{1}{e^2}$ point.

Figure 11 shows a typical laser cavity. The laser cavity is also called an optical cavity or a laser resonator. The basic laser cavity is comprised of a lasing medium (active medium), a high reflector and an output coupler. A lasing medium could be in the form of a gas, liquid, or solid. A lasing medium contains atoms that have

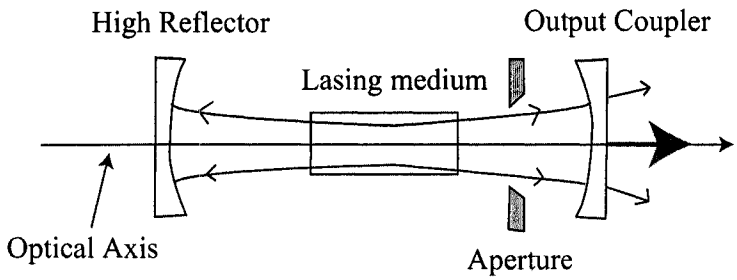

FIG. 11: Schematic diagram of a basic laser resonator. It is comprised of a high reflector, a lasing medium, and an output coupler.

metastable states and hence a population inversion can be built and stimulated emission can be initiated. The laser needs energy to excite the atoms to the metastable states. A gas laser uses a discharge system to excite the atoms while the liquid laser and solid-state laser usually use light from a lamp to excite the atoms. The lasing medium also acts as a light amplifier. The high reflector and the output coupler act as a feedback mechanism. The high reflector has 100% reflectivity and the output coupler has reflectivity a little less than unity to couple out some of the laser beam.

In the laser cavity, laser light bounces back and forth between the mirrors at a MHz rate. The laser light waves can travel in both directions at the same time and hence interference can result. This motion gives rise to standing waves or longitudinal waves. These standing waves help determine the characteristics of the laser light frequency and the wave length in the cavity. Figure 12 shows longitudinal modes in a laser cavity. The standing waves in the laser cavity should satisfy the condition that nodes are located at each end of the cavity. In addition, the standing waves between points exists as long as an integral number of half-wavelengths can fit exactly between the mirrors such that

$$N\frac{\lambda}{2} = L \; or \; N = \frac{2L}{\lambda}. \tag{47}$$

Here, N is the total number of half-wavelength, L is the mirror spacing, the wavelength of the N^{th} mode is given by

$$\lambda_N = \frac{2L}{N}. \tag{48}$$

The frequency of the N^{th} mode and the frequency spacing between mode are given as

$$\nu_N = N\frac{c}{2L}, \;\; \Delta\nu = \frac{c}{2nL}. \tag{49}$$

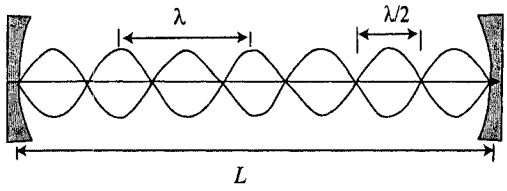

FIG. 12: A longitudinal mode between the two mirrors of the laser cavity separated by a distance L.

Here, c is the speed of light in the cavity and n is the refractive index of the active medium. A laser output is not exactly monochromatic, it has a bandwidth $\Delta\lambda$, and often many longitudinal modes with spacing $\Delta\nu$ can fit within the bandwidth and thus exist simultaneously in the cavity. Pulsed lasers can be created from a cw cavity laser by inserting an electro-optic modulator or an acousto-optic modulator in the laser cavity. There are two types of pulsed laser output; single pulse and repetitive pulse. A single pulse laser produces one pulse of light per laser operation while a repetitively pulsed laser produces a train of pulses at equal spacing whenever the laser is in operation. The repetitively pulsed laser is known as a cw mode-locked laser. The output of a cw mode-locked laser is shown in Fig. 13. The separation of the pulses is equal to the time required for the light to make one round trip around the laser cavity $\tau = 2L/c$, this value is also defined as the "pulse repetition time." The pulse repetition rate of the mode-locked laser is defined as $1/\tau$ and the pulse width as T. In most cases, the output of a mode-locked laser is characterized by measuring the average power of the laser using a power meter and determining of the pulse width and the pulse repetition time using a fast photodiode and an oscilloscope. The maximum power of the pulse equals the average power divided by the duty cycle of the pulse. The duty cycle is the ratio of the time the laser is on to the time the laser is off.

II.5 PULSED FORT

In Sec. II.3, the theory of an optical dipole force trap using single frequency, continuous wave laser light has been derived and it is well discussed in the literature [42, 52]. In this section, the derivation of an optical dipole force trap using a pulsed or mode-locked laser which is detuned far from an atomic resonance will be discussed.

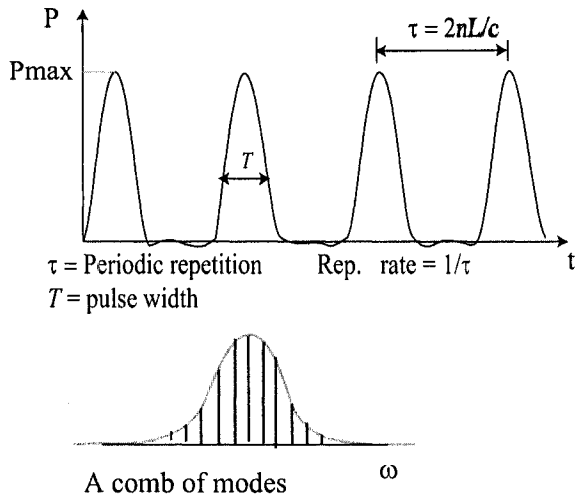

FIG. 13: The output of a mode locked laser, train of pulses.

The discussion is based on the derivation by [38].

As discussed in Sec. II.4, a pulsed laser beam produced by a mode-locked laser in the time domain consists of a train of pulses with a certain pulse width, temporally separated by a repetition time. In the frequency domain, each pulse is comprised of frequency components or a comb of modes whose bandwidth equals the inverse of the pulse width. Each of these frequency components gives rise to an AC Stark shift as defined in Eq. (37) and (41) and their combined effect is the sum of the shifts. This approximation is only valid for laser detuning larger than the mode-locked laser bandwidth. For smaller detuning, the interaction between individual modes has to be included. As for our experiment, the requirement is satisfied since the Nd:YAG laser we used, which is operated mode-locked, has pulsewidth $\sim$ 100 ps equivalent to a bandwidth $\sim$ 10 GHz, while the laser frequency detuning $\Delta\omega$ from the resonance frequency of ^{85}Rb $\simeq$ 645 THz.

In a time domain point of view, the atoms are portrayed as receiving a series of mechanical kicks at the pulse repetition rate. The time-averaged effect would be the same as that of a cw beam with the same average power unless the repetition rate of the laser beam equals one of the characteristic frequencies of atomic motion in the trap which can drive a parametric oscillation of the atoms [38]. This is unlikely to happen in our trap since the repetition rate of the Nd:YAG laser is 82 MHz while typical trap oscillation frequencies are in the kHz range.

The scattering rate for a pulsed FORT can also be considered as the sum of the scattering rates due to each frequencies component of the mode-locked laser beam. Equation (42) is still valid since the laser bandwidth is much smaller than the laser detuning even though the instantaneous intensity I_p of each pulse is very large. This is justified from Eq. (50) below

$$p_e \cong \frac{\xi^2}{2(1+\xi^2)}, \tag{50}$$

where

$$\xi^2 = \frac{4\Gamma^2 I_p}{\Delta^2 I_{sat}} \tag{51}$$

because the fractional population of the upper state for a 10 Watts average power laser beam which is focused down to a $1/e^2$ intensity radius 15 μm still has ξ^2 and p_e on the order of 10^{-3} [39].

II.6 HEATING AND LOSS

Trapping ultracold atoms in an optical dipole force trap requires cooling to load the trap since the dipole force is conservative instead of dissipative. Efficient cooling techniques are very important to load atoms into a dipole trap since the trap depths are usually only $\sim$ 1 mK. The standard procedure to load the atoms is from a magneto-optical trap (MOT) which is capable of trapping ultracold atoms with temperature $\sim$ 100 μK (or less). Further cooling can be applied to the trapped atoms using some of the cooling techniques that have been developed for a dipole trap [25, 27]. The number of atoms in the dipole trap depends of the heating and trap loss due to collisional processes taking place during loading and after the loading is complete.

II.6.1 Heating

A fundamental source of heating in an optical dipole force trap is the fluctuations in absorption and spontaneous re-emission processes of the trapped photons from the far detuned dipole trap light. The photon scattering leads to ground state spin relaxation, i.e. transition between different ground states (hyperfine levels). As one of the interests in using an optical dipole force trap is to reduce this scattering rate which is proportional to $1/\Delta^2$, this scattering rate is reduced as the laser frequency is detuned far from the atomic resonance.

The heating due to fluctuations in absorption corresponds to an increase of the thermal energy by $E_{rec} = k_B T_{rec}/2$ per scattering event. The spontaneous process also contributes one recoil energy per scattering event, the overall heating thus corresponds to $2E_{rec}$ per scattering event. The total heating power corresponds to the increase of the mean thermal energy $\bar{E}$ of the atomic motion with time. It is related to the scattering rate which is defined in Sec. II.3 by

$$P_{Heat} \equiv \frac{d\bar{E}}{dt} = 2E_{rec}\bar{\Gamma}_{sc} = k_B T_{rec}\bar{\Gamma}_{sc}. \tag{52}$$

Here T_{rec} is the recoil temperature. The heating rate can be derived by assuming a thermal equilibrium condition of an atomic gas in a dipole trap. In thermal equilibrium, the average kinetic energy per degree of freedom is $\frac{1}{2}k_B$T and in harmonic potentials, the potential energy equals the kinetic energy, $\bar{E}_{pot}$ / $\bar{E}_{kin} = 1$, giving the average total energy in a three-dimensional trap $\bar{E} = 3k_B$T. Combined with Eq. (52), the equation for the heating rate becomes

$$\frac{dT}{dt} = \frac{T_{rec}}{3}\bar{\Gamma}_{sc}. \tag{53}$$

In addition to this fundamental heating, technical heating can also occur because of intensity fluctuations and pointing instabilities in the trapping fields [52]. In an optical trap, however, loss by heating from the trap laser is usually negligible compared to loss by collisions which will be explained in next section.

II.6.2 Cold Collisions

Since the development of laser cooling techniques in the early 1980's, there are two mutual results emerging from laser cooling experiments. First, it was found that the collision between cold atoms in optical traps was one of the limiting factors in the achievement of high density samples. Second, laser cooling and trapping techniques also allow for the advancement in the study of the physics of cold collisions [56]. In fact, knowledge of collision processes in atom traps was critical for achieving high density samples. There are some unique differences between typical atomic collisions (fast and high energy collisions) and ultracold ones [57]. For high energy collisions, a collision happens during a very short time-much shorter than the lifetime of any electronic excited states. In contrast, a low energy collision happens with longer time, many absorption-emission cycles may occur in the light field during the collision, and collisions between excited atoms may occur. Collisional processes can lead to

substantial trap loss. Extensive studies have been done to understand the collisional processes involved in optical traps [58, 59, 60, 61] theoretically and experimentally.

Accurate determination of density-dependent collision rates requires an accurate determination of the density. Density measurements on trapped atoms are usually done by counting the number of atoms with either absorption (absorption imaging) or emission (fluorescence detection) techniques, combined with measurements of the spatial distribution of the cloud of the trapped atoms. Collision rates are typically extracted by observing the time dependence of the atom number either as the trap loads or as it decays. The number of atoms in a trap with no loading can be described by a general loss (decay) equation [52]:

$$\frac{dN(t)}{dt} = -\alpha N(t) - \beta \int_V n^2(r,t) d^3r - \gamma \int_V n^3(r,t) d^3r. \tag{54}$$

Here, the first term with α as the single-particle loss coefficient represents the loss due to the collision process between the trapped atoms with the background gas in the vacuum apparatus. α is very small for an ultra high vacuum ($\sim 10^{-11}$ Torr) and higher for a vapor cell experiment. The second term describes the trap loss due to inelastic-ultracold binary collisions that reveals a wide range of interesting physics. The quantity β is the two-body loss coefficient which contains the probabilities for inelastic process such as fine-structure changing collisions, radiative escape, and photo-association. The last term represents three-body losses with loss coefficient γ. It is only relevant at extremely high density traps and will not be considered below.

In general, because of the spatial variation of atomic density *n(r,t)* a detailed integration over the whole volume occupied by the atoms [56] is required. However, the spatial density distribution of the trapped atoms can be in one of the two possible limits. First, at low density, radiation trapping is negligible and the trap distribution is close to Gaussian hence the integration over volume is trivial.[6] Second, at high density, radiation trapping dominates and the density is approximated by a "flat-top" profile. For the low density case, the density can then simply be replaced by the number of atoms measured divided by the volume. In this experiment, the first limit is considered, hence Eq. (54) can be re-written as

$$\frac{dN(t)}{dt} = -\alpha' N(t) - \beta' N^2(t). \tag{55}$$

[6]This situation is typical for our experiment.

Here the prime is used to differentiate it from the coefficients which are defined with respect to the spatial density: α and β.

Two types of collisions may happen between the trapped atoms; elastic and inelastic. Elastic collisions do not necessarily change the internal state of the atoms but can lead to thermalization of the trapped sample due to momentum transfer and may cause atom loss from a trap by evaporation. This type of collision is very useful for evaporative cooling to achieve Bose-Einstein Condensation, however, elastic collisions can also cause problems such as for high precision frequency measurement, since a small systematic shift results from this type of collision. Inelastic collisions change the internal state of atoms. The exchange energy in the collision process leads to an excess of kinetic energy causing trap loss especially in the optical trap with a shallow potential depth.

In terms of the internal state of atoms, there are three classes of collisions that occur between the trapped atoms [62] that depend on the short and long-range potentials. First is a ground state collision where both atoms are in their ground electronic states. Like higher temperature collisions, the atomic motion is governed by conservative interatomic forces, the collisions are sensitive to the potential interaction shape. Elastic collisions dominate in this class of collision since they interact only through the weak, short range $1/R^6$ van der Waals interaction and usually occur at low intensity light field. Here R is the interatomic separation. An important contribution to trap loss due to ground-state collisions, which mostly involves alkali atoms, is the inelastic hyperfine-state-changing process. This process gives an increase in the kinetic energy of each of the colliding atoms of $h\nu_{hfs}/2$, where ν_{hfs} is the atomic ground state hyperfine splitting.

The second class of cold collisions is the collision involving a ground state atom with an excited atom. This class of collision is of interest because it is very important in a MOT or FORT. For homonuclear atoms, the interaction is dominated by a long range $1/R^3$ dipole-dipole interaction [62, 63]. At long range, this collision is dominant over the ground state collisions, it mostly occurs at high intensity laser light where light scattering is likely to occur. There are three inelastic processes involved in this type of collision; Radiative escape (RE), fine structure changing (FCC) collisions, and hyperfine structure changing collision. The latter has a small contribution to the total trap loss.

The third class of collision involves two excited atoms. This doubly excited state

collision is also dependent on the long-range potential, interaction with external fields, and spontaneous emission. The collisional rate is smaller compared to the collisional rate of the second class collision since the doubly excited interaction potentials are relatively weak, $1/R^5$ range and is usually characterized by a quadrupole-quadrupole interaction.

In our experiment, the ultracold atoms are loaded into the FORT from a MOT. There are two stages during loading when collisional processes play a role. First is in the loading stage where the MOT laser beams are still present to transfer atoms from the MOT to the FORT. The second stage is the holding stage where the MOT laser beams have been turned off (loading is terminated). Trap loss because of light-assisted binary collision (radiative escape) and excited-state fine structure-changing collision strongly affect a MOT but are negligibly small for a FORT because of the extremely low excitation probability. They can be important in the FORT if near-resonant cooling light is present or the FORT light is not far-detuned. Equation (55) is somewhat modified to represent both stages. The loading stage has an additional term which include the loading rate R_0 and a new parameter γ_{mot} which characterizes the change to the MOT dynamics during the FORT loading stage:

$$\frac{dN}{dt} = R_0 e^{(-\gamma_{mot} t)} - \Gamma_L N - \beta'_L N^2, \tag{56}$$

and for the holding stage, the number of atoms remaining in the trap is the solution of

$$\frac{dN}{dt} = -\Gamma_H N - \beta'_H N^2. \tag{57}$$

Equations (56) and (57) will be used frequently in the analysis of this experiment. The index L and H are used to differentiate the collision rates between both stages.

CHAPTER III

THE EXPERIMENTAL SETUP

A major challenge in doing research in experimental atomic physics is to prepare a sample in such condition as to avoid the interaction with the surroundings and any circumstances that obscure the experimental result. In laser cooling and trapping experiments, the atom sample is cooled and confined in a high or ultra high vacuum chamber with very low background gas pressure. Applying techniques to get high vacuum while still maintaining a relatively simple optical arrangement is just one of the details of the experimental setup that we will discuss in this chapter.

The simplified experimental setup of the cw and pulsed FORT system for confining rubidium atoms is shown in Fig. 14. It begins with a ^{85}Rb MOT. The MOT consists of three pairs of counter propagating trap laser beams (sometimes called the MOT primary laser beam) and two pairs of horizontal counter propagating repump laser beams. The trap beams come from a Master-Slave configuration diode laser system (not shown). The repump laser beam comes from a separate laser for easy intensity and frequency control. The output of the lasers is coupled to a fiber optic cable for easy alignment to the vacuum chamber. A pair of anti-Helmholtz coils (not shown) with a magnetic field gradient about 10 G/cm is used to trap Rb atoms in the MOT. After a stable MOT has been achieved, the atoms in the MOT are transferred to the FORT, first by overlapping the rubidium cloud with the waist of a Nd:YAG laser beam at the center of the chamber for a certain amount of time, then all the MOT laser beams and the magnetic field are switched off while the FORT laser beam remains on. The atoms captured in the FORT potential well are held by the FORT laser beam for a couple of seconds before being ejected from the trap. An imaging system using a CCD (CCD2) camera aimed down the bore of the FORT beam is used to monitor the alignment of the MOT cloud to the waist of the FORT beam. While the Camera CCD1 is just used to monitor the MOT cloud. The number of atoms in the FORT is determined by measuring the fluorescence of recaptured atoms in an optical molasses phase, where the MOT beams are on but no magnetic field is present. Fluorescence is detected with a photomultiplier tube.

In this chapter, all the aspects of the experimental setup will be explained in detail including the vacuum chamber, the external cavity laser systems, optics for the MOT, and the Nd:YAG laser system for cw and pulsed FORT operation. The detection

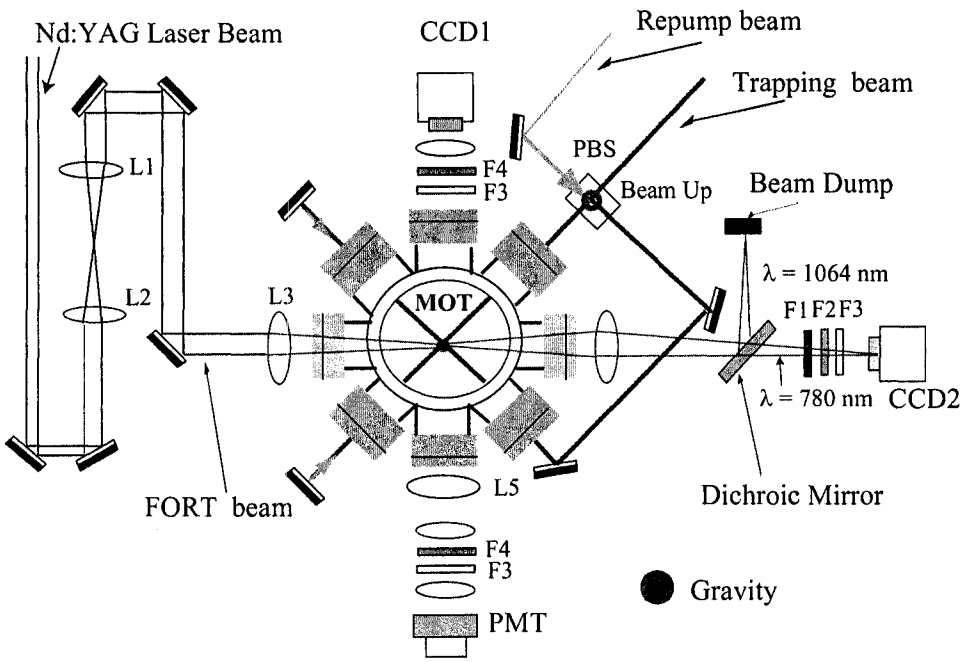

FIG. 14: The experimental setup for cw and pulsed FORT. L1 = 100mm and L2 = 200mm. F1 = neutral density filter, F2 = colored glass filter, F3 = interference filter, and F4 = short pass filter. PBS = polarized beam splitter and PMT = photomultiplier.

system and the data acquisition system will be discussed in the next chapter. Details of the experimental arrangement for performing spectroscopy of atoms in the FORT will be described in Chapter V.

III.1 VACUUM SYSTEM

The vacuum system is the center of the laser cooling and trapping experiment where the atoms are cooled, confined, and manipulated. Vacuum denotes that air or other gases have been substantially removed [64]. The amount removed depends on the application, and creating a vacuum is done for many reasons. In this case, the collisions between background gases and the cooled atoms will result in atoms being ejected from the optical trap (trap loss). The loss rate depends on the density and the velocity of background gases and also depends on the collision cross section. The removal of the background gases in a vacuum system is done by many methods, for example: by displacement pumps or by capture pumps. Here the chamber is first evacuated to low pressure from atmospheric pressure by a turbomolecular pump and is then pumped to even lower pressure by an ion pump. The suitable pressure for laser cooling and trapping experiments is in the range of 10^{-7} to 10^{-12} Torr, which is referred to as ultra high vacuum (UHV) to extreme high vacuum.

In this experiment, the vacuum system is a custom-built cylindrical chamber with ten of 2-3/4″ conflat ports. Six of the ports are used for the MOT lasers, two for the FORT beam, and two for detection. The chamber is continuously pumped by an 11 l/s ion pump, resulting in a pressure which is estimated to be in the low to mid 10^{-9} Torr range. Figure 15 displays the vacuum system used for this experiment, it shows the outlets for the ion pump and Rb dispenser. The preparation of the vacuum system follows the standard procedure [54] and will not be explained in detail here.

III.2 DIODE LASER SYSTEM

As mentioned in Sec. II.4, a simple laser cavity is comprised of a laser medium and two reflecting mirrors. The operating frequency ν is determined by the cavity mirror spacing L, and the energy difference E between the two energy levels used for the stimulated emission. Two relations which must be satisfied for operating the laser are [65]:

$$\nu = N\frac{c}{2nL}, \tag{58}$$

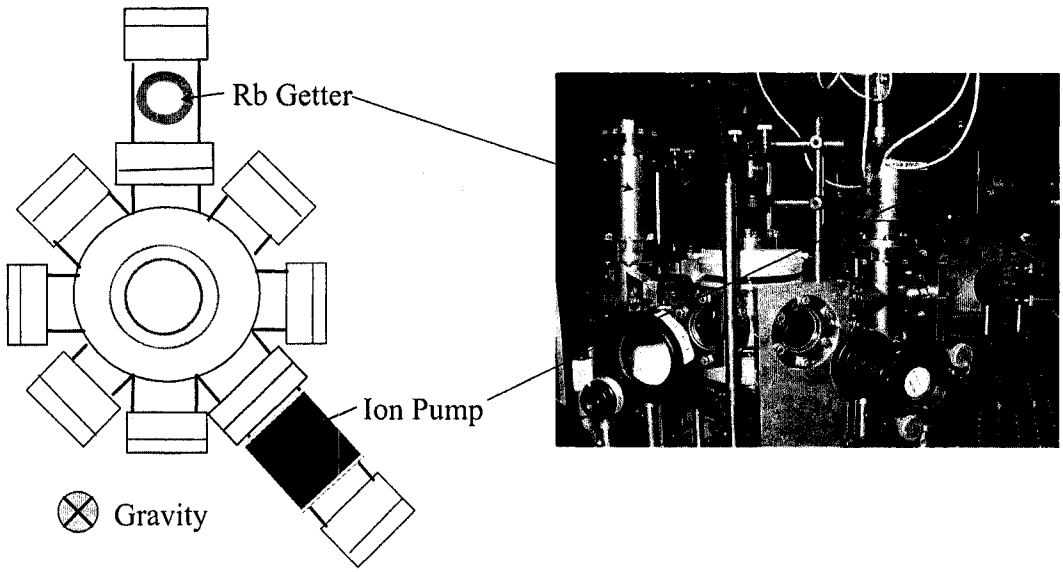

FIG. 15: The vacuum system used in this experiment.

$$\nu = \frac{E}{h}. \tag{59}$$

Here N is an integer, c is the speed of light, h is Planck's constant, and n is the index of refraction between the reflectors.

From Eq. (59), it can be shown that the uncertainty principle, $\Delta\varepsilon\Delta t \sim h$ can give rise to a finite linewidth of the laser frequency where $\Delta\varepsilon$ is the uncertainty of the level's energy and Δt is the uncertainty in its lifetime. Random motion of the atoms or molecules in the laser medium also contributes to the linewidth where there is a finite gain bandwidth which is a measure of the range of frequencies that satisfy Eq. (59). Due to this bandwidth, many longitudinal modes with spacing $\Delta\nu$ can fit within the bandwidth and thus exist simultaneously in the cavity. The quantitative representation of the laser output is given by Schawlow-Townes linewidth (limit) [65]:

$$\Delta\nu = \frac{h\nu_0}{2\pi} c^2 \frac{(1-R)^2}{PL^2}. \tag{60}$$

Here $h\nu_0$ is the average photon energy, c is the speed of light in the laser medium, P is the output power, L is the cavity length, and R is the reflectivity of the output mirror. Equation (60) shows that the linewidth can be reduced by changing the cavity length and the output mirror reflectivity. The linewidth is decreased by lengthening the cavity and increasing the output mirror reflectivity. From Eq. (58), it can be seen

that frequency fluctuations can arise from the fluctuations in the index of refraction n and the cavity length L. Both of the fluctuations are mostly due to environmental influences such as vibration and temperature.

Commercial diode lasers are fortunately suitable as a light source for laser cooling and trapping experiments. The cooling transition of most alkalis is accessible by the frequencies of the inexpensive diode lasers which also are tunable [54]. In addition, diode lasers for other elements beyond the alkalis have been produced as well to replace some of the state of the art, expensive lasers such as a dye laser or a Ti:S laser. However, free running diode lasers have linewidths on the order of tens of MHz and can be tuned continuously only within certain limited spectral regions [55]. Moreover, because of their short laser cavities, their frequencies are sensitive to changes in temperature and injection current, fluctuation on the current and the temperature create some fluctuation in the frequency output, which is unsuitable for laser cooling and trapping experiments. Most laser cooling experiments demand laser systems that are tunable around a resonance frequency of atoms and highly stabilized and capable of remaining "locked" at or near the atomic resonance for long periods of time. Various methods to reduce the necessary linewidth and stabilization of the frequency have been developed [55, 66, 67]. The most commonly used is an external cavity equipped with a diffraction grating and a piezo electric transducer (PZT) [55]. Using this scheme, one is able to tune the diode laser over a range up to ≈ 25 nm and narrow the linewidth down to less than 1 MHz. This diode laser system is known as an external cavity diode laser (ECDL). The next section will discuss the ECDL, laser stabilization, trap laser and repump laser. A MOT setup is also described.

III.2.1 External Cavity Diode Laser (ECDL)

An ECDL has three basic components, a commercial diode laser, a collimating lens and a diffraction grating. There are two typical configurations widely used for the external cavity, Littman-Metcalf configuration and Littrow configuration. In Littrow configuration, an external cavity is built using the back facet of the diode laser internal cavity and the grating surface as reflectors. The laser frequency is tuned by changing the angle of the grating. Typically, the angle adjustment is performed by sending 0–200 V voltage to a PZT which is mounted behind the grating. The first order laser light is sent back to the laser diode internal cavity and the zeroth order is used as the laser output. For the Littman-Metcalf configuration, an external mirror

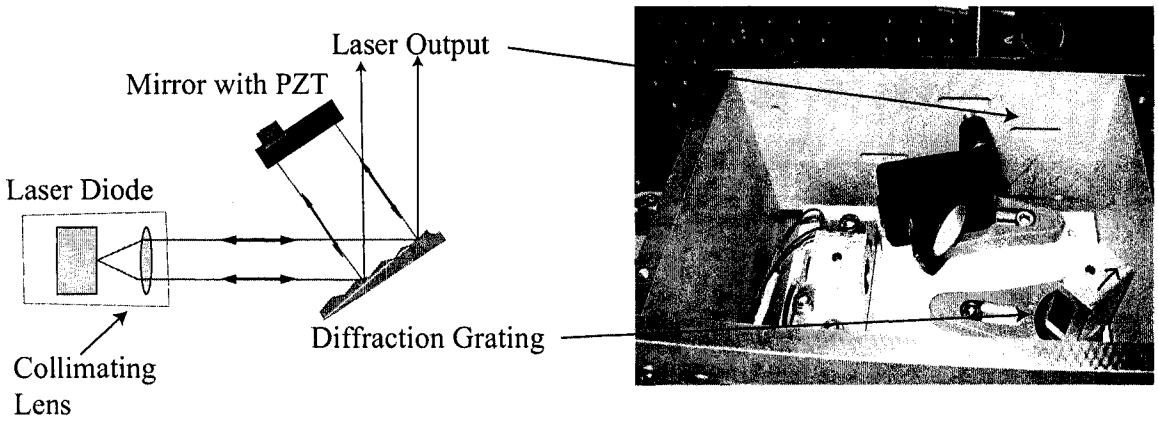

FIG. 16: The components of an ECDL in Littman–Metcalf configuration.

is added. The grating is no longer positioned in Littrow configuration and the PZT is attached to the horizontal adjustment screw of the mirror mount instead, as shown in Fig. 16. The laser frequency is tuned by adjusting the mirror angle.

The frequency fluctuations of the diode laser are due to the fluctuations in temperature of the diode and the external cavity, injection current for the diode, and mechanical fluctuations – minimizing them needs some effort and is time consuming. In our experiment, some steps have been taken to reduce the mechanical fluctuations which are mostly due to frequent vibrations in the building. The principal method for reducing vibrations is by floating the optical table, the second is to mount the laser system on a mechanically stable base plate. This base plate is mounted on three legs for height adjustment and the legs are mounted onto the optical table using rubber pads. The laser system is also enclosed by an aluminum box to reduce the air movement and sensitivity to frequent temperature changes in the lab. This box has outlets for laser beam output and for adjusting the cavity mirror. The temperature of the diode is stabilized using a Peltier cooler, sometimes it is referred to as a "thermoelectric cooler" (TEC). The laser diode and the collimating lens are enclosed within a collimating tube (Thorlabs LT230P-B), and mounted on a mounting block. This block is mounted on another aluminum block such that the TEC can be placed between the two blocks. Its temperature is monitored using a thermistor that is inserted into a small hole near the collimating tube. The TEC and the thermistor are connected to a feedback circuit of a homemade temperature controller. The diode

injection current is controlled by a homemade current controller.

III.2.2 Saturated Absorption Spectrometer (SAS) and Diode Laser Stabilization

In our experiment, the temperature and the injection current of the diode laser are set to a constant value by the temperature and the current controller, respectively, and generally then need only a small adjustment if the room temperature causes mode hopping[1] to the laser due to changes in the cavity length of the external cavity.[2] Usually, if the adjustment cannot solve the problem, tweaking of the cavity mirrors is needed. It is inconvenient to tune the laser frequently if one needs to do measurements for a long period of time, therefore long-term stabilization of the laser frequency is needed. The stabilization is usually achieved by using electronic feedback and locking the laser frequency to an external frequency reference. Here, the most suitable external reference for locking the laser frequency is a narrow peak in a rubidium saturated absorption spectrum (SAS).

The saturation absorption technique was developed by Schawlow and Hansch in 1970's as a practical way to use nonlinear interactions of laser light with atoms to produce spectra without Doppler broadening. This technique is known as Doppler-free Saturated Absorption Spectroscopy/spectrometer. The setup for the saturated absorption spectrometer is shown in Fig. 17.

In this setup, a small portion of the laser beam that will be used for an experiment is diverted to the SAS using a beam splitter (BS1) and split into two probe beams and one pump beam at BS2. The laser source is an external cavity diode laser whose frequency can be swept through atomic absorption lines by varying the voltage across a PZT which changes the laser cavity's resonant frequency. An optical isolator is often used to prevent unwanted reflected light from going back into the laser system. Both probe beams pass through a low density rubidium vapor cell which is used as a reference cell. The pump beam, which is much more intense than the probe beams enters the cell from the opposite side and is superimposed on one of the probe beams. The probe beam that is overlapped with the pump beam is called the

[1]Mode hopping is a phenomenon that occurs when the wavelength λ or the laser cavity length has changed such that an additional $\lambda/2$ of light can fit within the diode's laser cavity. $\Delta\lambda = \frac{2n_0 l_c}{m(m+1)}$. Here $\Delta\lambda$ is the size of the mode hop, m is integer, n_0 is the diode refraction index and l_c is the cavity length.

[2]No TEC is used to control the temperature in the external cavity.

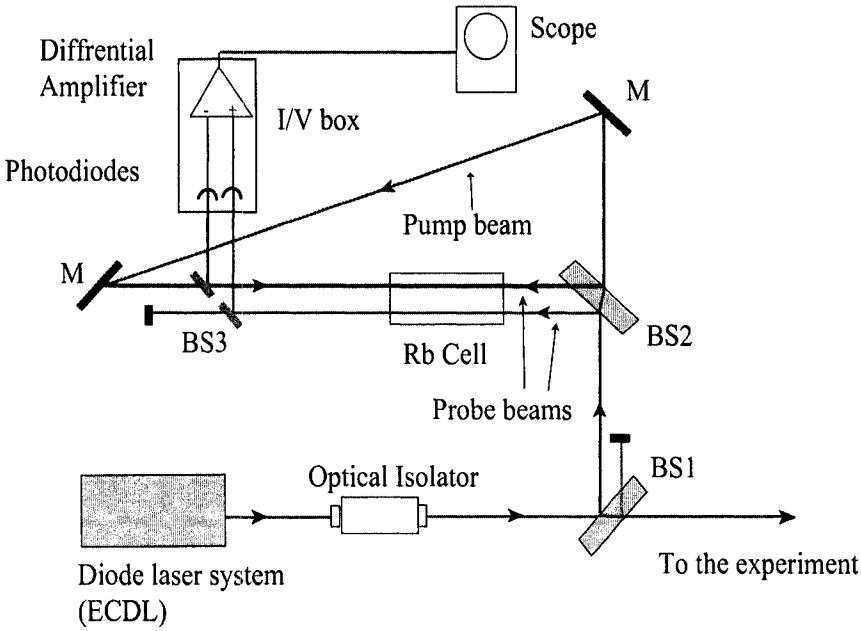

FIG. 17: The optical setup for Rb saturated absorption spectrometer. BS is beam splitter, M is mirror. I/V box is a current to voltage converter which is comprised of two photodiodes and a differential amplifier.

"saturated beam" and the other probe beam is called the "reference beam." Each of the probe beams is sent to a separate photodiode by two small beam splitters (BS3). The signals from the photodiodes are sent to a differential amplifier which outputs the amplified difference between the two signals.

The Doppler effect, discussed in Sec. II.2.1, plays a crucial role in this technique. It is known that in conventional laser spectroscopy, the closely spectral lines arising from atomic fine structure or hyperfine structure are often not resolved because of Doppler broadening (Doppler broadened absorption lines) [68]. The Doppler broadening arises because of the thermal (random) motion of atoms. When a laser beam propagates through an atomic vapor cell, thermal (random) motion which has a Maxwellian distribution of velocities will cause most of the atoms to absorb photons from the incident light at frequencies Doppler shifted away from the atoms's resonant frequency. For example, an atom moving with velocity v in the direction of propagation of the light will absorb photons with frequency $\omega = \omega_0(1+v/c)$, where ω_0 is the resonance frequency of the atom. If the laser frequency is tuned to ω_0, only those atoms that have no component of velocity along the line of the incident light will be

resonant with it. In another example, if the laser frequency is tuned to the Doppler shifted ω, the light will be resonant with just those atoms that have velocity along the laser beam such that $v/c = (\omega - \omega_0)/\omega_0$. $v > 0$ if the atoms move in the direction of the laser beam and $v < 0$ if atoms moves toward the laser beam. Therefore, if the laser frequency is varied,[3] the laser light will interact with a different part of the thermal distribution of the velocities of the atoms, resulting in an absorption profile which is a function of laser frequency ω. The intensity of the absorbed radiation as a function of frequency ω is given by

$$I(\omega) = I_0 \exp[-mc^2(\omega - \omega_0)^2/(2kT\omega_0^2)]. \tag{61}$$

Here I_0 is the intensity at $\omega = \omega_0$. The profile has the shape of a Gaussian (Doppler broadened absorption line shape) with full width at half maximum (FWHM) given by [68]

$$\Delta\omega_D = \sqrt{8k_B \ln 2}\,\frac{\omega_0}{c}\sqrt{\frac{T}{M}}, \tag{62}$$

where k_B is the Boltzmann constant, M is the mass of an atom, and T is the vapor temperature. This FWHM corresponds to the linewidth due to the Doppler broadening which is about 3.24 GHz for rubidium at room temperature.

The saturated absorption spectrometer, as shown in Fig. 17, eliminates Doppler broadening. When the saturated beam is blocked, the reference beam is absorbed by the atoms if the laser frequency equals the Doppler shifted frequency seen by the atoms and hence the absorption signal displays the usual Doppler broadened absorption profile. However, when the reference beam is unblocked, the saturated beam still displays the broad Doppler profile, but at certain laser frequencies additional narrow peaks are revealed. When both probe beams are sent to the differential amplifier (where they are subtracted), only the narrow peaks remain (Doppler-free absorption signal). The narrow peaks arise because of the interaction of the saturated beam and the pump beam with atoms in the vapor cell. If the laser frequency is different from the resonance frequency of the atoms, one of the beams interacts with one set of atoms with velocity v, the other beam interacts with the other set of atoms with velocity $-$v. However, when the laser frequency is tuned to the atomic resonance frequency, the pump beam and the probe beam will interact with the same set of atoms which are the atoms that have approximately zero velocity (at rest) along the axis of the beams. Under these circumstances, the stronger pump beam will excite

[3]The frequency is usually scanned using the piezo electric transducer PZT.

most of the atoms, leaving very few for the probe beam to interact with. So the saturated probe beam travels through the vapor cell without being absorbed in a very narrow range of frequencies corresponding to the linewidth of the atomic transition which for rubidium is about 6 MHz.

In a SAS experiment, there are four saturation absorption spectra which will be seen on the scope, two for each isotopes (^{85}Rb and ^{87}Rb) if one is able to scan the frequency of the laser for a certain frequency range. The two spectra for each isotope can be used to lock the trap laser and the hyperfine/repump laser. The spectrum for locking the trap laser can be seen in Fig. 18. The spectrum has main peaks as a result of transitions from F = 3 to F′ = 2, 3, 4 and crossover peaks F = 3 to F′= (2,3), (2,4), (3,4). These crossover peaks occur when two transitions share a common ground state, but different excited state. Crossover peaks are often more intense than the normal transitions. We lock the trap laser at a crossover peak (2,4) whose frequency ~ -92 MHz from F′=4. In order to detune the laser frequency $\Delta = -2\Gamma = 12$ MHz from the resonance frequency, the laser light going into the experiment is shifted +80 MHz by an acousto-optic modulator. As discussed earlier, the frequency of an ECDL can be stabilized by locking it to an external reference such as narrow peaks from a Doppler free - saturation absorption spectrum (SAS). "Locking" means tuning the laser cavity by either adjusting the piezoelectric transducer continuously or changing the injection current using a feedback circuit to the reference frequency. The former is most commonly used. The laser frequency can be locked either to the side (side locking) or to the peak (peak locking) of a narrow, saturated absorption line [55]. Side locking uses the fact that on the side of a narrow absorption line, the output $V(\omega)$ of the differential photodiodes has a steep slope as a function of the laser frequency ω, to lock the laser to a frequency ω_0 for which $dV(\omega)/d\omega|_{\omega_0} \neq 0$, a reference voltage $V(\omega_0)$ is subtracted from the output signal to produce an error signal $err(\omega) = V(\omega) - V(\omega_0)$. This error signal serves as the input to the feedback circuit which adjusts the laser frequency to produce $err(\omega) = 0$. This locking technique is sensitive to the fluctuations in beam intensity and laser alignment which can alter the lock point. Peak locking is chosen to avoid this fluctuation dependence. However, on the peak of the saturated absorption line, the derivative of the output voltage is zero. If the laser frequency is locked to frequency ω_0, a drift toward higher or lower frequency causes a decrease in the output voltage of the photodiodes and the error signal is no longer zero. A nonzero error signal alone is

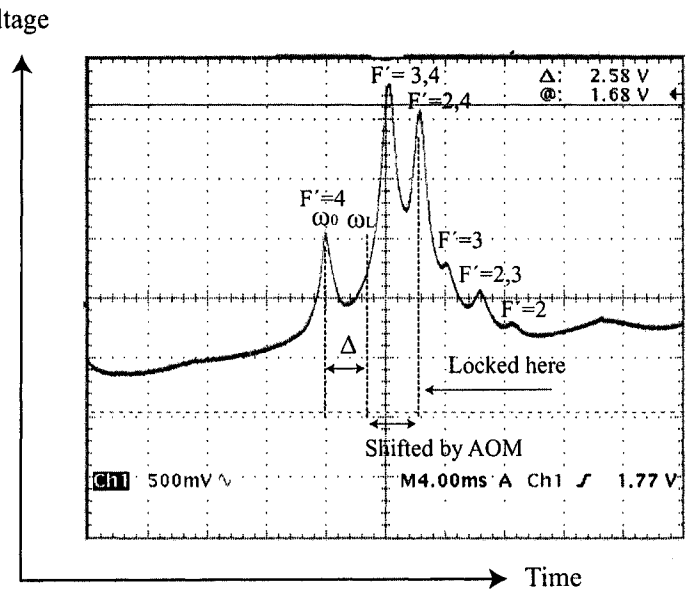

FIG. 18: The saturated absorption spectrum of ^{85}Rb for transitions from F = 3 to F′, there are 3 crossover peaks shown here. The trap laser is locked at crossover peak (2,4) and shifted to the desired frequency ω_L from resonance frequency ω_0 using an acousto-optic modulator, detuning is $\Delta = \omega_0 - \omega_L$.

insufficient to determine whether the laser frequency should be adjusted. The most common way to solve this problem is by using phase sensitive detection to provide an error signal which closely resembles the derivative of the saturation absorption line. This derivative shape is known as a dispersive-like error signal. A dispersive-like error signal can be obtained by modulating the laser frequency with an ac signal and then demodulating the signal from the saturated absorption spectrometer using a lock-in amplifier (dither-locking method). The effort to produce a dispersive-like error signal, especially without modulation, is of current interest in atomic physics, where a number of new techniques have recently been developed for this purpose [69, 70, 71].

In this experiment, we implement a dither-locking method using a lock-in amplifier. In this technique, the laser frequency is dithered slowly at a frequency Ω such that $\omega = \omega_0{}' + \Delta\omega\cos(\Omega t)$. Technically, an ac signal with frequency $\Omega/2\pi \sim 10$ kHz is fed from the reference connection of the lock-in amplifier into the current controller and hence the output voltage of the differential photodiodes results in $V(t) = V(\omega(t))$

$\simeq$ V[$\omega_0{}'$ + $\Delta\omega$cos(Ωt)]. Here $\omega_0{}'$ is the frequency of the laser when it is not dithered. This output voltage becomes the input signal of the lock-in amplifier. If $\Delta\omega \gg \Omega$, the voltage signal behaves as if the laser frequency were slowly oscillating back and forth and hence the true signal from the SAS is also modulated at this frequency. The lock-in amplifier will then produce an error signal which is the Fourier component of V(t) at frequency Ω. By assuming V(ω) as a Gaussian peak, the expansion of V(ω) for $\omega \sim \omega_0$ can be written as

$$V(\omega) \approx V(\omega_0) + A(\omega - \omega_0)^2. \tag{63}$$

The expansion of V(t) can be written as

$$V(t) = V[\omega_0' + \Delta\omega cos(\Omega t)] \simeq V(\omega_0') + \frac{dV}{dt}(\omega_0') \cdot \Delta\omega cos(\Omega t) + ..., \tag{64}$$

so the error signal is defined as

$$err(\omega) \sim \frac{dV}{d\omega}(\omega) \cdot \Delta\omega \sim 2A(\omega - \omega_0). \tag{65}$$

The error signal has the desired property that err(ω) = 0 and its derivative $\neq$ 0, hence it is suitable for a feedback circuit. However this method has some disadvantages. The dither method needs a sometimes expensive lock-in amplifier and has a limited recovery range. The schematic of the electronics for frequency locking used in this experiment is shown in Fig. 19.

III.2.3 Laser Beam Setup

Two external cavity diode lasers are used in this experiment, one for the MOT trap laser beams and one for the repump laser beams. One could use one laser with an added sideband to replace the need for the second laser [72]. We purposely use a second laser for the repump laser beams in order to be able to obtain fine intensity control during the FORT loading process. The MOT trap laser light is used to excite the atoms from the ground state F = 3 to excited state F$'$ = 4. The MOT trap laser is constructed using a master-slave configuration to provide high power laser beams. The trap laser setup is shown in Fig. 20. The master laser is an ECDL laser with most of its output beam sent to injection lock the otherwise free running slave laser. Both lasers are built using a diode laser Sanyo DL 7140-201S. The power output of the master laser after being split to the saturated absorption spectrometer (SAS) is $\sim$ 8 mW while the output power of the slave laser before going into a fiber

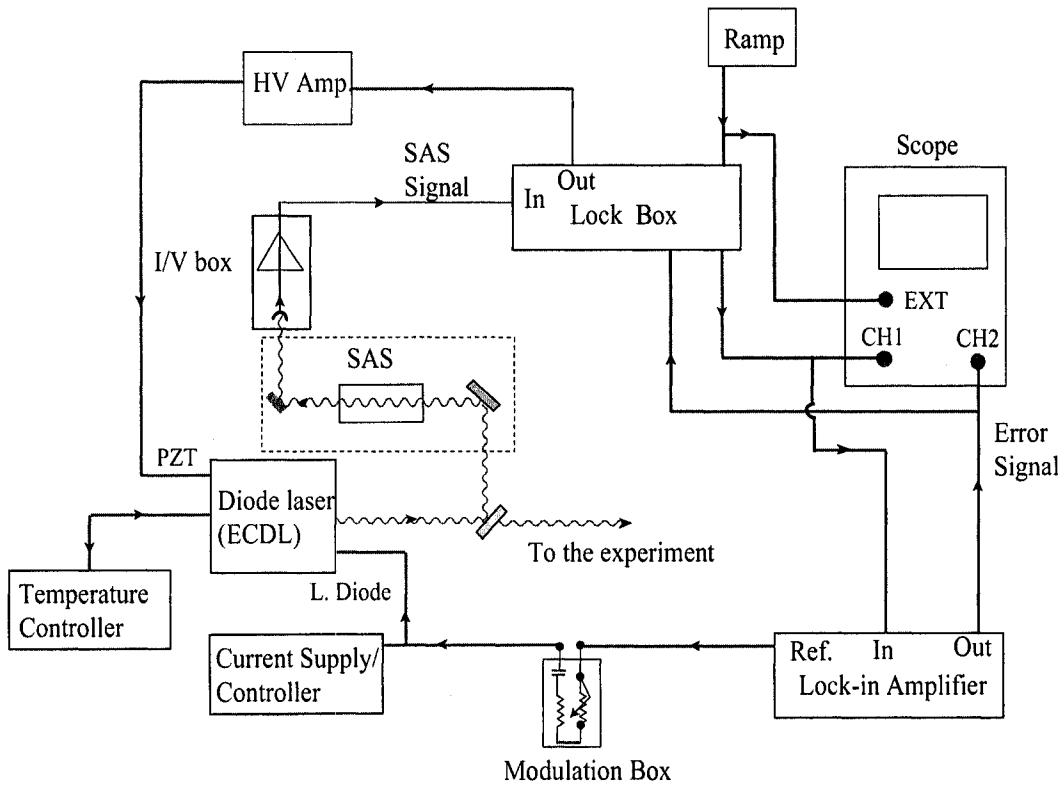

FIG. 19: Schematic of the electronics used to lock the laser frequency.

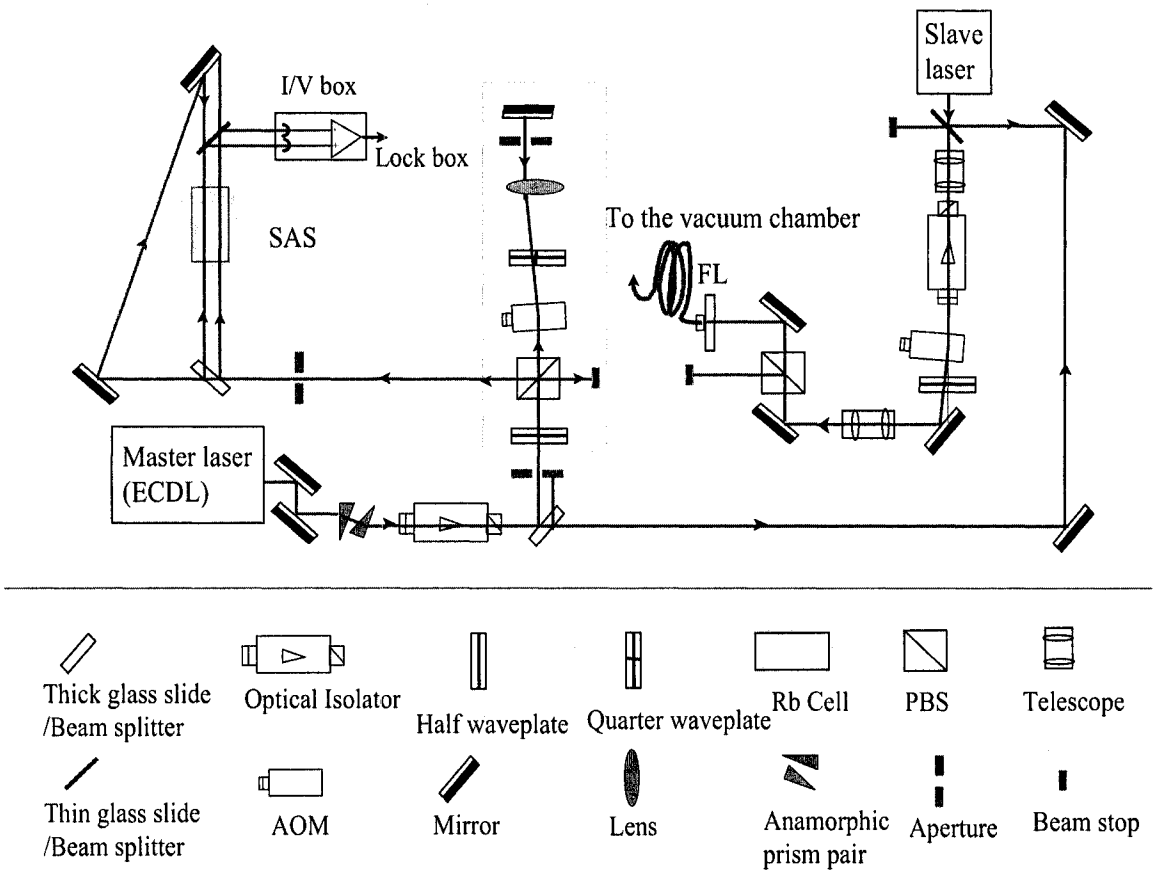

FIG. 20: The optical alignment of the master-slave laser system. Here FL = fiber launcher.

launcher (FL) is $\sim$ 17 mW. Coupling as much of the slave laser output as possible to a single mode fiber optic cable needs a certain effort. We use a telescope with magnification $1\times$ to collimate the beam going into the fiber cable launcher. This telescope is mounted on a translation stage for adjusting the collimation. We found that every time we switched the slave laser AOM on and off, the light polarization at the other end of the fiber optic cable (which is not a polarization maintaining fiber) changes. Using a half wave plate and a polarized beam splitter cube, we were able to overcome this problem. We used a polarization maintaining (PM) fiber once, but it gave less coupling than the current setup. The coupling setup we used results in about 8 mW trap laser light going into the vacuum chamber.

There are two ways to detune the frequency of the MOT trap laser, using a single pass or using a double pass AOM system. A double pass system is preferred if one

uses fiber optics to send the laser beam to the vacuum chamber since the detuning will cause a beam walk and uncouple the beam from the fiber optics in the case of a single pass system. However for the convenience of using a double pass system one will pay the price of losing up to half of the laser beam power because the beam passes the AOM twice before going to the fiber optics, and the AOM typically has 70–80% efficiency. A thorough explanation about a double pass system can be found in [73]. Since we have only 8 mW trap laser power from the slave laser output going into the vacuum chamber, we set the double pass system before a saturated absorption spectrometer (SAS) as seen in Fig. 20. We use a 30/70 beam splitter to split the laser beam from the master laser, 70% goes to the slave laser and 30% goes to the double pass system. This is slightly more power than one usually needs for an SAS system, but the double pass system has only about 50% efficiency. Since we use an AOM before the SAS absorption, another AOM has to be added at the slave laser beam. In order to have detuning $\Delta = -2\Gamma$, the AOM inside the double pass system is shifted -80MHz, the result will be shifting the master laser $+160$ MHz and the AOM in the slave laser setup is shifted -80 MHz in order to get a total shift $+80$ MHz then detuning is $\Delta = -2\Gamma$. The purposes of an AOM in the laser beam setup is twofold. The first is to shift the laser frequency to the desired one and the second is to switch the laser beam on and off. The circuitry to control the AOM by feeding a TTL signal from a LabVIEW program and the voltage controlled oscillator to produce a radio frequency (RF) signal is shown in Fig. 32. The discussion of the switching system for an AOM is presented in the next chapter.

The repump laser setup is shown in Fig. 21. The repump laser is also an ECDL laser and used to optically pump the atoms that fall to the ground states F = 2 as shown in the ^{85}Rb energy levels in Fig. 1. It is built using a Hitachi HL7851 diode laser. Since we do not need to have high intensity for repump laser output, the laser system does not need a master-slave configuration. The laser power output before entering the fiber launcher is $\sim$ 1.4 mW and, after the fiber optic cable is coupled, only 500 μW. This is more than adequate for the repump beam of the MOT. The frequency of the repump laser and MOT trap laser are locked using the dither locking method. According to [42], the maximum loading of ultracold atoms from a MOT to a FORT happens when the detuning of the repump laser is zero. We use a saturated absorption signal for the transition from F = 2 to F$'$ = 1, 2, 3 of ^{85}Rb and lock the repump laser frequency at the peak of the transition from F = 2 to F$'$ = 1 and use

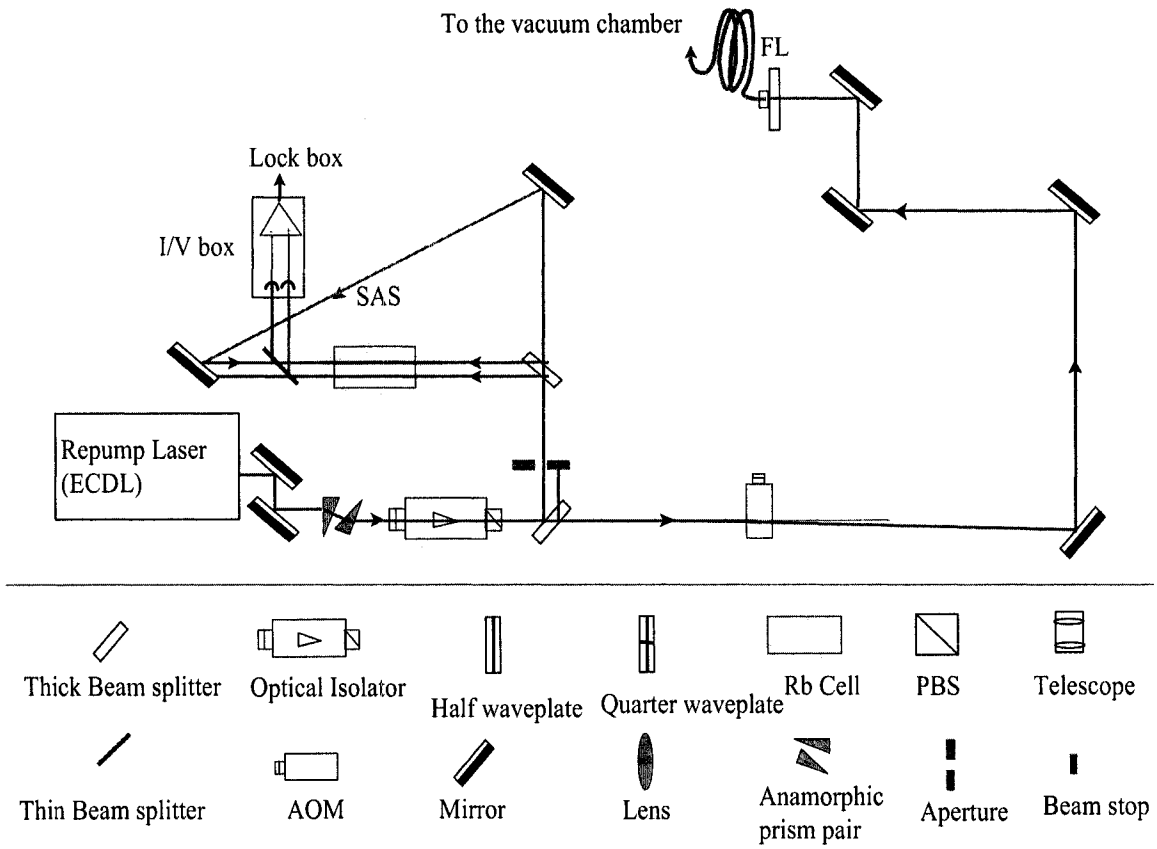

FIG. 21: The optical setup of the repump laser beam. Here FL = fiber launcher.

an AOM to shift it 92.7 MHz to F′ = 3. The AOM is also switched by a LabVIEW program to follow the loading time sequence as discussed in the next chapter. The intensity of the repump laser beam going to the vacuum chamber can be varied by adjusting the RF power going into the AOM, this is done using a voltage controlled attenuator as shown in Fig. 32. The variation of repump laser intensity is needed to investigate the intensity dependence of the FORT loading rate.

III.3 MOT SETUP AND PERFORMANCE

The MOT consists of three sets of counter-propogating trap laser beams (sometimes called the MOT primary laser beam) and two horizontal counter propagating repump laser beams. The trap beams come from a Master-Slave configuration diode laser setup as shown in Fig. 20 and the repump laser beam comes from a repump laser setup as shown in Fig. 21. The output of both lasers is coupled to a fiber optic cable for easy alignment to the vacuum chamber. The beam alignment for the MOT is shown in Fig. 22. The trap laser beam which comes out of the fiber optic cable is divergent, a collimator lens T2 (Olympus 41.7 mm) is used to collimate the beam. The beam is then expanded by a beam expander T3 (1.67×) to a $1/e^2$ beam radius entering the chamber of 0.55 mm. The beam is then split by a polarized beam splitter cube (PBS) such that 1/3 of the beam is reflected up for the upper beam of the trap laser beam to be sent to the vacuum chamber and the rest is transmitted. The transmitted beam is split further by an unpolarized beam splitter cube, the transmitted one and the reflected one, both are sent by mirrors to the chamber. There is a half wave plate (HWP) mounted before the beam expander to balance the intensity of the three beams that go to the chamber. Each beam that goes to the chamber is circularly polarized by a quarter wave plate (QWP) that is mounted before the chamber window. After entering the chamber the beams passing through the opposite window and are retro reflected. These retro reflected beam are also circularly polarized by a QWP. The repump laser beam is collimated and expanded by collimator T1 after it comes out from the fiber optic cable hence the beam radius is equal to the beam size of the trap laser beam. In order to be able to calculate the intensity of the repump laser beam, the beam alignment is somewhat critical. With given beam radius, the maximum intensity of the trap laser beam is 23.1 mW/cm^2 and the maximum intensity of the repump laser is 1 mW/cm^2. A pair of anti Helmholtz coils is mounted outside the chamber which give a magnetic field

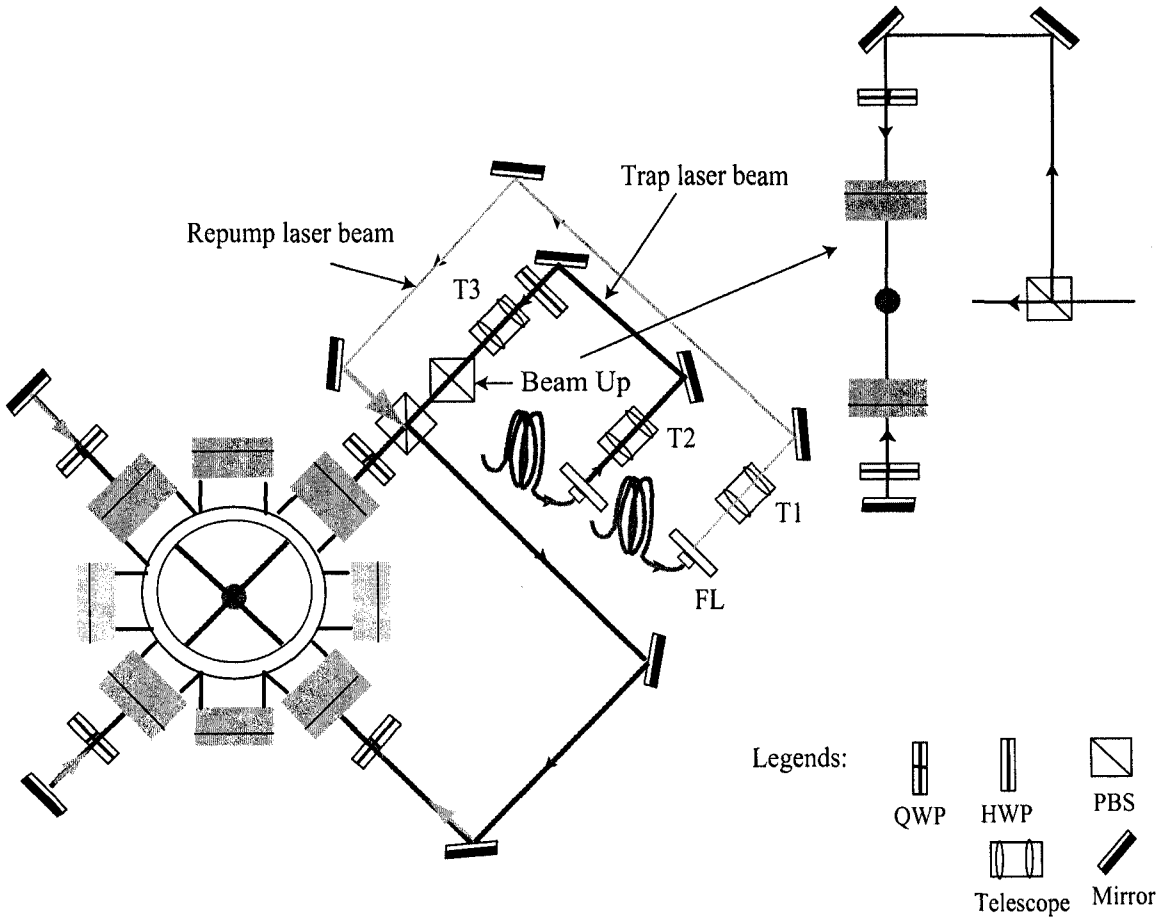

FIG. 22: The optical setup of MOT laser beams. Here FL is fiber launcher, T2 is a beam collimator, T1 and T3 are beam expanders. QWP is a quarter waveplate and HWP is a half wave plate.

gradient of about 10 G/cm used to trap Rb in the MOT. This magnetic field gradient can be varied by adjusting the current supply, it also can be turned on and off by a B-field switching circuit. We use a Hewlett Packard power supply and a homemade B-field switcher. The switching is controlled by the LabVIEW program as shown in Fig. 30.

To operate the MOT, first the Rb oven is turned on by turning on the current supply for the dispenser. The current is set above 3 A at first to fill the chamber with Rb atoms– especially if the MOT has not been turned on for more than a week. After one hour, the current can be lowered to avoid saturation. Then, the anti Helmholtz power supply is turned on and both trap laser and repump laser are locked to the lock points. If there is no fluorescence seen in the chamber, it usually means that the laser lock is not correct or the slave is not following the master in the case of the trap beams. For the latter a simple current adjustment usually solves the problem. A Rb MOT cloud should be seen at the center of the chamber.

At first, every time we turned the MOT on, we noticed that the Rb cloud was not at the center of the chamber. We found that this was due in part to stray magnetic fields around the vacuum chamber especially due to the ion pump magnet. This is a problem if we want to reproducibly overlap the MOT with the focused FORT laser beam. So we set five shim coils around the chamber. Each shim coil is independently controlled with a separate power supply. The position of the Rb cloud at the center of the chamber can be adjusted by varying the current for each shim coil. To approximately null any stray magnetic fields, the MOT image is observed on a TV monitor or using a photodiode detection connected to a digital oscilloscope while only the anti-Helmholtz magnetic field is quickly switched off. If the magnetic field is nulled, the atoms (now in an optical molasses only) should disperse slowly. In reality, because reflective losses on windows and other optics cause the MOT laser beams to have slightly different intensities, this technique is essentially balancing the *forces* felt by the atoms. Ideally, for efficient FORT loading both the forces will be balanced and the fields will be nulled at the center of the chamber. The MOT optimum performance is obtained at $\sim$3 A Rb dispenser current, and 4.5 A current of anti-Helmholtz coils. These settings give about 1.5×10^7 Rb atoms trapped.

III.4 ND:YAG LASER SYSTEM

The laser system used as the FORT laser in this experiment is a Spectra-Physics Model 3800 Nd:YAG Laser which can be operated in continuous (cw) and cw mode-locked mode, both at 1064 nm wavelength. Although not used in this experiment, the laser can also be Q-switched. The cw mode-locked mode can also operate at 532 nm wavelength using a frequency doubler. The average power for cw mode is 11 Watts while for mode-locked it is 10 Watts. The laser system consists of the Model 3800 laser head, the Model 3242 mode locker, Model 3275 acousto-optic stabilizer/Q-switch and the power supply [74].

Since this laser system is rated as a class IV-high power, safety and fire hazards become an important issue when one is operating the laser. The accidental exposure to both direct and the reflected beam must be avoided. The diffuse as well as the specular beam reflections can cause severe eye or skin damage. Also because the output of this laser is invisible (1064 nm), the proper goggles with the right wavelength rating should be used all the time during the laser operation and only limited and laser safety-trained personnel are allowed in the laser operation area.

There are four parts of the laser system that needed to be installed and tested before the whole system could be operated safely and with high performance. The first is the power supply which controls everything in the laser system; shutters, water cooling flow, current to the krypton lamp in the laser head, and electrical connections to the laser head. The second is the laser head which consist of the laser/optical cavity; Nd:YAG Rod with krypton arc lamp (lasing unit), high reflector, output coupler, pinhole, shutter and polarizer. The third is the mode locker system which consists of mode locker modulator, mode locker driver, and stabilizer. The last part is switching system which consist of an acousto-optic modulator (AOM) and Model 3275 acousto-optic stabilizer/Q-switch for driving and controlling the AOM frequency. Since the laser system had not been used for a long time and had been taken apart and moved several times before coming to our lab, the laser head, mode locker system and switching system needed to be installed and aligned.

The control center of the laser system is the power supply. It has a front and back control panel. The front panel displays a key switch, knobs, meter and indicators. A key switch in the front panel is used to turn the main power on and off and start the water pump. The indicators are the emission indicator, power supply on and off indicator, lamp start, low water resistivity, low water level, and the interlock

indicators which displays the water temperature, water flow, shutter closed or opened condition. Moreover, the panel also displays the meter indicating the lamp current. The rear panel contains circuit breakers, maximum/minimum water indicator, water hose connections to the city water and to the laser head.

Before turning on the power supply, there are some steps that have to be done. First, one must make sure that all the electrical connections are secured in place. The power supply is operated at 220 Volt voltage rating; a special cable plug with proper grounding is needed. Second, the water cooling hoses have to be installed and inspected carefully for leaks. The cooling system has two loops; a primary loop which circulates deionized water from a water reservoir inside the power supply panel in and out to the lasing unit in the laser head and the secondary loop which circulates the city water (external water) through heat exchanger where it absorbs heat from the deionized cooling water in the primary loop. The external water flow rate must be at least 2.0 US gal/min with a differential pressure between 20 to 60 psig. The deionized water must be about 7 US gal with resistivity at least 100 k Ω/cm in the water reservoir. When the power supply is turned on, checking for water leaks on the laser head must be done. The indicators on the front panel and on the laser heads will alert the user if something still is wrong in the power supply system when the power supply is turned on. Should a warning light appear, one should refer to laser manual for complete instructions and troubleshooting. The proper sequence of steps in turning on and off the power supply including when one should turn on/off the city water has been made and printed and placed near the power supply panel for reference. Following these steps is very important to avoid any damage to the krypton arc lamp and to prolong its lifetime. The power supply front and rear panels are shown in Fig. 23.

After the power supply is working properly, the next step is to align the laser head components; lasing unit, high reflector, output coupler, shutter, polarizer and aperture. The lasing unit is where the Nd:YAG rod and krypton arc lamp are located. No alignment is needed inside the unit. Some laser system accessories such as alignment targets, a set of threaded apertures, infrared detector card or an infrared viewer, a set of four foot clamps and He-Ne laser are needed for the alignment. Figure 24 shows the components of the laser head.

The first step for alignment of the laser head components is to make sure the height of the laser head surface is the same everywhere, it is done by adjusting the

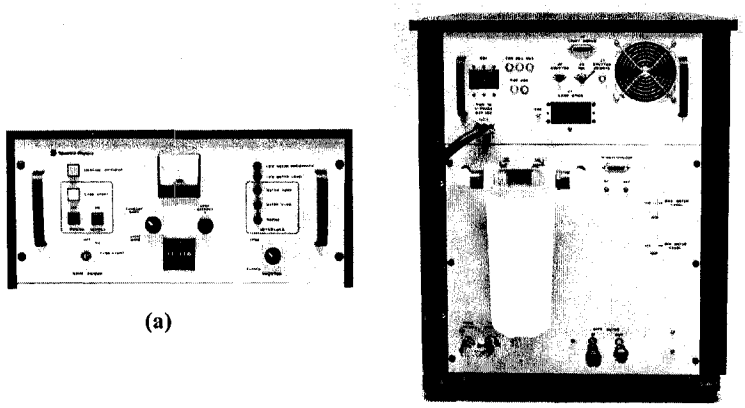

FIG. 23: The power supply panels of Spectra Physics Nd:YAG laser system Model 3800.

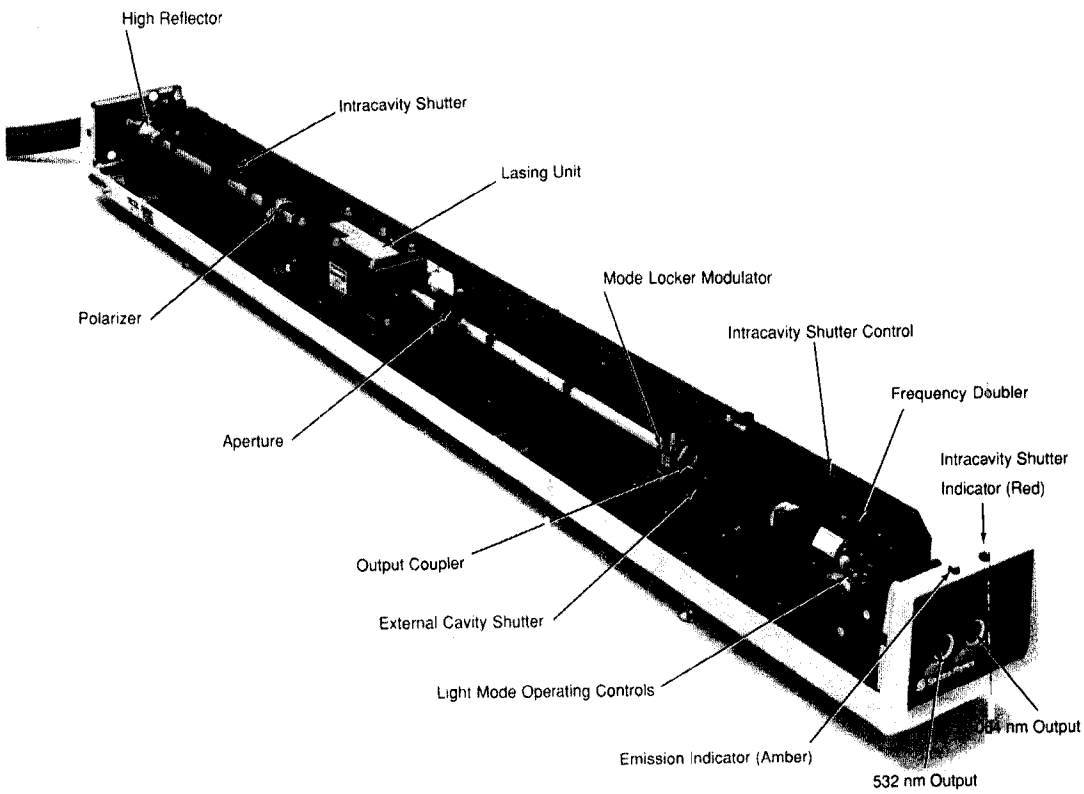

FIG. 24: Parts of the Spectra Physics Nd:YAG Laser Head Model 3800.

four foot clamps. Next, the He-Ne laser beam is centered and aligned using two mirrors at the output aperture of the laser head through output coupler holder, through the polarizer and through the center of the high reflector mirror plate. For guidance, a threaded alignment target is installed at the output coupler holder. After that, the lasing unit is placed at its position and adjusted with its laser rod centered on the He-Ne beam. Next, the high reflector holder is loosely placed in position by adjusting the high reflector mirror plate, centered on the He-Ne beam. Then the high reflector mirror with cavity length adjustment is put in its holder, and adjustment is made to the mirror plate to retro reflect the He-Ne beam to the output coupler. When this is done, the output coupler can be installed and adjusted to retro reflect the He-Ne beam to the He-Ne laser output. Finally, the intracavity shutter and aperture can be placed in their positions. The He-Ne laser can now be turned off and removed from the output, and a power meter is placed at the output of the laser head.

After the alignment is done, the power supply can be turned on. A 10-30 minute warm up is required while the lamp current is 25 A. Then, the intracavity shutter can be opened. Any time the intracavity shutter is opened, eye protection must be worn. With the shutter open, fluorescence spots can be seen at the aperture using an Infra Red (IR) Viewer. By adjusting the output coupler mirror, the spots are centered to the laser rod in the lasing unit until a flash of laser light can be seen. After that, maximum power can be reached by adjusting the aperture, the high reflector mirror, the polarizer, the lamp current, and the output coupler. After the maximum power is reached, the aperture can be replaced with one of smaller size to get a laser beam with a good Gaussian mode, and the mirrors need to be adjusted again to get maximum power. However, the original maximum output power will be reduced if a smaller aperture is used. The power of the laser is about 2.5 Watts at 25 A Krypton Lamp current and with a pinhole with size 1.1 mm while at the 29 A current setting and with the same pinhole size, the output power is about 10.6 Watts. The pinhole size 1.1 mm was used for the entire experiment because it gave a nice gaussian mode while still giving good output power. The laser can provide a power of more than 10 Watts but the current will be right at the edge of the full scale of the power supply's Ammeter which is 29.5 – 30.0 A and is likely to overload the krypton lamp. The output power maximum at the same current can change over day to day operation. In order to get to the same power, after turning on the power supply and the lamp for

about 30 minutes to warm up, the high reflector mirror and pinhole can be tweaked at until maximum power is once again reached.

After the laser head has been successfully operated in cw mode, the mode locker modulator can be installed inside the laser cavity just before the output coupler. The mode locker modulator, a standing wave acousto-optic modulator (AOM) is an antireflection coated, high Q device. It only requires a low-level RF driver signal. It has its own translation stage where the Bragg angle, horizontal, and vertical position can be adjusted. The mode locker modulator is centered on the beam path using the vertical and angle controls. Using an infrared viewer, two spots can be seen on the aperture; a bright spot and dimmer spot. The dimmer spot is the retro-reflection from the output coupler and needs to be overlapped with the bright spot by adjusting the output coupler. When these spots are overlapped, lasing will occur. Both output coupler and high reflector mirrors then can be adjusted to get maximum output power. The laser head is also equipped with a small beam splitter and a photo detector module which splits a small amount of the laser output and sends it to the amplified photodiode. The output signal can be monitored using an oscilloscope. This monitoring is very important when the laser is operated in mode-locked mode in order to know whether the laser is being mode-locked properly. The photodiode can measure the repetition rate of the pulse train, but does not have sufficient bandwidth to accurately measure the pulse width.

The mode locker modulator is driven by a RF signal from a mode locker driver which is connected by an RF cable, and temperature-stabilized with the mode locker stabilizer which is connected by a heater cable. The mode locker is operated at a frequency of 41 MHz with an insertion loss less than 10%. After the stabilizer and the driver are turned on, it takes at least 20 minutes to warm up and for the oven light to turn off, indicating the temperature has been stabilized. Mode-locked operation can be initiated by turning on the RF power, adjusting the frequency and lock of the frequency driver. The combination of adjusting the frequency and cavity length is needed until the pulse train can be seen on the oscilloscope monitor which occurs when the RF frequency is matched the cavity length of the laser.

After the laser is mode-locked, both mirrors still need to be tweaked to get maximum power. Figure 25 shows the pulse train in mode-locked operation. The repetition rate of the pulse train as measured by the provided photodiode (slow photodiode) is 82 MHz and the locked synthesizer RF frequency is between 40.9725 MHz - 40.9840

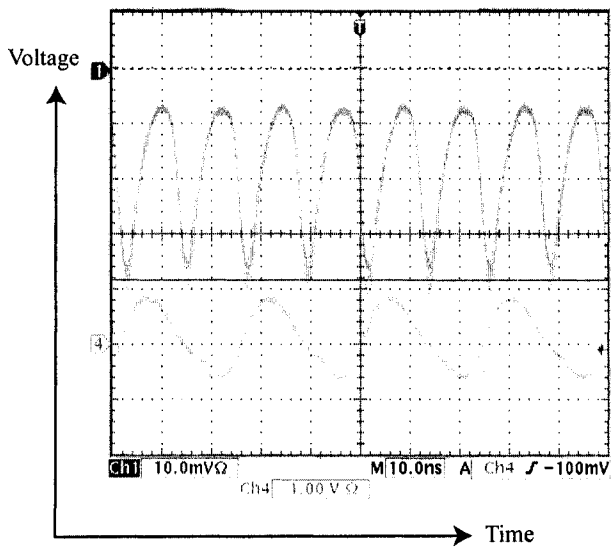

FIG. 25: The output of the mode-locked Nd:YAG laser detected using a slow photodiode. The top signal is the mode-locked signal and the bottom signal is the RF signal from Spectra Physics Model 3275 Mode locker driver. This signal is obtained at a Nd:YAG lamp current of 27 A.

MHz. At the same lamp current as the cw mode laser, the maximum average power for mode-locked operation is much less than the maximum power when the laser is operated in cw mode. At 25 A lamp current, only 2 Watts average power can be reached, while at 29 A, the average output power is only 7 Watts. The output powers for cw mode and mode-locked operation are measured after the beam expander, before the beam enters the chamber. The actual power which determines the intensity at the center of the chamber is the measured power minus $\sim 8\%$ due to the uncoated window of the chamber. A Molectron PowerMAX 500D power meter is used to measure the laser power for cw mode operation, while for mode-locked operation, a Molectron PowerMAX 500A power meter is used.

The laser system can be operated in cw and mode-locked configurations without uninstalling the mode locker modulator. To return to cw mode, the mode locker driver and stabilizer have to be turned off. There is no significant change in alignment observed for cw operation with the presence of the mode locker modulator in the cavity. One thing that is very important is to maintain the cleanness of the optical components by using a purge system. The laser head is equipped with purge tubing

along the optical cavity. After the laser cavity alignment is complete, the purge tube can be installed. At first, nitrogen was used for the purge system, it was found out that it is not an efficient way to do it because the nitrogen supply runs out quickly. At last, a commercial, simple purge system is used which has a small-Aqua Nature aquarium pump equipped with a filter to clean the air and desiccator cartridge to remove any moisture.

In the loading process of ultracold atoms from the MOT to the cw or pulsed FORT, the Nd:YAG beam needs to be on or off at certain times. Therefore, a switching system is needed to turn on and off the Nd:YAG laser at the FORT location. This can be done using an AOM as an optical switch. The Nd:YAG laser system is equipped with a Model 3275 acousto-optic stabilizer/Q-switch for driving and controlling the AOM frequency. The Model 3275 has two functions; as a stabilizer in conjunction with the model 3695 pulse compressor to reduce noise from dc to 20 kHz and to provide long term stability for frequency doubled output, as Q-switch to provide low insertion loss and high Q-switched power. The model consists of a beam splitter/photodetector module which is used also for monitoring the mode-locked signal, an AOM, a driver module, and a remote control module. In this experiment, the driver is used to drive the AOM to diffract the Nd:YAG output to the first order and hence can be switched on and off from the zero order. The RF driver has maximum power of 10 Watts and RF carrier frequency of 27 MHz. Unfortunately, this AOM can only give 30% of the laser output to the first order. As a replacement, an Intra-Action Model AOM-272AH AOM is used for the switching system. This AOM is also operated at 27 MHz. Instead of using a new driver, the RF driver module model 3275 was modified such that the trigger of the RF signal is made external instead of internally triggered while the characteristics of the new AOM still match the original AOM. The trigger signal comes from the digital output of a LabVIEW program that will be explained in the next chapter. Using 4.5 Watts RF power, 80% laser output power is transferred to the first order. The separation between orders is big enough to block the zero order and others. So, using this AOM, the maximum power of the first order beam in cw mode is 8.7 Watts while running at 29 A lamp current, while for mode-locked operation, the maximum power reached is 7 Watts at the same lamp current.

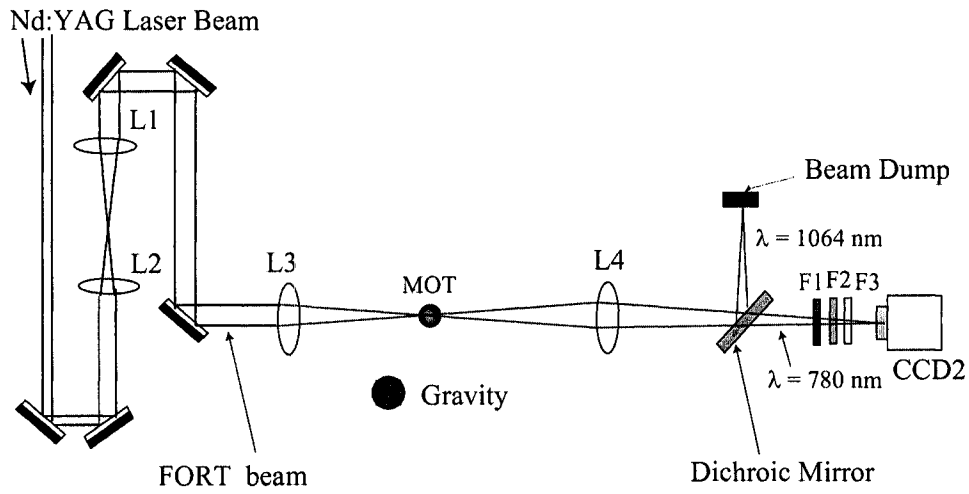

FIG. 26: The experiment setup for sending the FORT beam to the vacuum chamber.

III.4.1 FORT Laser Beam Setup

After the Nd:YAG laser system can be operated in cw and mode-locked mode, the beam is ready to be sent to the vacuum chamber. First, since the height of the output beam from the laser head is lower than the center of the chamber by about 4 cm, a periscope is used to increase the beam height. The upper mirror of the periscope needs to be rotated 90^o to keep the beam on the optical table since the Nd:YAG laser head length covers almost the entire length of the optical table. The output beam then propagates right at the edge of the table. One should be careful about the zero order beam since it has about 20% of the original beam power. A beam stop with suitable heat sink is used to stop the zero order beam before the beam enters a beam expander while the other orders (with much less power) are simply covered by a white card. The beam size coming out of the laser is about 1 mm, a beam expander which consists of 100 mm and 200 mm lenses is used to increase the size of the beam to a $\frac{1}{e^2}$ intensity radius 4.2 mm and collimate it before going into the chamber.

Figure 26 shows the optical setup of the Nd:YAG laser beam going into the chamber. An anti-reflected coated achromat lens (Thorlabs LAC506-B) with focal length 200 mm mounted in an XYZ stage is used to focus the beam to the center of the chamber. The waist of the beam at the center of the chamber is calculated to be 16 μm, the real waist size is certainly bigger due to the imperfect spatial mode of the

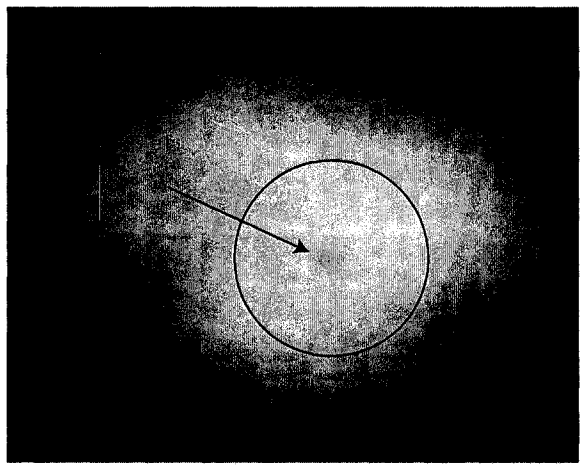

FIG. 27: The dark spot at the center of the MOT cloud.

Nd:YAG laser beam and the imperfection in the lens. The outgoing beam from the center of the chamber is divergent. A 100 mm lens is used to collect the beam and images of the MOT cloud and a dark spot to the CCD2 camera. Since the Nd:YAG laser beam used is 1064 nm in wavelength, all the mirrors and lenses used are for that wavelength. A dichroic mirror (CVI Model SWP RS1064/TU780) which passes the 780 nm beam to the CCD2 camera and reflects the 1064 nm Nd:YAG beam to the beam dump is a centerpiece in this optical alignment. The dichroic makes it possible to dump the remaining – still powerful Nd:YAG laser without damaging the CCD2 camera while allowing us to look down the bore of the Nd:YAG beam in order to observe the MOT cloud image with a dark spot in it from the Nd:YAG beam. The dark spot arises because the ultracold atoms at the focus of the Nd:YAG beam are AC stark shifted out of resonance with the MOT light. Figure 27 shows the image of the MOT cloud overlapped with the dark spot.

This scheme also makes it possible to align the focus of the Nd:YAG beam to the center of the chamber or to the center of the MOT cloud. The position of the Nd:YAG waist from the center of the MOT cloud affects the number of atoms that can be loaded to the potential well created by the FORT laser. This effect has been investigated by Corwin *et al.* [42] thoroughly and was not studied here. By assuming the MOT is at the center of the chamber which is inspected using CCD camera 1 and 2, the position of the focus along the Nd:YAG beam is adjusted by the XYZ stage of the achromat 200 mm lens. In this alignment, three filters are used; a neutral density

filter (Newport 0.3) to reduce the brightness of the MOT cloud image so the dark spot can be seen clearly without saturating the camera, an interference filter (Thorlabs FB780-10), and a colored glass filter (Thorlabs FGL850SP). The interference filter and colored glass are used to block any stray 1064 nm light passed by the dichroic mirror and reflected from other surfaces in the chamber.

CHAPTER IV

MEASUREMENT AND DATA ACQUISITION CONTROL

When all the experimental operating conditions are correctly set, (a stable MOT cloud seen at the center of the chamber, the FORT laser waist has been aligned to the center of the MOT cloud, both trap and repump lasers of the MOT beams have been locked to the correct locking points...) a control and data acquisition (DAQ) system is needed to run the experiment automatically by controlling the timing of lasers and magnetic fields and measuring the MOT level and FORT level with millisecond accuracy. This chapter describes the detection method and the DAQ control system used.

IV.1 MOT AND FORT DETECTION

There are two standard methods used to measure the number of atoms in a MOT or FORT; fluorescence measurement and absorption imaging. The most common one is the fluorescence measurement which is sometimes called a passive method. Fluorescence is the photon being emitted by an excited atom and it can be detected by a photodiode or a photomultiplier tube (PMT) and converted to a voltage. By knowing the laser parameters, as well as the geometry and efficiency of the detector, the total number of scatterers (atoms) can be deduced. The imaging absorption method is used if one needs the detailed characteristics of the MOT or FORT cloud in addition to the number of atoms such as the shape or the density of the MOT cloud and it is performed using a resonant laser beam sent through the center of the chamber overlapped with the MOT being measured and viewed with a CCD camera (with a frame grabber device) to record the beam absorption. In this method, the size of the beam is made larger than the size of the MOT cloud while the beam intensity is set much lower than the saturation intensity of the ^{85}Rb transition. When the beam passes through the MOT cloud, the trapped atoms absorb the light and the beam loses its intensity. By comparing the beam intensity before and after absorption, the optical density of the trap can be measured. It is typically found that measurements using both of these methods agree to within a factor of two. In this experiment, the fluorescence measurement is used.

Figure 28 shows the optical and electronic setup to convert the fluorescence signal

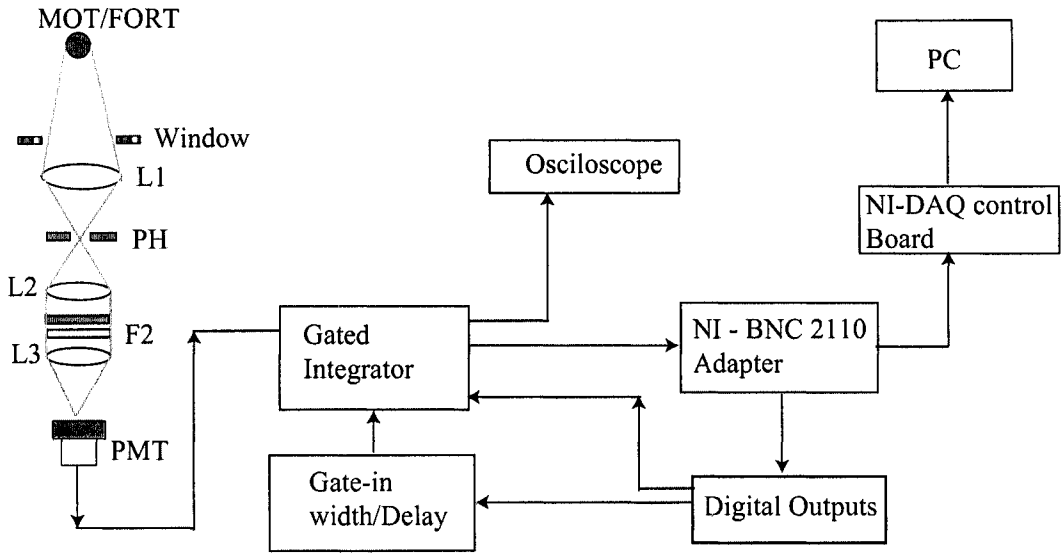

FIG. 28: Optical setup and electronics used to convert the fluorescence of the MOT and FORT cloud to voltage and to measure them with the DAQ system. L1 = 44 mm, L2 = 38.01 mm (KPX079 Newport), and L3 = 60 mm (LA1134 Thorlabs) are lenses. F1 = interference filter (MG03F1L056), F2 = short pass filter (FES0850 Thorlabs). PMT = photomultiplier tube (Hamamatsu R928), PH = pinhole.

to voltage and integrate it before sending it to the data acquisition (DAQ) system. The fluorescence of the MOT passes through one of the (uncoated) vacuum viewports and is collected by a 2 inch combination lens with an effective focal length of 44.5 mm. The lens holder and other optics holders are arranged on a rail to aide with alignment. An iris with adjustable xy position is placed at the focused MOT image. Before positioning the iris, the position of the focused MOT image is found using a CCD camera with a good adjustable lens, a TV monitor, and a white card. The camera is set to see the image on the card which is walked along the rail (other optics have not been installed yet). The focused and unfocused images can be seen on a TV monitor while walking the card. The position where the image is focused is marked and a pinhole is set there. This pinhole is used to block the unwanted scattering from outside and inside the camber surfaces. Next, a pair of lenses is used to collimate the image so that two filters can be installed before the image hits the PMT surface. It is a good idea to check the final image after collimation by the same technique explained above to position it on the center of the PMT surface. Care must be taken when it comes to installing the PMT. One needs to work in a dark room

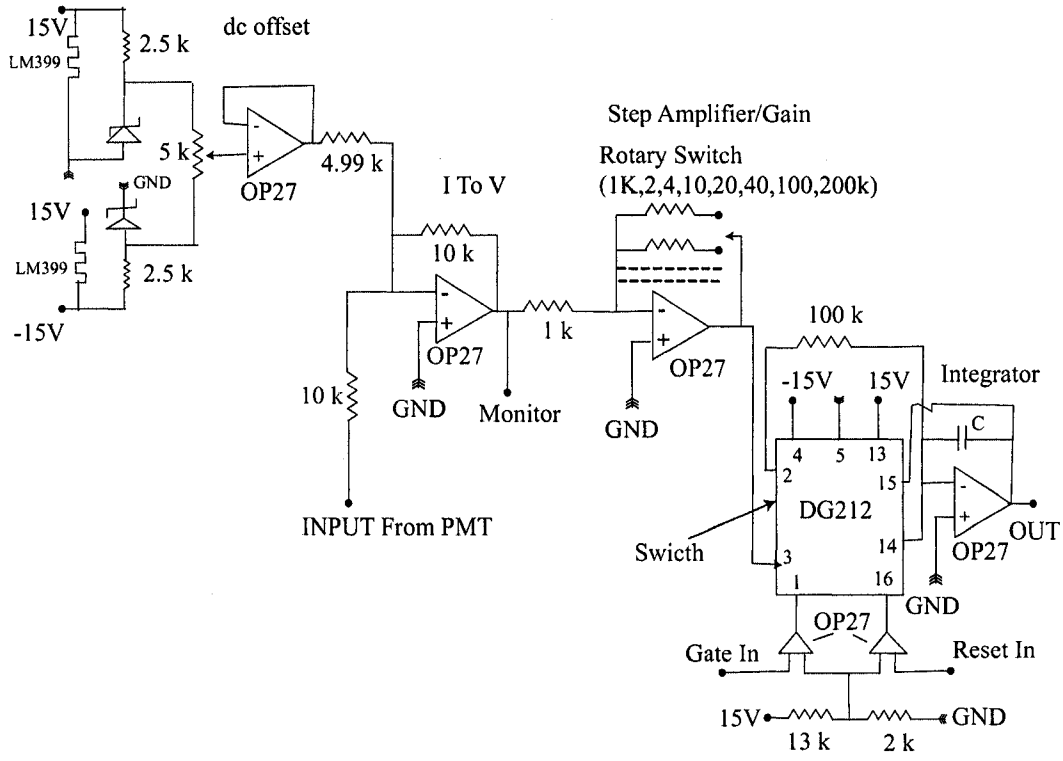

FIG. 29: Schematic diagram of a Gated integrator box.

when installing the PMT to avoid overloading its surface threshold and damaging it. All the optics used in this setup are enclosed with optical tubing to reduce the room and scattered light entering the PMT box which adds unwanted background to the measurement.

The current from the PMT output is sent to an integrator box as seen in Fig. 29. The integrator box consists of the I to V converter, step adjustable amplifier, an IC switch which allows control from the DAQ system, and an integrator. This box also contains a dc offset which allows one to null the background signal. The signal output before the switch and integrator is monitored by a multichannel digital oscilloscope. The box is fed with a Gate-in signal and Reset signal via the switch IC DG212 in the box. The Gate-in signal comes from a Gate-in circuit where the Gate width and delay can be adjusted. The TTL signals for Reset-in and for the Gate-in circuit input are supplied from the DAQ digital outputs which will be explained in the next section. The integrated output is then sent to the DAQ system.

The setup above is used to monitor and measure the MOT voltage and the FORT

voltage and compare them to determine how many atoms are loaded from the MOT to the FORT. The number of atoms is then determined by dividing the FORT level by MOT level and multiplying by the number of atoms in the MOT. The number of atoms in the MOT is measured in a separate setup using another viewport of the vacuum chamber. The MOT level is maintained to be stable during the measurement. A detailed explanation of the determination of the number of atoms in the MOT is given in Appendix A. We find the number of atoms in the MOT to be 1.5×10^7 atoms with a factor of two uncertainty.

IV.2 EXPERIMENT CONTROL

Timing control is very important in the FORT loading process. The entire MOT to FORT transfer process takes only several hundred milliseconds. Using the timing control system, one is able to run the experiment by switching the lasers in microseconds, and the magnetic field in a few hundred microseconds. Before using a personal computer (PC) and a LabVIEW program to control and acquire data, a simple timing box was designed and controlled by a programmed pulsed generator which has many signal outputs to provide the loading sequence pulses. A Stanford Research boxcar was also used to integrate the fluorescence signal from the PMT and send the result to a digital oscilloscope. However, as the experiment progressed, it was found that this system did not have the flexibility or scalability required to optimize the FORT loading, where the detuning of the MOT trap laser beam and reduction the repump laser intensity become a critical point to get higher loading, for example, requiring additional digital control ports. So a timing control system using a personal computer (PC), National Instrument data acquisition (DAQ) cards and breakout boxes, and a program using LabVIEW 6 to run the sequences of loading was implemented. The program controls the trap beam, repump beam, and FORT laser beam and the magnetic anti-Helmholtz current via switching circuits. It also control the intensity of the repump beam by connecting the analog output of the DAQ devices to the voltage-controlled attenuator in the switching circuit. The detuning of trap beam frequency also can be controlled by varying the output voltage of the voltage controlled oscillator (VCO) in the detuning system.

In general, a PC-based DAQ system consists of a PC, transducers, signal conditioning circuits, DAQ hardware, and software [76]. Figure 30 shows the schematics for the data acquisition and measurement control system. The transducer in this

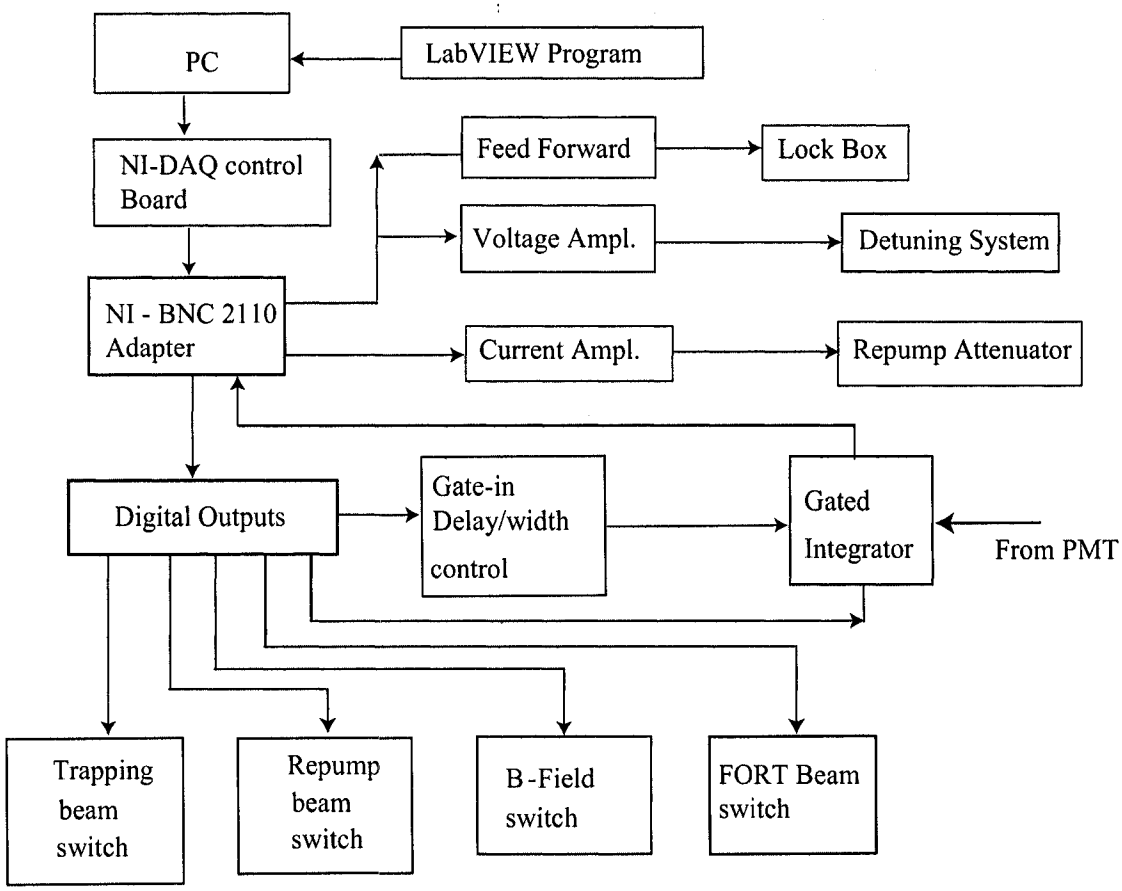

FIG. 30: Block diagram of data acquisition control.

system is a photomultiplier tube (PMT) which converts the photons from the MOT cloud to electrons while the conditioning circuit is represented by the Gated integrator and Gate-in delay and Gate-in width circuit. The Gate-in circuit supplies a Gate signal to the Gated integrator during the detection time. The PC used is a Gateway E-3200 Pentium III which has a 500 MHz clock speed, 6.0 GB Hard Drive, 128 MB RAM, and 3 PCI slots. The DAQ devices used are National Instruments (NI-DAQ) which consists of a PCI E Series plug and play board with measurement and automation explorer (MAX). This board is connected to a NI BNC-2110 adapter. The adapter has 3 types of connections from the PC to the experiment setup; analog inputs, analog outputs, and digital/timing I/O. Only one of the analog inputs was used in this experiment control which measures the signal from the Gated integrator box output. Because each BNC adapter only has two analog outputs, two PCI boards and two BNC adapters have to be used to accommodate the need to control the detuning of the trap laser frequency, attenuation of the repump laser intensity, and the attenuation of the trap laser intensity. The second PCI Board and BNC adapter used for the trap laser intensity is not shown in Fig. 30. The digital outputs on the BNC 2110 adapter are given extension BNC cable connectors for easy connection. There are 8 digital outputs used and coded from 0 to 7. Channels 0 and 1 of the digital outputs are used to control the switching for the trap laser and repump laser, respectively. Channel 2 is used for magnetic field switching, while channels 3, 4, 6 and 7 which have the same timing are used for Reset-in, Gate-in and triggering the digital oscilloscope and other electronics used. Channel 5 is used for FORT laser beam switching. Each of these digital outputs supplies a TTL signal pattern to each switch.

The TTL signal patterns that follow the time sequence as shown later in Fig. 33 are supplied by a LabVIEW program which we wrote using LabVIEW 6.0 codes from National Instruments . LabVIEW is a graphical programming language which is capable of connecting a computer to the hardware that is used to control data acquisition. Since we wrote the program, the codes have been upgraded by National Instruments to LabVIEW 9.0 codes. A LabVIEW program is comprised of two parts; a front panel and a block diagram. The block diagram contains of command icons as a replacement of command lines in other program languages such as FORTRAN and C. The front panel has controls and indicators that have a direct connection to the experiment hardware via a PCI card. Figure 31 shows a typical front panel of

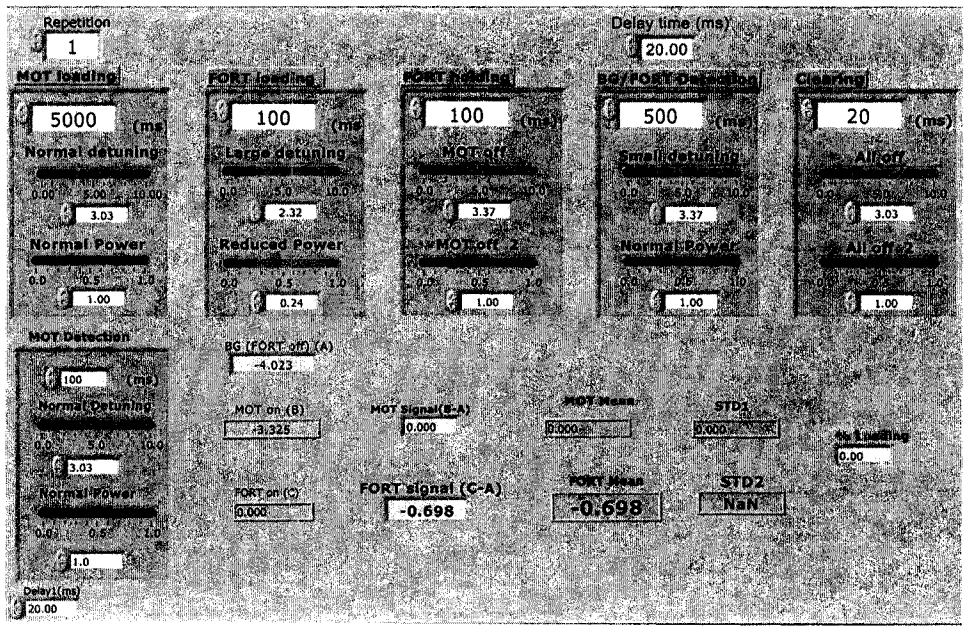

FIG. 31: A front panel of LabVIEW codes we have written to control data acquisition in this experiment.

our program.

Figure 32 shows the typical switching system for the trap laser beam, the repump laser beam, and for the detuning system where connections to the BNC 2110 connector or DAQ board are shown. The homemade voltage divider supplies a variable voltage to the voltage controlled oscillator (VCO) (Mini-Circuits Model ZOS-100) to vary the RF frequency for the acousto-optic modulator (AOM). Most of the switching components here are products of Mini-Circuits except the AOM and the homemade 35 dB RF power amplifier. The key component to reduce the intensity of the repump laser light and trap laser light is a voltage controlled attenuator (Mini-Circuits Model ZX73-2500, the voltage for this attenuator is supplied by the DAQ board. This attenuation system uses a 24dB RF power amplifier (Mini-Circuits ZHL3A-S). As explained in Chapter III, there are two AOMs used for the Master-Slave configuration Trap Laser system. The first AOM is used in the detuning system operated in double pass configuration while the second AOM is used in the slave laser beam before the fiber optics. The orientation of both AOMs is set such that the effective detuning for the MOT laser is similar to the detuning achieved when using only one AOM, but without the beam deflection.

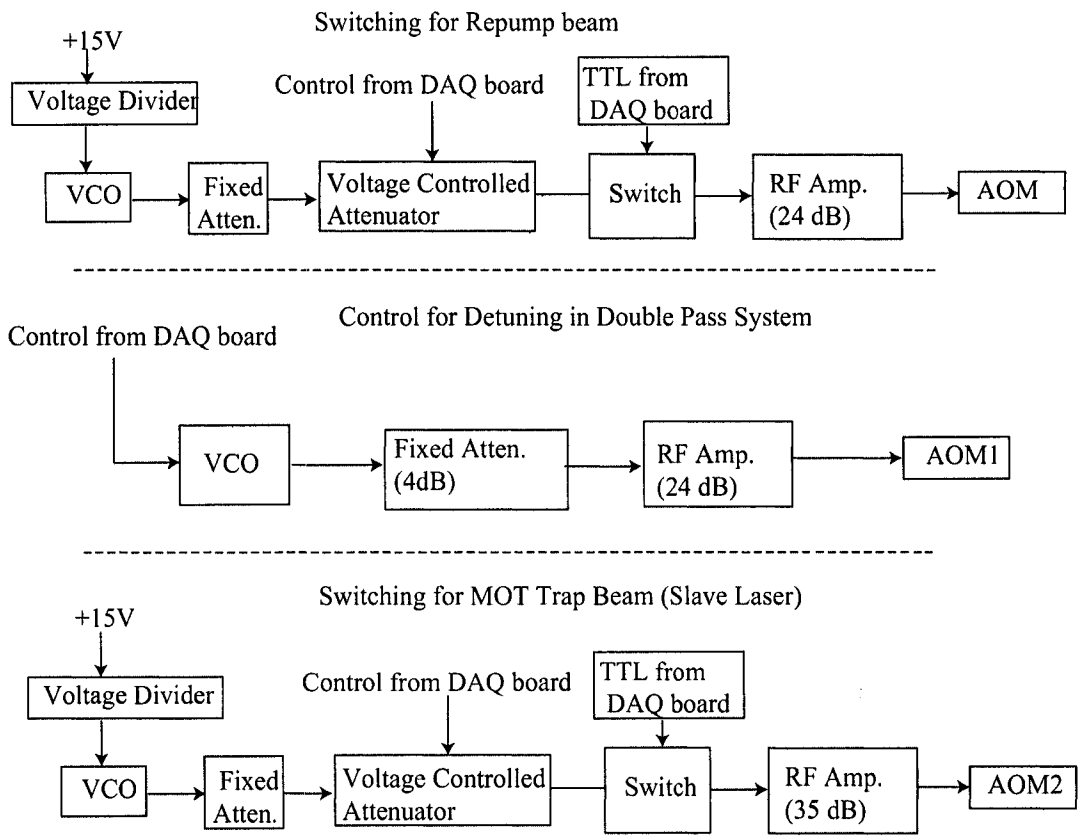

FIG. 32: Schematic diagrams of AOM switching for trap laser beam, repump laser beam, and detuning system.

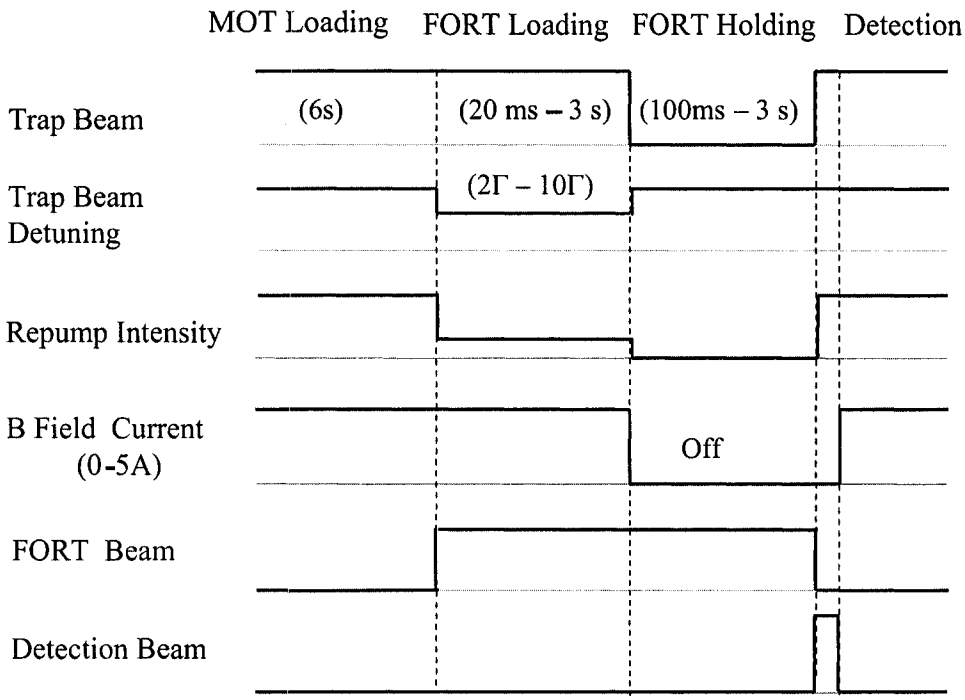

FIG. 33: Diagrams representing time sequences in FORT loading process.

IV.3 TIMING SEQUENCE

There are 5 stages in the loading process of ultracold atoms from a MOT to a cw or pulsed FORT; MOT loading, FORT loading, FORT holding, FORT detection, and clearing stage [41]. Figure 33 shows the timing sequence for each parameter controlled by the DAQ devices and a LabVIEW program; the MOT primary laser beam (trap laser beam), repump laser beam, trap laser detuning, repump laser intensity, anti-Helmholtz current or gradient magnetic field, FORT laser beam, and detection beam. The sequence of loading is as follows. It begins with loading the MOT for 6 s at detuning $\Delta = -2\Gamma$ in order to optimize capture by the resonant scattering force, at maximum repump beam intensity. The trap laser intensity is always kept at maximum. This stage is referred to as "MOT loading." Then, comes the "FORT loading" stage where the repump beam intensity is reduced to about 13.2 μW/cm^2 while simultaneously increasing the detuning of the trap laser frequency up to $\Delta = -10\Gamma$ (Γ = 6 MHz for ^{85}Rb) and turning on the FORT laser. The purpose of the repump laser intensity reduction is to limit the light-assisted collisions knocking the trapped atoms out while increasing the trap laser frequency detuning will help the

cooling process continue for atoms in the FORT. This stage time can be varied from 20 - 3000 ms. Next, the atoms transferred from the MOT are held in the "FORT holding" stage by the FORT laser beam alone. In this stage, the MOT trap laser, repump beam, and magnetic field gradient are turned off starting from 100 ms – 3 s. In the detection stage, the FORT beam is turned off, the magnetic field is still off but the MOT and repump laser beams are turned on to scatter photons off atoms which have remained trapped in the FORT. This stage time is set to 500 ms to see the decay of atom numbers on the oscilloscope, the integration time/detection time is set to only 8 – 9 ms (Gate-in width) with 1.2 ms delay after the FORT laser beam is turned off. The Gate-in width is set by comparing the output signal from the integrator box read by the LabVIEW program and by the oscilloscope while the delay time is adjusted so that the Gate-in starts at the peak of the decaying fluorescence signal, hence the voltage measured will represent the number of atoms held in the FORT. The last stage in the timing sequence is the clearing stage where the trap beam, repump beam and the magnetic field are back on. The detuning of the trap beam and reduction of the repump laser intensity are made only at the FORT loading stage, at other stages, the repump laser intensity is at maximum while the trap detuning is fixed at -2Γ.

Two time sequences are followed for each measurement. The first is called the "background measurement" where the FORT beam is turned off during the FORT loading and holding time. Ideally, during this sequence, since the FORT beam is turned off, the atoms from the MOT fall out of the MOT center quickly and no atoms will be trapped in the holding stage because the MOT light is turned off. In this sequence, the PMT measures only scattered light that results in a background signal. In the second sequence, the FORT beam is on during FORT loading and holding. The background signal is subtracted from the MOT level and FORT level. The net FORT level is then divided by the net MOT level to get the percentage of ultracold Rb atoms transferred from the MOT to the FORT.

IV.4 FEED FORWARD CIRCUIT AND CALIBRATION

In Chapter III, it was mentioned that a double pass AOM system has been installed before part of the master laser beam is sent to a saturated absorption spectrometer (SAS). Detuning of the trap laser frequency is performed by changing the VCO frequency of the AOM inside the double pass system, where the VCO frequency is

changed by varying the voltage going into the VCO. The voltage is sent from an analog output of the BNC adapter as seen in Fig. 32. By changing the frequency of the master laser beam before going to the SAS, the lock point is also changed. Since the switching happens quickly and the capture range of the lock loop is only on the order of the ^{85}Rb natural linewidth, the PZT in the laser cavity can not follow fast enough for the laser to remain locked. In other words, the bandwidth of the lock loop is not great enough for switching the laser on the time scale required in the experiment resulting in the laser becoming unlocked or becoming locked to a different part of the SAS spectrum. To allow for fast switching while keeping the laser locked, a feed-forward circuit was designed and installed on the master laser locking system.

In order to correct for the changing of the lock point position, the frequency of the external cavity diode laser must be adjusted quickly so that the new frequency is within the capture range of the lock for the shifted lock point when the laser detuning is changed. There are two ways to do this; by adjusting the PZT voltage or by varying the laser diode current [75]. The latter is slightly more difficult to do since it can cause instability of the laser frequency through a small temperature change. So adjusting the PZT voltage is a good choice. As discussed in Chapter III, the piezoelectric in the cavity is controlled by the output voltage of the locking circuity box. The PZT voltage is varied by the gain and scanning offset voltage adjustment. By adding a fast voltage correction to the PZT, the laser frequency can be adjusted to correspond to the new lock point frequency which is obtained when the voltage to the VCO of the detuning system is varied. The relationship between VCO control voltage change and PZT correction voltage is approximately linear, but an exact calibration is required.

Figure 34 shows a diagram of the feed forward circuit used. In order to know the appropriate voltage correction to give to the feed forward circuit when the detuning is changed, we need to know how the laser frequency changes when the PZT voltage changes. The change in laser frequency is determined by observing a SAS peak while simultaneously scanning the frequency of the laser and measuring the PZT voltage. We found that it takes 0.02216 V or 22.16 mV to shift 6 MHz (one Γ). So the voltage from the BNC 2110 analog output which is sent to an amplifier for the VCO is split so that part can be sent to the input of the feed forward circuit. This voltage has to be divided by 20.8 (calibrator) in order to match the change of frequency given to

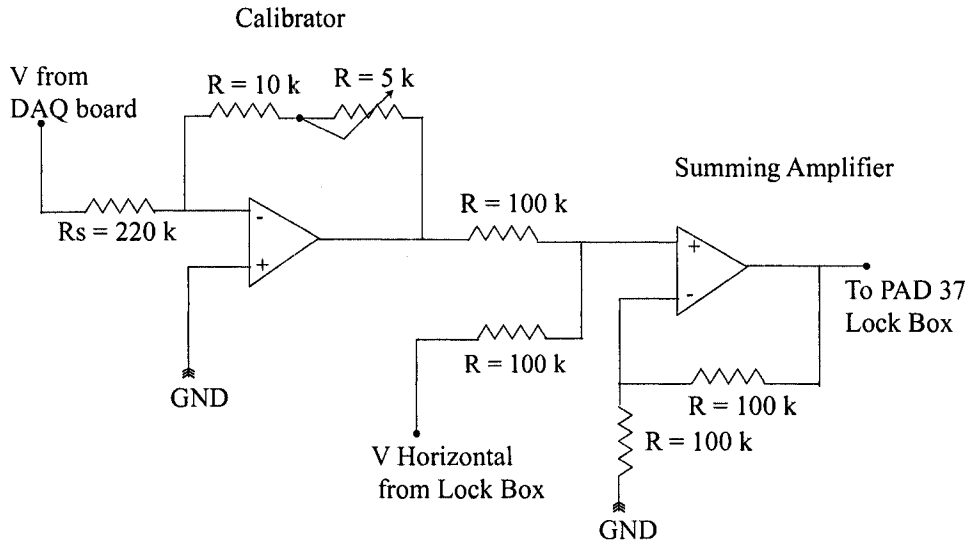

FIG. 34: Feed forward circuit needed for detuning of the trap laser frequency.

the VCO. The calibrated voltage is then summed to the voltage from the lock box (scanning voltage) and sent to the PZT.

After the feed forward circuit is installed in the lock box and the calibration is set, the peaks of the unlocked SAS signal and locked SAS signal are observed while the detuning system is switched. The peaks of the unlocked SAS do not move during switching, only small changes in the peak height are observed because the double pass efficiency is slightly frequency dependent. When the laser frequency is switched using the feed forward circuit, the new locked SAS signal level settles down in a time slightly less than 15 ms. This time sets a bound on the MOT laser detuning switch time during the FORT loading stage. Table. I shows the relation between the voltage supplied to the VCO of the detuning system to the amount the frequency is detuned from the ^{85}Rb resonance frequency (in terms of the natural linewidth Γ) for the MOT laser system. The amplifier has gain 3×, so the real voltage supplied to the VCO is 3 times the voltage displayed on the LabVIEW front panel. After the experiment is setup and the control system is complete and calibrated, data for cw and pulsed FORT dynamics are ready to be taken. At the beginning of each data run, the first thing to do before getting the MOT up is to turn on the Nd:YAG laser because it takes 30–45 minutes for the laser to warm up. If the pulsed FORT is being observed, the mode locker driver also needs to be turned on. After the MOT

TABLE I: Calibration of the required detuning system DAQ voltage.

V (LabVIEW front panels)	Detuning (Γ)
3.48 Volt	0
3.26 Volt	-1
3.03 Volt	-2
2.81 Volt	-3
2.57 Volt	-4
2.32 Volt	-5
2.07 Volt	-6
1.81 Volt	-7
1.55 Volt	-8
1.29 Volt	-9
1.03 Volt	-10

is on and the lasers are locked, one usually needs to wait for about 30 minutes to get a steady MOT. The level of the MOT is kept constant during the measurement to make sure the same number of atoms are being loaded to the FORT for a given set of loading parameters.

CHAPTER V

RESULTS AND DISCUSSION

A lifetime curve and a loading curve are often used to characterize the loading process from a MOT to a FORT. The number of atoms that is measured as a function of storage time or holding time is displayed as a holding or lifetime curve while the measurement as a function of loading time is presented as a loading curve [41]. For the holding curve, the dependence on the FORT laser power will be presented and the loss rates in the FORT during the holding stage will be calculated. The dynamics of the loading process from a MOT to a cw and pulsed FORT are explored by measuring the number of atoms in the FORT as a function of loading time for different loading parameters. The loading parameters we investigate are the power of the FORT laser, the intensity of the repump laser, the intensity of the trap laser, and the detuning of the trap laser frequency during FORT loading. From the loading curves, loading rates and loss rates during loading are obtained. The loss rates for the holding curves (lifetime curve) and loading rates and loss rates for the loading curves are found by curve fitting the solution of Eq. (57) for decay and Eq. (56) for loading to the experimental data using Solver, one of the 2000 Microsoft Excel Analysis ToolPax packages. Ref. [78] explores the applications of Solver, its accuracy and its weakness. It also gives some examples of equations that already have parameter values to test the accuracy of the Solver. With the parameters which characterize the dynamics of the FORT determined, a direct comparison between the physics of cw and pulsed FORT operation can be made.

V.1 HOLDING TIME

The lifetime curves represent the behavior of the number of atoms after they are loaded into the FORT. The ideal FORT has a long storage time and low loss rates. The number of atoms remaining in the FORT as a function of time is given by the solution of Eq. (57) which is rewritten as

$$\frac{dN}{dt} = -\Gamma_H N - \beta'_H N^2, \tag{66}$$

Γ_H is the loss rate due to background gas collisions and β'_H is the loss rate because of the two-body collisions. The index H in this equation is used to differentiate the loss

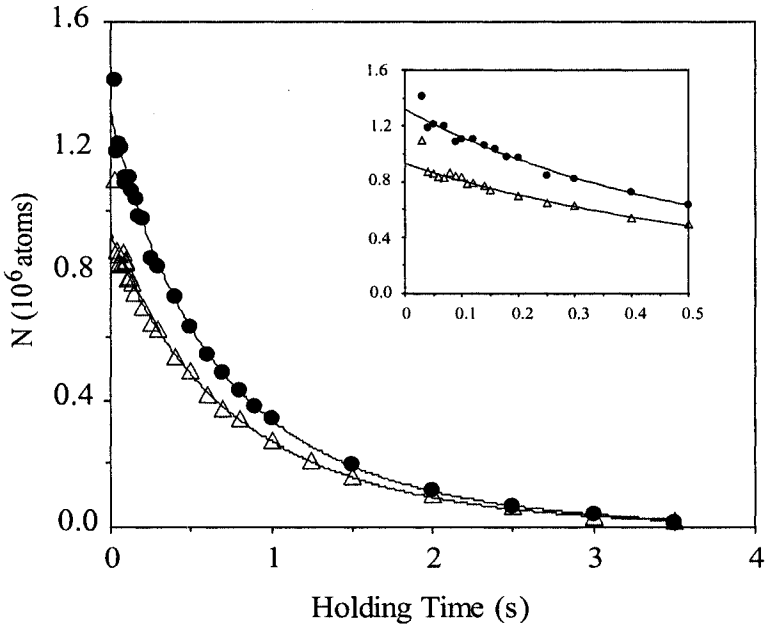

FIG. 35: Number of atoms vs holding time in cw (•) and pulsed (△) FORT for 7 Watts of FORT laser beam power, -8Γ detuning, 18.0 μW/cm^2 repump laser intensity, and 23.1 mW/cm^2 trap laser intensity

rates during holding from those during loading which sometimes are different. The prime on β'_H is to differentiate *number-dependent* loss rates from *density-dependent* loss rates. The solution of Eq. (66) is

$$N = \frac{N_0 e^{(-\Gamma_H t)}}{[1 + \frac{(\beta'_H N_0)}{\Gamma_H}(1 - e^{(-\Gamma_H t)})]} \tag{67}$$

where N_0 is the initial number of atoms loaded after the MOT light is turned off. This is when the holding stage begins.

Figure 35 shows a typical example of holding curves in both a cw and a pulsed FORT for $\sim$ 7 Watts (W) of FORT laser beam power, -8Γ MOT laser detuning during loading, 18.0 μW/cm^2 repump laser intensity during loading and 23.1 mW/cm^2 MOT trap laser intensity. Although FORT laser power is usually given in round numbers, corresponding to the measured power before entering the chamber, the actual FORT power is slightly less due to reflections on the vacuum viewport, which is not anti-reflection (AR) coated. The curve is fit to the solution of Eq. (67) and the fit parameters N_0, Γ_H, and β'_H are extracted from the curve fitting. The curve fit is taken for data starting at 100 ms, because before 100 ms holding time, some

MOT atoms which are not confined in the FORT remain in the trap region and some of the FORT atoms leave the trap through evaporation. The data before 100 ms is shown here to illustrate that the holding curve is not a simple exponential curve for short times. A holding time of 100 ms will be used when the holding time needs to be fixed (constant) in the data taking process while other parameters are varied. At the beginning of the curve, two body-collisions dominate the trap, but at long times, the background gas collisions are more important. The number of atoms in the pulsed FORT at the beginning of the holding period is always somewhat less than for the cw FORT. The reason for this does not appear to be fundamental. Instead, it most likely arises because the spatial mode of the pulsed trap is slightly irregular in comparison to the $\sim TEM_{00}$ mode of the cw FORT. Such a degradation of spatial mode quality can result in the pulsed FORT having a depth slightly less than the cw FORT for the same average power. Later in this chapter, the reason for the irregular spatial mode will be addressed again.

V.1.1 The Dependence on FORT Laser Power

The holding curves are taken at different FORT laser power to investigate the number of atoms held in the trap at different potential well depths. The potential depth of a red detuned FORT can be varied using three parameters; beam waist size, FORT beam wavelength and FORT beam power. In this experiment, the potential depth is changed by varying the FORT laser power and keeping the beam waist size and FORT laser wavelength constant. The power of the cw mode laser can be varied up to 8 Watts while the mode-locked laser can be varied only up to 7 Watts. The power for both lasers is measured at the same point outside the vacuum chamber, the actual value of the measured power at the center of vacuum chamber is less by about 8% due to reflection at the surfaces of the window of the vacuum chamber.

The well depth and the scattering rate of a CW FORT (applied also to pulsed FORT) as a function of FORT laser power are calculated using the general Eq. (31) and (32) and using the rotating wave approximation (RWA) Eq. (39) and (40) for each average power of the FORT laser as shown in Tables II and III. In this calculation, the 8% reflection loss due to the chamber window has been subtracted from each power measured outside the chamber in order to find the laser power at the focal point P; the power displayed on the tables are the measured power. The formula used for the intensity at the focal point is $I_0 = 2P/\pi w_0^2$, here w_0= 16 μm

TABLE II: Well depth of the CW FORT at certain average FORT laser power calculated using general Eq. (31) and Eq. (32).

FORT laser power (Watts)	Well depth(mK)	Scattering rate (s^{-1})
8	−2.9	10.5
7	−2.5	9.2
6	−2.1	7.9
5	−1.8	6.6
4	−1.4	5.2

is the calculated beam waist[1], there is also uncertainty in this calculation, the real beam waist could be larger than 16 μm because of imperfections of the beam spatial mode and because of lens abberations. For this reason, an achromatic lens is used to reduce spherical abberation.

We can see here that the well depths increase as the power increases, however the scattering rates increase also. To lower the scattering rates at the same well depth, the detuning of the laser frequency needs to be increased also. There is about 14% difference between both calculations for well depth and 45% for scattering rate. So, for large detuning, the general Eq. (31) and Eq. (32) are preferred.

The initial number of atoms held in the trap is shown in Fig. 36. From Fig. 36, we can see that the number of atoms loaded initially to the holding stage is less in the pulsed FORT than in the cw FORT, the most likely reason is simply the observed irregular spatial mode of the pulsed laser beam. Another possible reason, though, will be explained in the next section where the loading stage of FORT loading is discussed. From Fig. 36, we can see also that for cw FORT especially, the deeper the potential, the more atoms are trapped.

[1]The calculation is obtained by knowing the beam size of the laser before it is focused down by a lens with focal length f.

TABLE III: Well depth of the CW FORT at certain average FORT laser power calculated using RWA Eq. (39) and Eq. (40).

FORT laser power (Watts)	Well depth(mK)	Scattering rate (s^{-1})
8	−2.5	19.2
7	−2.2	16.8
6	−1.8	14.4
5	−1.5	12.0
4	−1.2	9.6

To obtain a good fit, the curve fitting using the Excel Solver is performed by adjusting the fit parameters until the lowest of the sum of squares of the residuals (SSR) is found. For a holding curve fit, only one minimum with the lowest SSR is found for each curve where other solutions with higher minima are scattered around it, this is true because Eq. (66) has an analytical solution. For the loading curve, which will be discussed later on, there are always two minima with lowest SSR which are found, but one of the minima always gives either a zero or a very big value for the fit parameters. The error bars in this graph and other graphs in this chapter are taken from the fluctuations/deviation around the minima. The amount of fluctuation (deviation) for each parameter is found by changing the value of the fit parameter around the accepted value and running the Solver program until it gives no solution. For holding curves, the errors bar for the fit parameters range from 3% to 30%. The total error is comprised of the errors due to this fluctuation and errors due to the propagation of error in calculating the number of atoms in the FORT and error in calculating the number of atom in the MOT. The number of atoms obtained from the calculation as described in Appendix A is only good to a factor of 2. For our experiment, the value is acceptable since we focus the analysis more on the comparison of the relative values of the cw FORT and the pulsed FORT

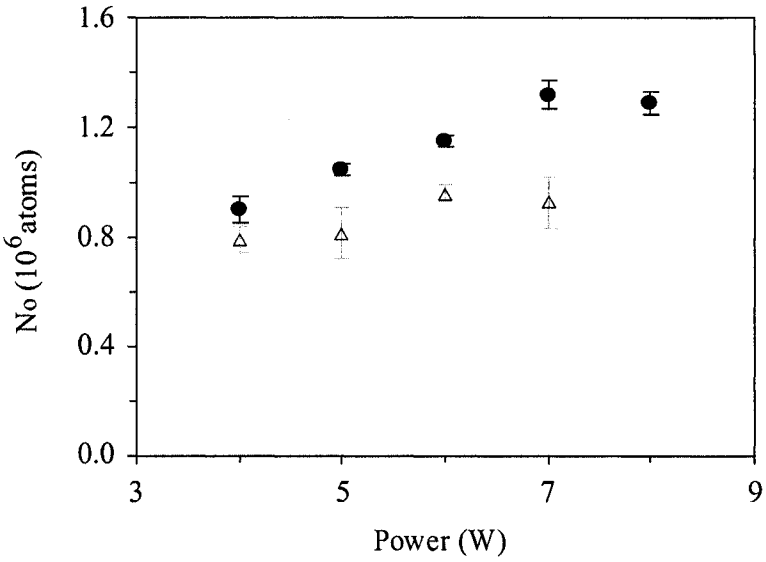

FIG. 36: Number of atoms loaded vs FORT laser power during holding stage in cw (•) and pulsed (△) FORT for -8Γ detuning, 18.0 μW/cm^2 repump laser intensity, and 23.1 mW/cm^2 trap laser intensity. The errors in this plot are from the fluctuation of the fit parameter as described in the text.

parameters. The error analysis is discussed further in the Appendix B.

The loss rates because of background gas collisions and light-assisted or two body collisions during the storage time are displayed in Fig. 37 and 38, respectively. From these figures we can see that Γ_H is essentially the same for each potential depth because the background gas collisions is set by the vacuum chamber system [41], it becomes lower for lower vacuum pressure. The average Γ_H is 1 atom/second per atom thereby making the life time of the trap $(1/\Gamma_H)$ equal to 1.0 s. This value is slightly bigger than the value obtained by Kuppen *et al.* [41] for ^{85}Rb which has $(1/\Gamma_H)$= 3.0 s from a 5×10^{-10} Torr MOT while we estimate a vacuum pressure on the order of 10^{-9} Torr. The loss rate due to two body collisions β'_H at the average FORT laser power of 7 Watts is $(4.2 \pm 0.7) \times 10^{-7}$ (atoms s)$^{-1}$ for the cw FORT and $(4.6 \pm 1.0) \times 10^{-7}$ (atoms s)$^{-1}$ for the pulsed FORT. β'_H for the pulsed FORT is slightly higher compared to the cw FORT but the error bar is larger. In the absence of MOT light, ground-state hyperfine changing collisions are the dominant contributions to values of the β'_H [41].

From Fig. 38, β'_H is found to decrease as the potential depth increases showing that as more cold atoms are trapped in the deep trap, the atoms do not have enough

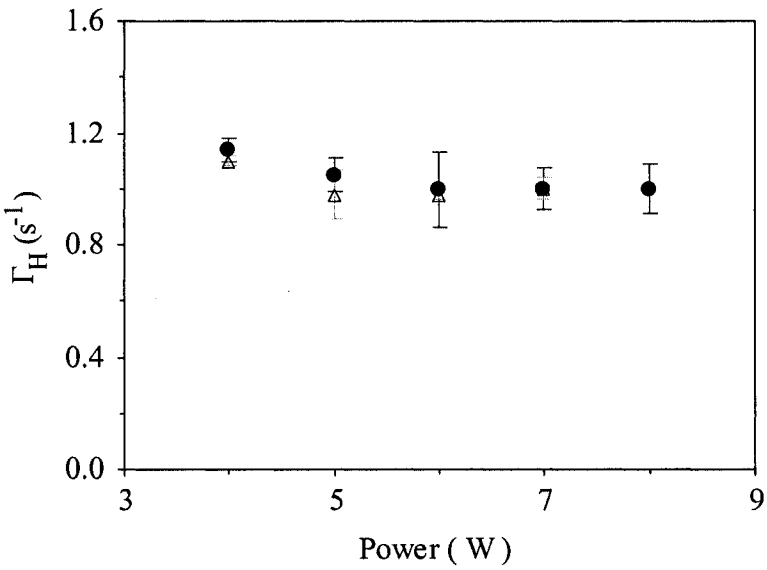

FIG. 37: Loss rates because of background gas collisions vs FORT laser power in cw (•) and pulsed (△) FORT for -8Γ detuning, 18.0 μW/cm^2 repump laser intensity, and 23.1 mW/cm^2 trap laser intensity. The errors in this plot are from the fluctuation of the fit parameter as described in the text.

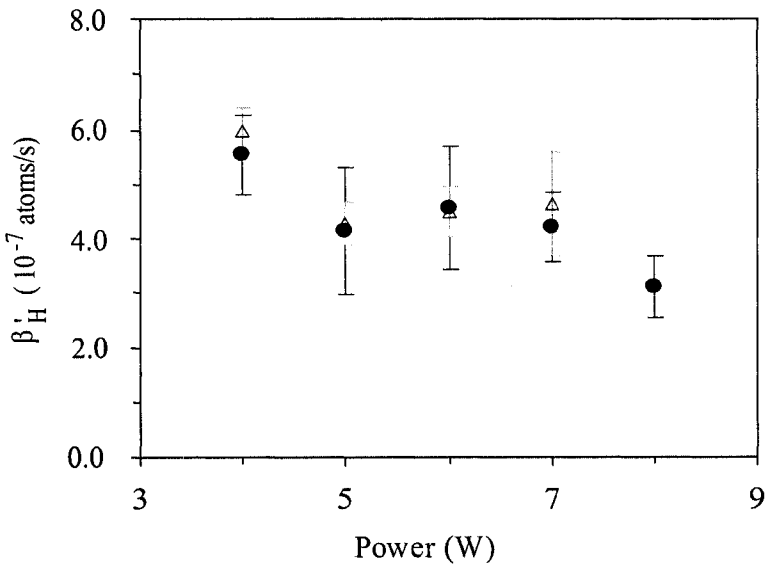

FIG. 38: Two body collision loss rates vs FORT laser power in cw (•) and pulsed (△) FORT for -8Γ detuning, 18.0 μW/cm^2 repump laser intensity, and 23.1 mW/cm^2 trap laser intensity. The errors in this plot are from the fluctuation of the fit parameter as described in the text.

energy to escape since the MOT light is turned off (eliminating MOT light assisted collisions). The value of β'_H obtained for the cw FORT, for example, at a well depth about $U_0 = -2.5$ mK and at 7 Watts FORT laser power is $\beta'_H = 4.2 \times 10^{-7}$(atoms s)$^{-1}$ which is lower than the value obtained by Kuppen *et al.* [41] of $\beta'_H = 1.3 \times 10^{-6}$(atoms s)$^{-1}$ at a well depth $U_0 = -1.8$ mK at 540 mW because our FORTs are red detuned very far off resonance while their FORT was detuned by only a few nm from resonance.

V.2 LOADING TIME

One of the goals of this project is to investigate the dynamics of the loading process of ultracold atoms from a MOT to a cw and pulsed FORT. The dynamics of the loading process can be observed from the data taken during the loading stage (loading curve). The number of atoms in the trap during loading stage [42] is governed by

$$\frac{dN}{dt} = R_0 e^{(-\gamma_{mot} t)} - \Gamma_L N - \beta'_L N^2, \tag{68}$$

where R_0 is the loading rate, γ_{mot} is a parameter representing the change in the MOT behavior during the FORT loading stage due to a change in the MOT laser detuning and reduction of the repump laser power or trap laser intensity. Γ_L is the loss rate due to background gas collisions and β'_L is the loss rate because of the two body-collisions or light-assisted collisions during the loading stage. To find the number of atoms, Eq. (68) is solved numerically using a Runge-Kutta method written in Excel 2000, and then curve fit to the experimental data using the Solver, Excel 2000 ToolPax analysis package. The Runge-Kutta program is tested by solving some differential equations that have analytical solutions and the numerical results are compared to the analytical solutions.

Figure 39 shows loading curves of the cw and pulsed FORT for 7 Watts of FORT laser power, -8Γ detuning, 18.0 μW/cm^2 repump laser intensity and 23.1 mW/cm^2 trap intensity. When loading curves are taken over the dependent parameter being investigated, all other parameters of the MOT and the FORT are set to their optimum values (where the maximum loading obtained). So, initially, an investigation is performed to obtain the optimum trap laser detuning, loading time, holding time, and trap laser intensity needed to get the best FORT loading.

The ultracold atoms start to load into the FORT with the number of atoms as a function of time as $N(t) = R_0 t$ at short time. At longer times the MOT parameter

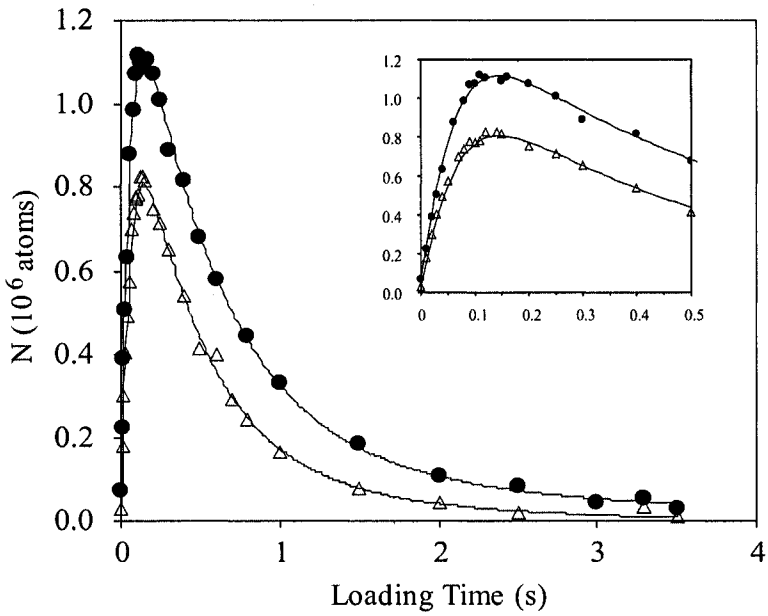

FIG. 39: Number of atoms as a function of loading time in cw (•) and pulsed (△) FORT for 7 Watt of FORT laser beam power, -8Γ detuning, 18.0 μW/cm^2 repump laser intensity, and 23.1 mW/cm^2 trap laser intensity.

γ_{mot} starts to affect the loading shape until it reaches the maximum number of atoms that can be loaded into the FORT. The loading time at maximum loading is always around 100 ms, so we use a loading time 100 ms when the loading time needs to be fixed in the data taking process. The fit parameters in curvefitting are R_0, γ_{mot}, Γ_L, and β'_L. In [42], R_0, γ_{mot} are measured directly and set as fixed parameters, only Γ_L, and β'_L are found using curve fitting. In this experiment, we also measured R_0 and γ_{mot}, but the measurement of γ_{mot} does not give a better fit. The agreement between the measured γ_{mot} and the γ_{mot} obtained from the fit is the same within a factor of 2. R_0 is measured by taking the slope of the experimental loading curves at a short time (0 to 40 ms). The values of the R_0's measured from the slope are smaller than the values of the R_0's obtained from curve fitting (by setting R_0 as a free parameter) by a factor of two. This is because the slope from 0 to 40 ms is not linear. The slope should be taken at time much less than 40 ms. To get an accurate slope measurement for R_0, more data points are needed at short loading time. So, we set R_0, γ_{mot}, Γ_L, and β'_L, all as free parameters (four free parameter fit) to analyze the loading curves. The fluctuations of the values of the fit parameters for the loading curves range from

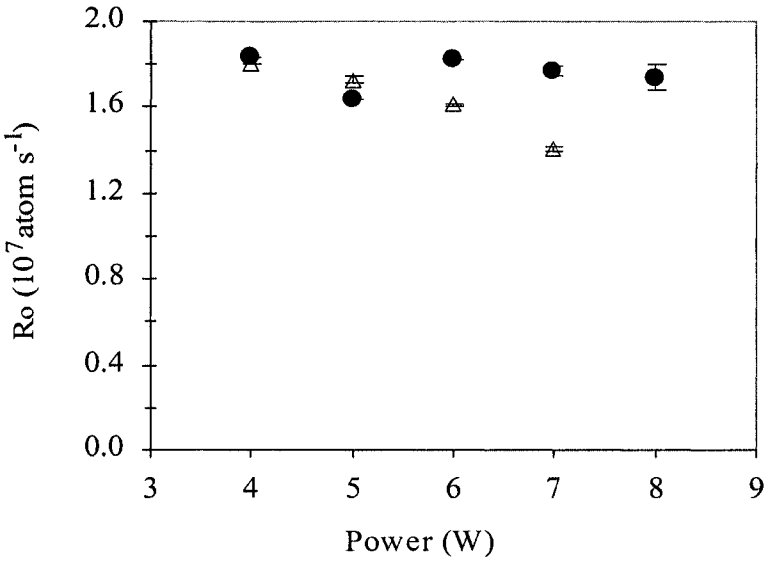

FIG. 40: The loading rates as a function of average FORT laser power in cw (•) and pulsed (△) FORT for -8Γ detuning, 18.0 μW/cm^2 repump laser intensity, and 23.1 mW/cm^2 trap laser intensity.

5% to 30% depending on the loading curve shape. For example at -2Γ detuning (see Fig. 53 and Fig. 54), the curve shape is flat after the loading time reaches 100 ms, the curve fitting gives an unusually large deviation/fluctuation.

V.2.1 The Dependence on FORT Laser Power

The number of atoms that can be loaded depends on the potential well depth. The loading rates and loss rates as a function of average FORT laser power are presented in Fig. 40 and Fig. 41. There is not much difference in loading rates R_0 between cw and pulsed FORT in term of average FORT laser power. Since the MOT level or number of atoms in the MOT is maintained the same during loading, the number of atoms loaded into the FORT is roughly the same for the two traps at a given well depth.

The values of β'_L are found to be larger for lower FORT laser power because for a shallow potential well, the trapped atoms can more easily gain enough energy to exit the trap. β'_L is slightly larger for the pulsed FORT than for cw FORT. The instability in the mode-locked laser intensity or modes could be the reason for the discrepancy where the higher the FORT laser the more unstable the intensity, hence

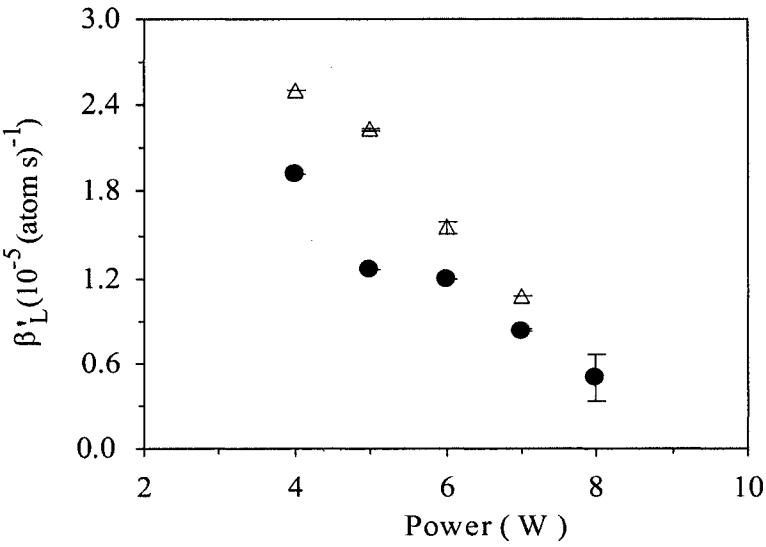

FIG. 41: Loss rates as a function of average FORT laser power in cw (•) and pulsed (△) FORT for -8Γ detuning, 18.0 μW/cm^2 repump laser intensity, and 23.1 mW/cm^2 trap laser intensity.

parametric heating of the cold atoms being loaded into the FORT may be taking place. This will need to be investigated in future studies.

At 7 Watts average laser power, the loss rate β'_L at -8Γ detuning, 18.0 μW/cm^2 repump laser intensity and 23.1 mW/cm^2 MOT trap intensity for the cw FORT is $(8.4 \pm 0.1) \times 10^{-6}$(atoms s)$^{-1}$ while for the pulsed FORT it is $(1.1 \pm 0.0) \times 10^{-5}$(atoms s)$^{-1}$. These values are smaller than typical loss rates during loading obtained by Corwin *et al.* [42] for the cw FORT, for example, they measured at 305 mW, detuning 4.5 nm, and beam waist 26 μm a $\beta'_L = (1.56 \pm 0.22) \times 10^{-5}$(atoms s)$^{-1}$. This is because our FORT laser frequency is detuned far from resonance (1064 nm). Moreover, the loss rate β'_L for the loading stage is larger than β'_H for the holding stage due to MOT light presence in the loading stage. The loss rates due to background collisions from curve fitting results in very small values which are close to zero. This means that β'_L, two-body collision process dominates the FORT loading process. In the presence of MOT light, radiative escape collisions induced by the MOT light give a big contribution to the values of β'_L [42]. The roles of the parameter γ_{mot} in the loading process will be explored in the next section.

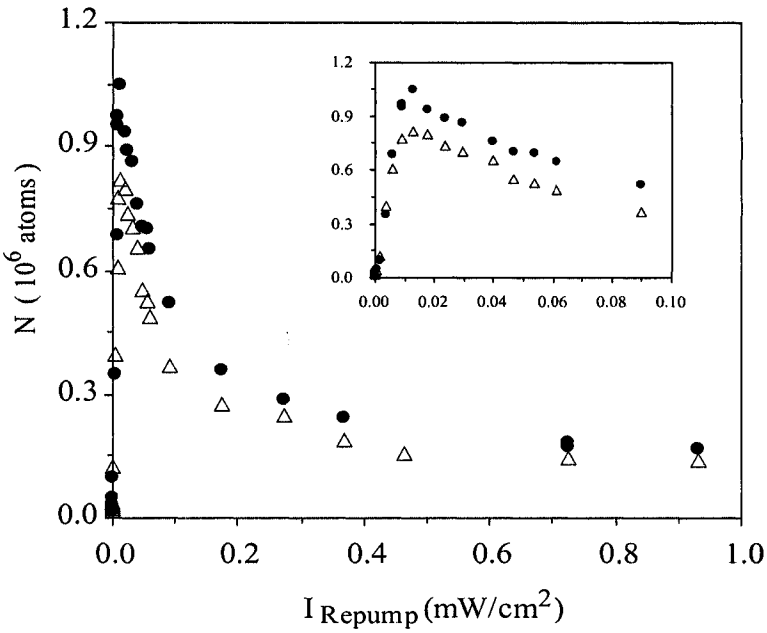

FIG. 42: Number of atoms vs repump laser intensity in cw (•) and pulsed (△) FORT for 7 Watts FORT laser power, -8Γ detuning, and 23.1 mW/cm^2 trap laser intensity.

V.2.2 The Dependence on Repump Laser Intensity

The other MOT parameter that strongly affects the loading efficiency from a MOT to a FORT is the repump laser intensity as mentioned earlier. Figure 42 shows the number of atoms loaded versus the repump laser intensity at 7 Watts FORT laser power and 23.1 mW/cm^2 trap laser intensity. During the course of this experiment, we found two similar values of the repump laser intensity during the loading stage that gave rise to the highest loading efficiency for both FORTs. One is 18.0 μW/cm^2 and the other is 13.2 μW/cm^2. The second value arose after a small realignment of optics for the repump laser beam. The 18.0 μW/cm^2 was used when we measured the number of atoms at different FORT laser power, MOT trap laser detuning, repump laser intensity while 13.2 μW/cm^2 was used to measure the loading rates and loss rates for loading efficiency dependence on MOT trap laser detuning, repump laser intensity and MOT trap laser intensity. There is no major difference in FORT performance due to the slightly different value.

From Fig. 42, it can be seen clearly that only one relatively low value of repump laser intensity can be set during the loading stage to obtain the highest loading

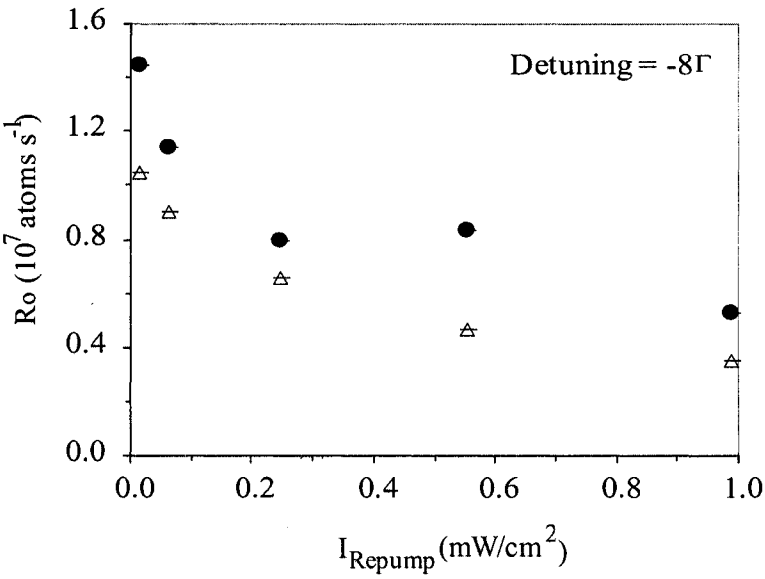

FIG. 43: Loading rates vs repump laser intensity for 7 Watts FORT laser power, -8Γ detuning, 23.1 mW/cm^2 trap laser intensity.

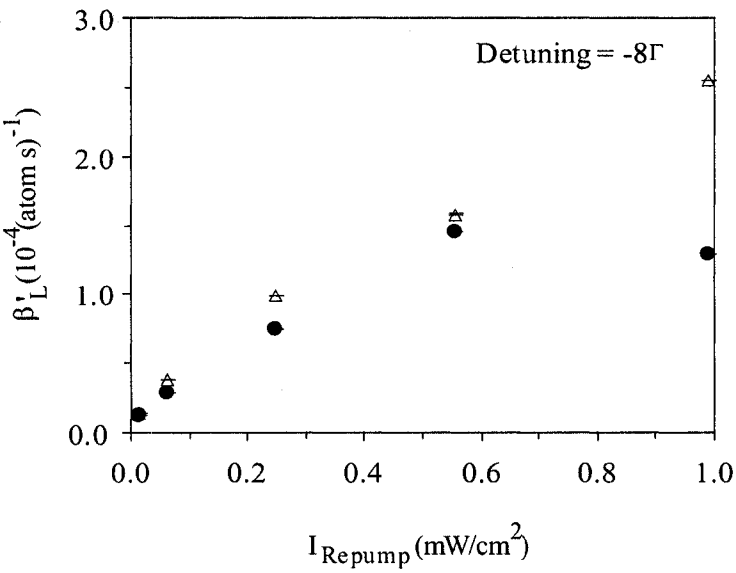

FIG. 44: Loss rates vs repump laser intensity in cw (•) and pulsed (△) FORT for 7 Watts FORT laser power, -8Γ detuning, and 23.1 mW/cm^2 trap laser intensity.

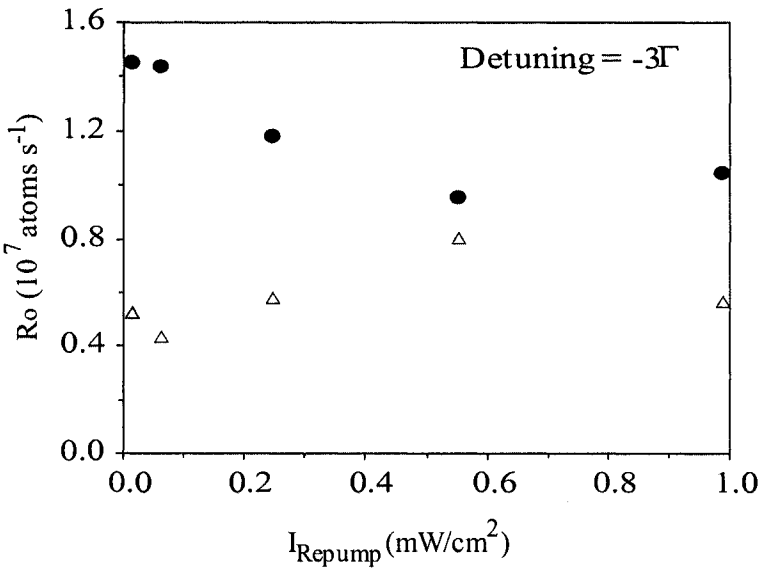

FIG. 45: Loading rates vs repump laser intensity in cw (•) and pulsed (△) FORT for 7 Watts FORT laser power, -3Γ detuning, 23.1 mW/cm^2 trap laser intensity.

efficiency. This value was found to be the same for both FORTs. It depends only on the performance of the MOT system. At lower repump intensity, the MOT itself does not operate well and there are few atoms to be loaded into the FORTs, while at higher repump intensity, the loss rates in the FORT during loading become larger due to light-assisted collisions. The optimal repump intensity for FORT loading occurs where there is a balance between maximizing MOT performance while minimizing collisional losses. Figure 43 and Fig. 44 show the loading rates and loss rates during the FORT loading stage as a function of the repump laser intensity. These rates are obtained at -8Γ trap laser detuning and obtained using a four free parameter fit. The fluctuations/deviations around the minima are less than 7%. There are always 2 minima resulting from the curvefit, with the secondary minima giving a very large γ_{mot} and a very small β'_L, for example, the minima we use has $\gamma_{mot} = 1.14$ per second and $\beta'_L = 1.59 \times 10^{-4}$ (atom s)$^{-1}$ for 0.55 mW/cm^2 repump intensity while the other minima with the same repump intensity has $\gamma_{mot} = 60.98$ per second and $\beta'_L = 9.06 \times 10^{-7}$ (atom s)$^{-1}$. This secondary result is not consistent with the known physical conditions in the trap and must be discarded.

The dependence of the loading rates and the loss rates on the repump laser intensity is the same for both FORTs at -8Γ detuning. However, for small trap laser

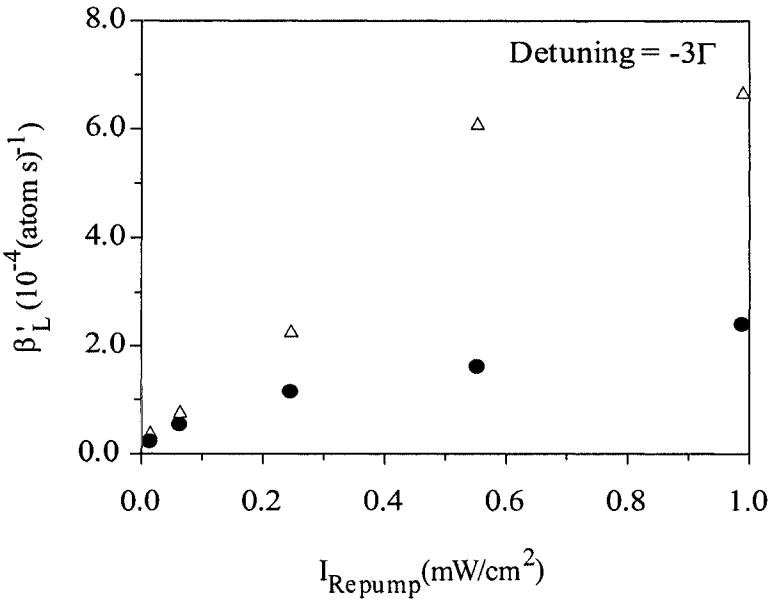

FIG. 46: Loss rates vs repump laser intensity in cw (•) and pulsed (△) FORT for 7 Watts FORT laser power, -3Γ detuning, and 23.1 mW/cm^2 trap laser intensity.

detuning during loading, the loading rate for the pulsed FORT is much smaller and constant at higher repump laser intensity while the loss rate is much larger at higher repump intensity. These are shown on Fig. 45 and Fig. 46. We also measured the loading and loss rates dependence on MOT trap laser detuning at higher repump laser intensity. For higher repump laser intensity, the loading rates as a function of trap laser detuning decrease by a factor of two for both FORTs, with the exception for the pulsed FORT, the loading rates are almost the same for smaller detuning. The loss rates for the cw FORT increase by a factor of two for higher repump intensity while for the pulsed FORT, the increase is 3 times. So the trap laser detuning and repump laser intensity play a big role in the loading efficiency. Both parameters have a bigger affect on the loss rates for the pulsed FORT than for the cw FORT. The dependence on MOT trap laser detuning will be discussed later in this chapter.

V.2.3 The Dependence on MOT Trap Laser Intensity

The loading efficiency for both the pulsed and cw FORT depends on the trap laser intensity only before the MOT reaches its maximum performance. The MOT performance also depends on such parameters of the MOT system as the vacuum chamber

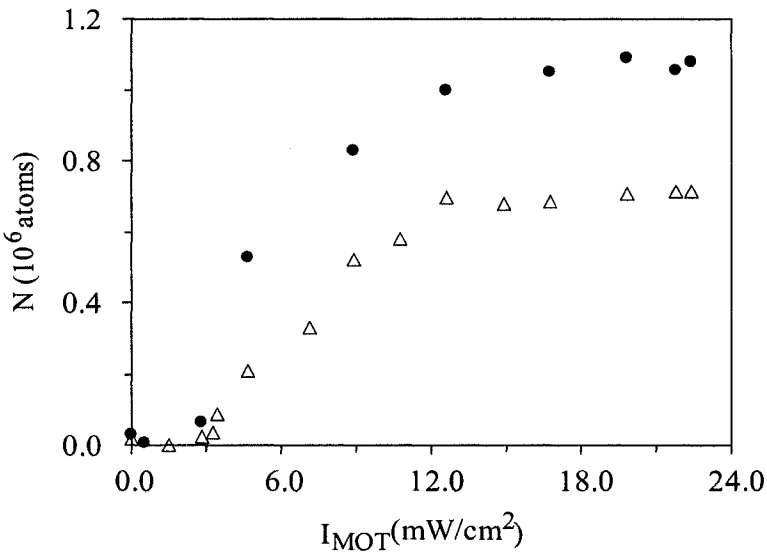

FIG. 47: Number of atoms as a function of trap laser intensity in cw (•) and pulsed (△) FORT for 7 Watts FORT laser power, -8Γ detuning, 18.0 μW/cm^2 repump laser intensity.

(background gas pressure), numbers of rubidium atoms in vapor in the chamber (alkali dispenser current), gradient magnetic field used, and the beam size of the MOT laser. Figure 47 shows the number of atoms as a function of trap laser intensity for both FORTs. After the maximum number of atoms have been trapped toward the MOT center, increasing the trap laser intensity does not affect the number of atoms loaded into the FORT. Although lowering the MOT intensity during FORT loading could aid in sub-Doppler cooling, we did not find an enhancement here in the FORT loading efficiency when the MOT laser intensity was lowered.

From Fig. 48 and Fig. 49, we see that the loading rate and the loss rate are constant after the MOT reaches its maximum performance, hence the number of atoms loaded into the FORT does not depend very much on trap laser intensity in the "high" intensity regime. The turning point where the number of atoms, loading rates, and loss rates become constant is at about half of maximum intensity; 12.7 mW/cm^2. So, for measurements on other FORT parameters, the trap laser intensity was set to the maximum achievable intensity which is 23.1 mW/cm^2.

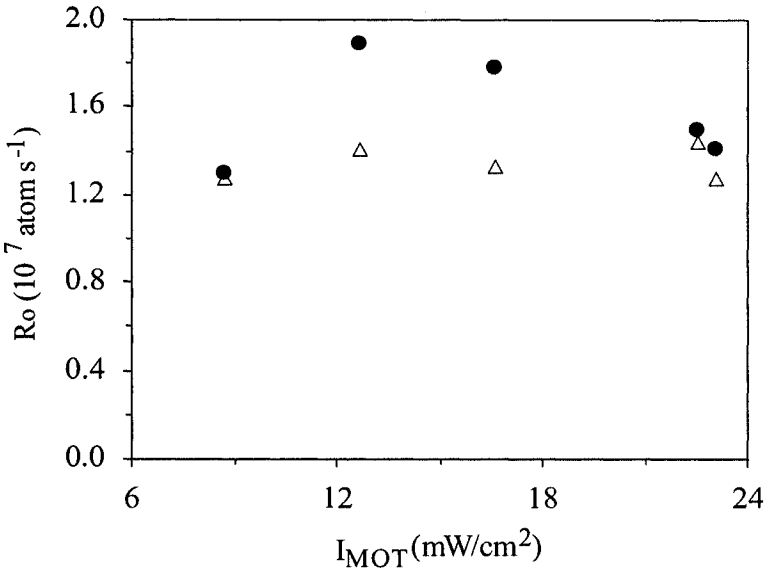

FIG. 48: Loading rates as a function of trap laser intensity in cw (•) and pulsed (△) FORT for 7 Watts FORT laser power, -8Γ detuning, 13.2 μW/cm^2 repump laser intensity.

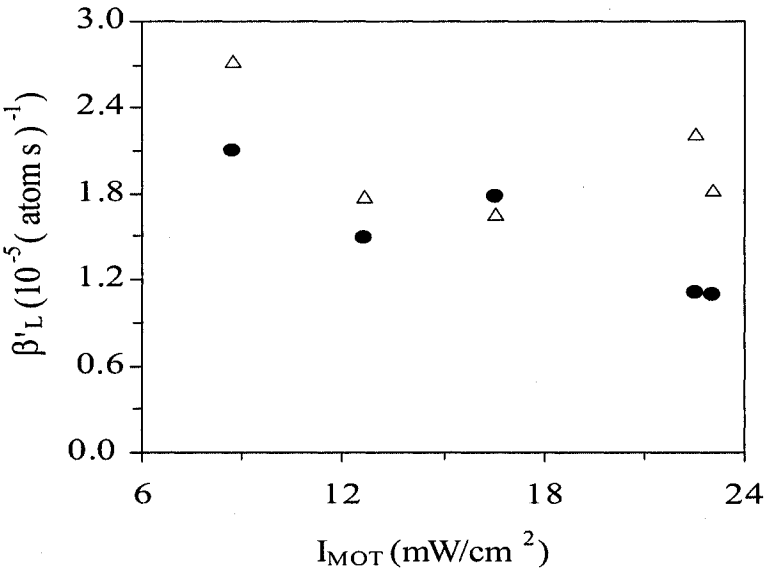

FIG. 49: Loss rates as a function of trap laser intensity in cw (•) and pulsed (△) FORT for 7 Watts FORT laser power, -8Γ detuning, 13.2 μW/cm^2 repump laser intensity.

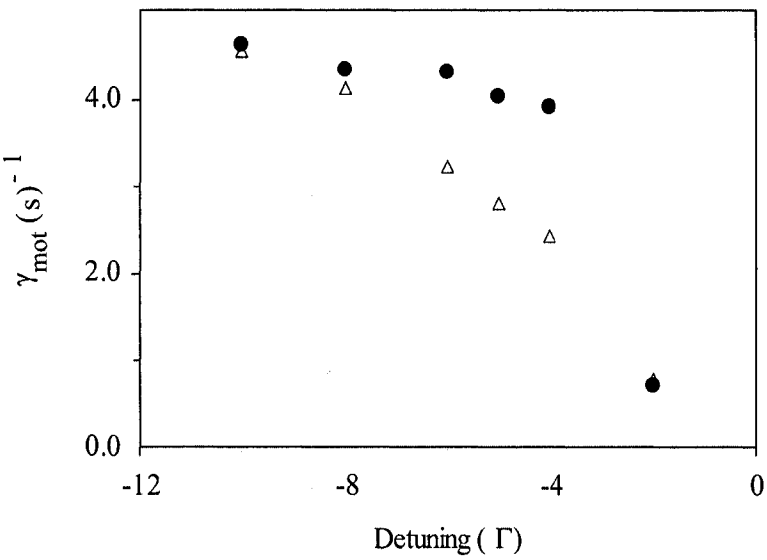

FIG. 50: MOT parameter γ_{mot} as a function of trap laser detuning obtained from the curvefit in cw (•) and pulsed (△) FORT for 7 Watts FORT laser power, 13.2 μW/cm^2 repump laser intensity, and 23.1 mW/cm^2 trap laser intensity.

V.2.4 The MOT Performance Parameter γ_{mot}

As mentioned before, the parameter γ_{mot} represents the change to the MOT performance during loading arising from changes to MOT laser frequency and detuning and the repump laser intensity (or detuning, if applicable). Typically, we only change the repump laser intensity and MOT trap laser detuning during loading. Optimizing the FORT loading by decreasing the repump laser intensity or by changing the MOT laser detuning results in an increase in the value of γ_{mot} because in both cases normal MOT operation is disrupted. Figure 50 shows the values of γ_{mot} versus detuning. These values are obtained from a four parameter fit. The values are larger when the trap laser frequency is detuned far from atomic resonance during loading, as expected. There is a difference in γ_{mot} values for cw and pulsed FORT. We find the γ_{mot} decreases smoothly for the pulsed FORT. γ_{mot} can be measured approximately by observing the MOT fluorescence decay at a time T_D before FORT loading would begin [42]. Figure 51 shows the values of the measured γ_{mot} using this method. We can see that the values for γ_{mot} are smaller than the ones obtained from the curvefit. This is not surprising since the measurement does not incorporate the change to the MOT in the region of the FORT volume.

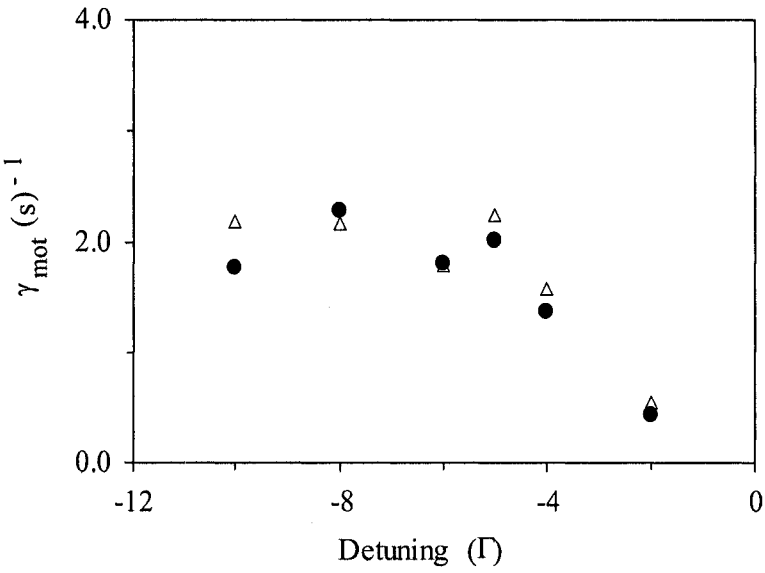

FIG. 51: MOT parameter γ_{mot} vs trap laser detuning measured in cw (•) and pulsed (△) FORT for 7 Watts FORT laser power, 13.2 μW/cm^2 repump laser intensity, and 23.1 mW/cm^2 trap laser intensity.

V.2.5 The Dependence on MOT Trap Laser Detuning

Up to this point, we have seen that the cw and pulsed FORTs tend to behave quite similarly. To first approximation, one would indeed expect comparable performance for traps with the same average potential well depth. Such similar behavior, however, is not universal. As we now discuss, a significant difference in cw and pulsed FORT dynamics was observed when the FORT loading as a function of MOT laser detuning was investigated.

In the FORT loading stage, the trap laser detuning has an important role in getting the largest percentage transfer of ultracold atoms in the MOT to the FORT [41]. As the FORT only confines–but does not cool– atoms, it is important to maintain the cooling process as atoms are loaded into the FORT. Of course, while atoms in the MOT/FORT overlap region are being cooled, atoms outside of the FORT volume must also be transported to the FORT region to be loaded. So the greatest overall loading efficiency occurs by detuning the MOT light in order to maximize the cooling of atoms as they load into the FORT while reducing any negative impact to MOT atom transport that a detuning change could bring.

Figure 52 shows the number of atoms loaded during the loading stage as a function

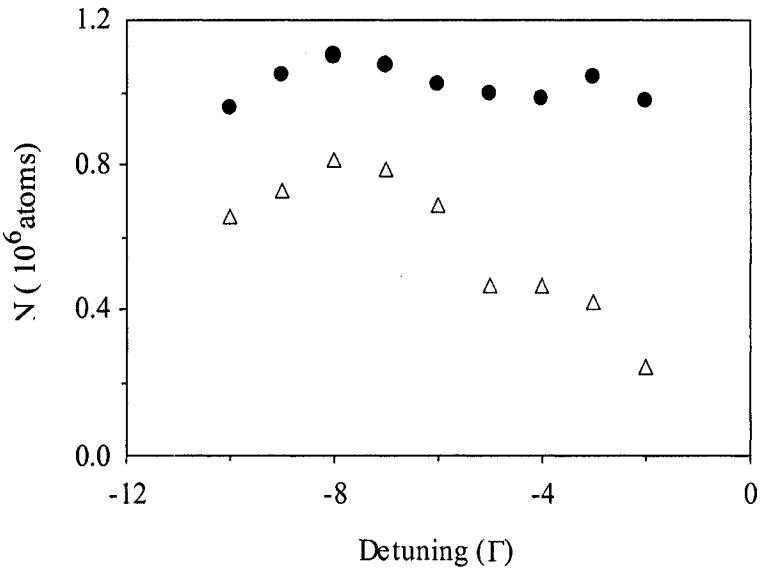

FIG. 52: Number of atoms as a function of trap laser detuning in cw (•) and pulsed (△) FORT for 7 Watts FORT laser power, 18.0 μW/cm^2 repump laser intensity, and 23.1 mW/cm^2 trap laser intensity.

of the detuning of the MOT trapping laser. Here we can see a crucial difference between cw and pulsed FORT performance. The pulsed FORT works well when the frequency of the MOT trapping laser is detuned far from the atomic resonance and, indeed, both FORTs have maximum loading at -8Γ detuning. Closer to resonance, the cw FORT still loads approximately the same until the detuning reaches -2Γ, however, the pulsed FORT shows a marked degradation in FORT loading starting -5Γ and loads very poorly as the MOT detuning approaches resonance.

In order to uncover the physics responsible for this difference, loading curves at a series of MOT laser detunings were taken and the loading and loss rates were extracted as described above. Again, we determined the loading rate R_0, MOT parameter γ_{mot}, loss rate due to background gas collisions Γ_L, and loss rate due to light-assisted collisions β'_L. We employs a 4 free parameter fit to obtain these parameters. Figure 53 and Fig. 54 show the loading curves for cw FORT and pulsed FORT at different detuning. We can see that the loading curves for each detuning for the cw FORT are quite comparable, whereas the loading curves for the pulsed FORT are far apart. These results are consistent with Fig. 52.

Figure 55 and Fig. 56 show the loading rates and the loss rates during loading

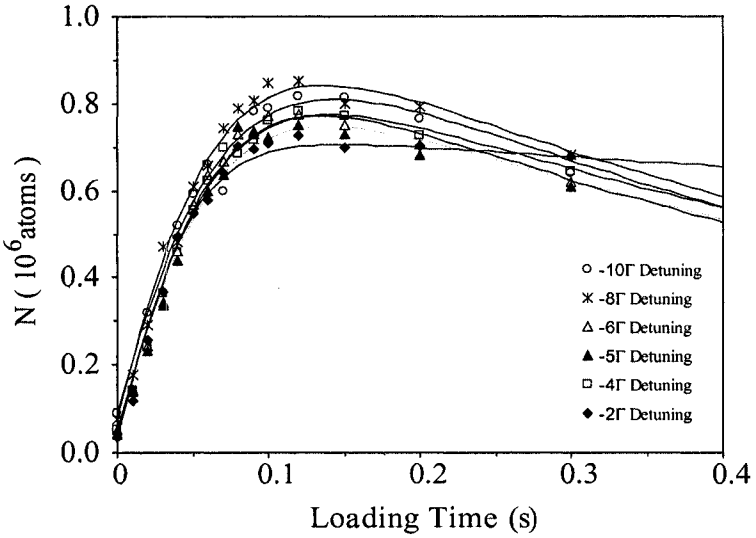

FIG. 53: Number of atoms as a function of loading time in cw FORT for different trap laser detunings at 7 Watts FORT laser power, 13.1 μW/cm^2 repump laser intensity, and 23.1 mW/cm^2 trap laser intensity.

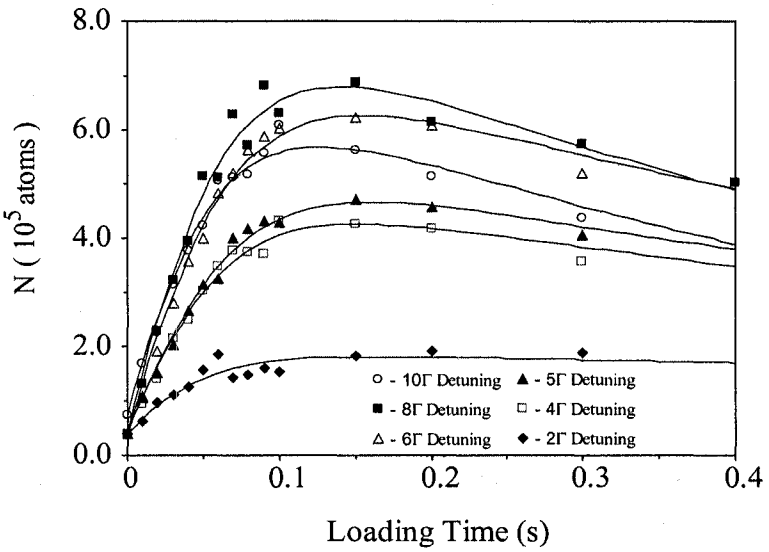

FIG. 54: Number of atoms as a function of loading time in pulsed FORT for different trap laser detunings at 7 Watts FORT laser power, 13.1 μW/cm^2 repump laser intensity, and 23.1 mW/cm^2 trap intensity.

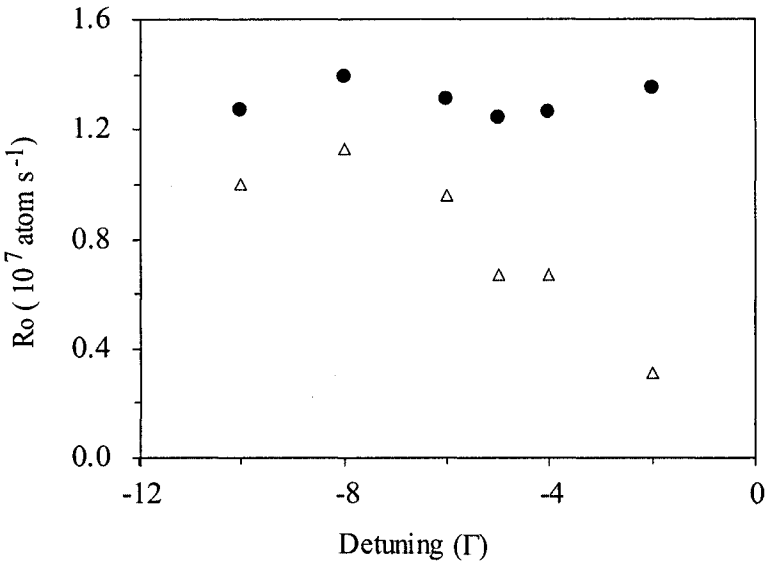

FIG. 55: The loading rates vs trap laser detuning in cw (•) and pulsed (△) FORT for 7 Watts FORT laser power, 13.2 μW/cm^2 repump laser intensity, and 23.1 mW/cm^2 trap laser intensity.

versus MOT trap laser detuning. The difference between the cw and pulsed FORT performance at lower detuning arises because the loading rate in the pulsed FORT is lower at smaller detuning than for the cw case, while at the same time, the loss rate in the pulsed FORT is higher at smaller detuning compared to the cw FORT. The loading rates and the loss rates as a function of detuning in a cw FORT obtained by Corwin *et al.* [42] are very much the same shape as those obtained by us; the principal difference being in the loading rate detuning dependence where they obtained a maximum loading at -5Γ, though our cw data does not show a strong detuning dependence in this region. The loss rate β'_L is larger at smaller detuning because more atoms are in the excited state; the excited atoms scatter more photons when they decay back to the ground state hence create heating. The Γ_L values obtained from the curvefit tend to be very small and close to zero, the loading curve shape is dominated more by γ_{mot} and β'_L than any background collisions characterized by Γ_L.

Simulation of the loading curves, using various combinations of values for loading and loss rates, indicates that although the difference between the cw and pulsed FORT loading at small detuning arises from the differences in both the loading and loss rates, it is primarily the difference in the *loading rate* which is responsible for

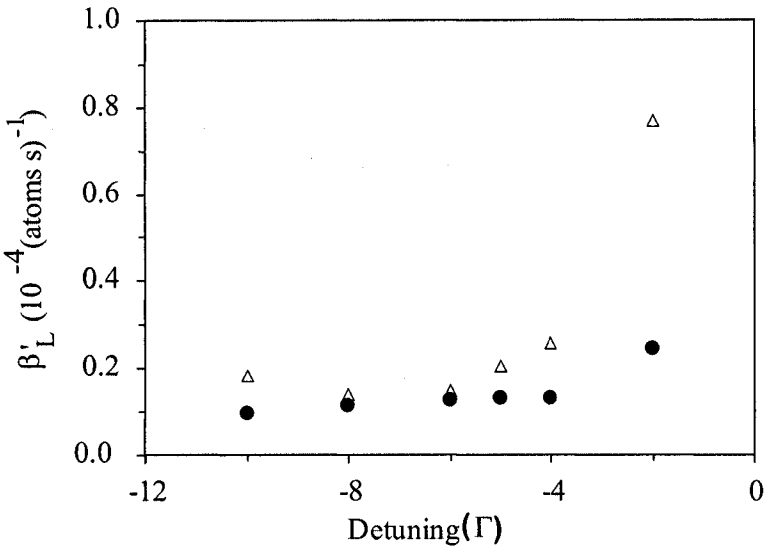

FIG. 56: The loss rates vs trap laser detuning in cw (•) and pulsed (△) FORT for 7 Watts FORT laser power, 13.2 μW/cm^2 repump laser intensity, and 23.1 mW/cm^2 trap laser intensity.

the difference in the number of atoms loaded into the FORT.

At smaller detuning, there are several possible factors which could cause the loading rates to be lower and the loss rates to be higher in the pulsed FORT compared to the cw FORT. We investigated this case further by measuring the number of atoms versus detuning at different FORT power and at different repump laser intensity.

Beginning with the FORT power dependence study, we noticed that the shape of the curves for a cw FORT at lower power is rather similar to the curve shape for the pulsed FORT at all powers studied. However, the number of atoms loaded in the cw FORT, even at low power and detuning is still greater than the pulsed case with comparable parameters. Figure 57 and Fig. 58 show the number of atom as a function of detuning for different FORT laser power. For the cw case, as the power is increased the atom number loaded into the FORT at low detuning rises quickly. In others words, as the trap potential well depth becomes deeper, more atoms are loaded. In both cases, the maximum number of atoms loaded occurs -8Γ, independent of FORT power. For a pulsed FORT at low detuning, however, the number of atoms loaded is increased as the FORT power is larger, but only slightly in comparison to the cw case. All of these results strongly suggest that the loading

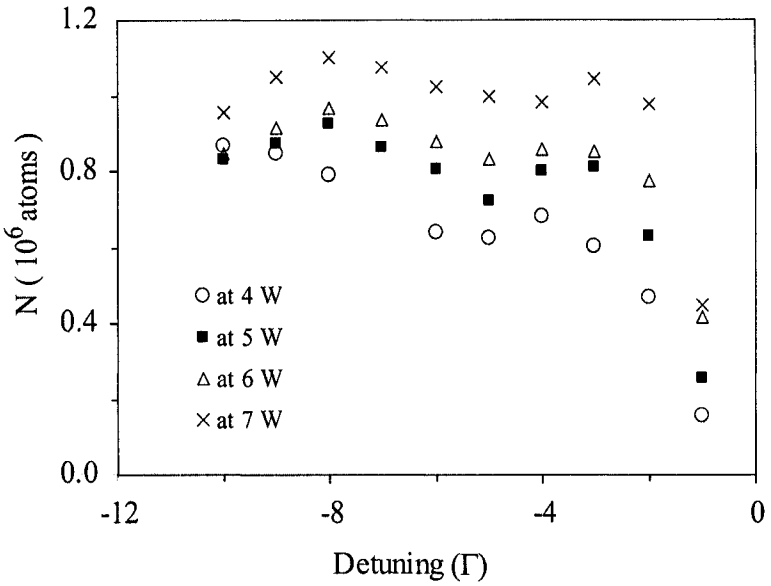

FIG. 57: Number of atoms as a function of trap laser detuning in cw FORT for different FORT laser powers.

of the pulsed FORT at low detuning is different because the *cooling during loading at small detuning is not exactly the same for cw and pulsed operation.*

This unexpected result has opened the way for future investigation in order to confirm that a modification of the cooling is indeed responsible for the observed difference in FORT loading and to understand exactly how the cooling is being modified. As a first step in that research direction, we have performed spectroscopy of atoms confined in the FORT in order to ascertain their response to near-resonant light in the presence of both cw and pulsed 1064 nm trapping light.

V.3 FORT SPECTROSCOPY EXPERIMENT

The multi level structure of atoms used in an optical dipole trap can affect the performance of the trap itself. An optical dipole trap relies on the spatially-inhomogeneous ac Stark shifts to trap atoms. In a two-level system, the energy shifts of the two levels coupled by a perturbing field are opposite to each other. This will lead to an inhomogeneous broadening of a transition between the two levels inside, because atoms in the trap are not completely localized. Such broadening can reduce the Doppler cooling of atoms inside an optical dipole trap or becomes an obstacle for precision

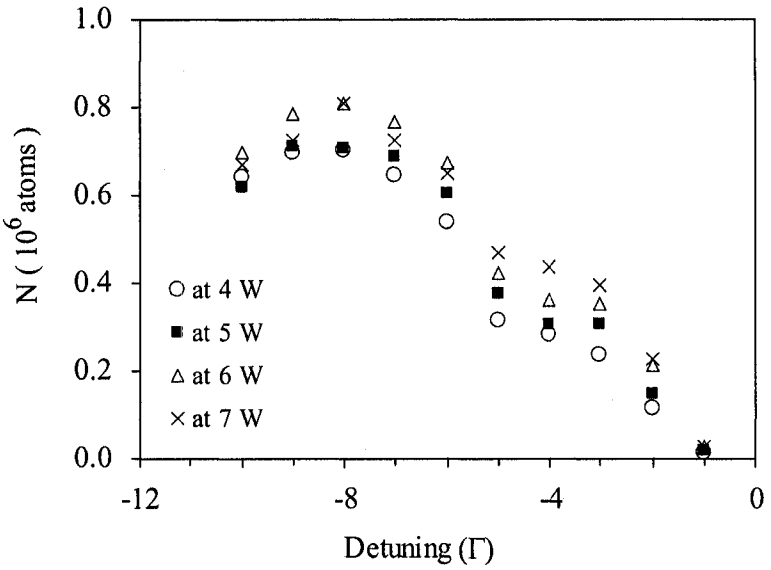

FIG. 58: Number of atoms as a function of trap laser detuning in pulsed FORT for different FORT laser powers.

spectroscopy experiments. We have performed spectroscopy of atoms in both a cw and a pulsed FORT, in order to observe the atomic response to the near resonant light which is responsible for cooling atoms while they are loaded into the FORT. We use a "kick" beam to push atoms out of the FORT and then measure the number of atoms which remain as a function of kick beam detuning.

Figure 59 shows the optical setup of the experiment. Sending another beam in addition to the MOT and FORT laser beams to the vacuum chamber is quite challenging since we have a vacuum chamber with a limited number of optical windows. The kicking beam comes from a separate ECDL laser system built in a master-slave configuration. The laser setup is the same as the one for the MOT trap laser where a double pass system is employed in order to have a convenient tunability of the frequency. We are able to detune the kicking beam frequency from -24 MHz to +52 MHz from the resonance frequency of Rb. In order to perform this experiment, the LabVIEW program as described in Chapter IV is modified such that an additional digital output is used to control the TTL signal for the AOM inside the double pass system of the laser beam. The kicking beam is turned on during the FORT holding, 50 ms before the FORT holding stage ends or 50 ms before the detection stage begins. The choice of a 50 ms duration for the kicking beam was obtained after several

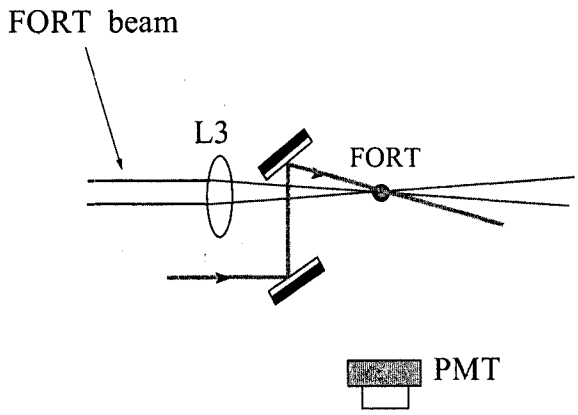

FIG. 59: Experimental diagrams for spectroscopy of atoms confined in a cw and a pulsed FORT.

trials on different kick beam powers and kick beam time and it was found that 50 ms kick beam time and 250 μW kick beam power with 3.5 mm beam radius yielded the biggest attenuation. Before entering the chamber, the beam is collimated and expanded– the diameter of the beam is made bigger than the MOT cloud to ensure uniform illumination of atoms confined in the FORT.

Figure 60 and Fig. 61 show the number of atoms versus kick beam detuning around the resonance frequency of ^{85}Rb for a cw FORT and a pulsed FORT. Several features are apparent from the graph. Given that the kick beam is identical for both the cw and pulsed experiments, it appears that the response for the cw FORT to the kick beam is greater in amplitude than that of the pulsed FORT. It is not clear whether this is a fundamental difference or a technical factor like pulsed FORT beam pointing stability. Also observable from the figures is that the magnitude of the frequency shift is somewhat different for cw and pulsed FORTs of equal average power. This result is completely consistent with the earlier observation that the spatial mode quality of the mode-locked laser is not as good as the cw beam, resulting in a slightly larger focussed beam waist and hence a slightly smaller potential well depth. We know that the cw FORT loads slightly more atoms than the pulsed FORT of equal average power as shown in Fig. 35 and Fig. 39. The data is also consistent with Fig. 57 and Fig. 58. These preliminary data indicate that further investigation of the interaction of atoms in the pulsed FORT with near-resonant light is needed.

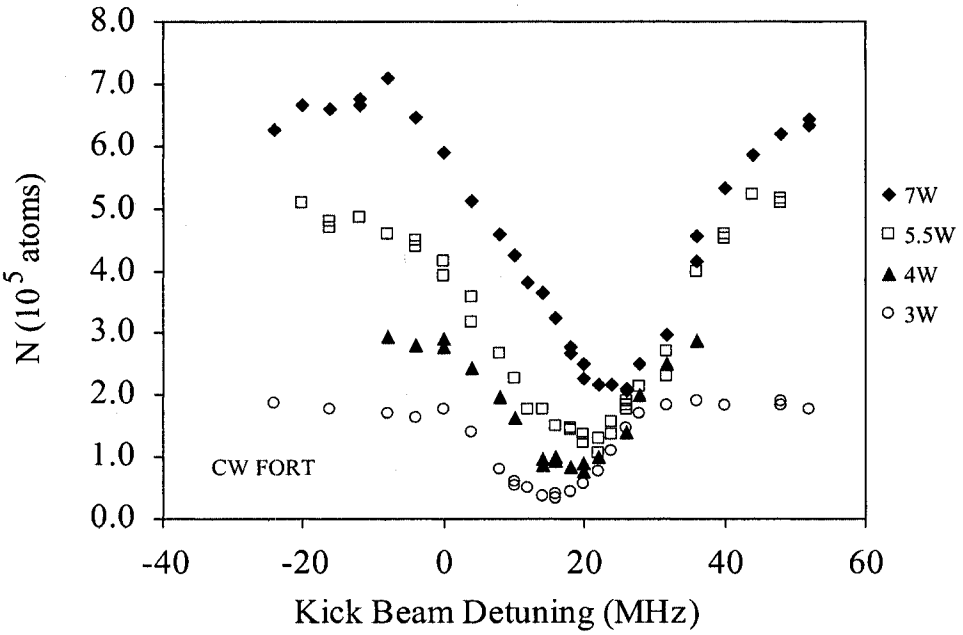

FIG. 60: Number of atoms in the cw FORT vs kick beam detuning for different FORT laser powers, 250 μW kick beam power, beam radius 3.5 mm, and 50 ms kick time.

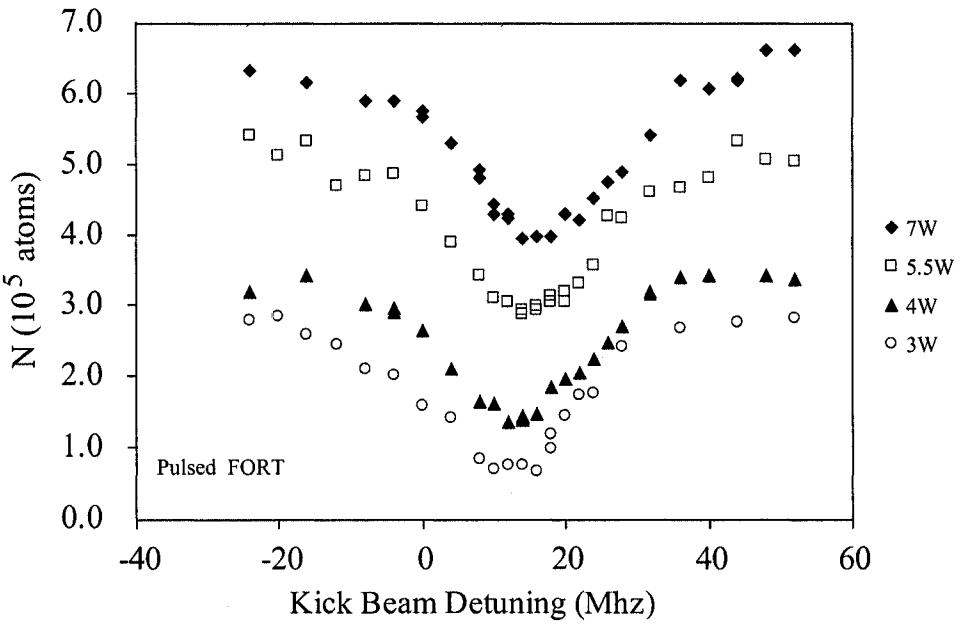

FIG. 61: Number of atoms in the pulsed FORT vs kick beam detuning for different FORT laser powers, 250 μW kick beam power, beam radius 3.5 mm and 50 ms kick time

CHAPTER VI

CONCLUSION AND OUTLOOK

This dissertation reports on the design, construction, and investigation of a pulsed optical dipole force trap (pulsed FORT). The main objective of the research was to investigate whether there was an appreciable difference in the physics of pulsed FORT loading in comparison to cw FORT loading, which had been studied previously by other groups. Our principal finding is that in most respects, they are similar in behavior for equivalent average potential well depth; however, there is notable difference in the FORT loading efficiency dependence on the detuning of the MOT trap laser frequency during the loading phase.

The pulsed and cw FORTs were built by focusing a Nd:YAG laser beam to the center of a MOT and loading the atoms from the MOT to the FORTs. There were about 1.5×10^7 ultracold rubidium atoms in the MOT before FORT loading began. We have investigated the behavior of the FORT loading both with respect to FORT and MOT laser parameters, as well as to the transfer process sequence timing. At $\sim$7 Watts FORT laser power, about 8% of the atoms are loaded successfully into the cw FORT and about 5% into the pulsed FORT under similar conditions. There is evidence that the spatial mode of the pulsed FORT is responsible for this difference. Both FORTs depend strongly on FORT laser power, where the higher the power, the deeper the trap, and the more atoms that are loaded. The number of atoms in each FORT depends also on the loading time and holding time. The highest loading efficiency is obtained at 100 ms of loading time while the average lifetime of both FORTs is 1 s, limited by background gas collisions. The maximum loading for both FORTs is reached at 13.2 μW/cm^2 repump laser intensity and at -8Γ trap laser detuning during FORT loading.

We have begun to investigate the physical mechanism(s) that are responsible for the observed difference in the FORT loading dependence on MOT trap laser frequency. Our analysis shows that for the pulsed FORT, as compared to the cw FORT at the same low trap laser detuning, the FORT loading rate is lower, while the loss rate during loading is higher. Both rates are responsible for the smaller number of atoms loaded into the pulsed FORT at smaller detuning. A simulation has shown that it is the lower loading rate which is principally responsible for the observed difference. The results are consistent with a reduction of the cooling of atoms during

FORT loading. Spectroscopy of the atoms in the FORT was performed in order to investigate the atomic response to near resonant light, and some differences between atoms in the cw and pulsed FORT were observed. Future studies will include further spectroscopic investigation as well as detailed temperature measurements of atoms loaded in the FORT.

FORT loading is a complicated dynamical process and there are many aspects of the physics of FORT loading which require future investigation. In addition to continued studies of the dependence on the detuning, future studies should include the dependence of loading on the polarization of the FORT laser light (circular and elliptical FORT), the dependence of the characteristics of the mode-locked laser (FEL or sub-ps Nd:YAG), the dependence on FORT to MOT size ratio, and a study of how the *temperature* of atoms in the FORT depends on the many loading parameters.

REFERENCES

[1] R. Grimm "Research groups working with atoms traps," retrieved on May 2006 from http://www.uibk.ac.at/exphys/ultracold/atomstraps.html

[2] G. Gwinner, J. A. Behr, S. B. Cahn, A. Ghosh, L. A. Orozco, G. D. Sprouse, and F. Xu, Phys. Rev. Lett. **72**, 3795 (1994).

[3] J. A. Behr *et al.*, Phys. Rev. Lett. **79**, 375 (1997).

[4] W. Ketterle and N. J. VanDruten, Adv. At. Mol. Opt. Phys. **37**, 181 (1996).

[5] P. D. Lett. *et al.*, Phys. Rev. Lett. **61**, 169 (1988).

[6] D.W. Keith, C. R. Ekstrom, Q. A. Turchette, and D. E. Pritchard, Phys. Rev. Lett. **66**, 2693 (1991).

[7] E. A. Hinds and I. G. Hughes, J. Phys. D **32**, R119 (1999).

[8] P. S. Jessen and I. H. Deutsch, Adv. Atom. Mol. Opt. Phys. **37**, 95 (1996).

[9] M. H. Anderson, J. R. Ensher, M. R. Mattews, C. E. Wieman, and E. A. Cornell, Science **269**, 198 (1995).

[10] K. B. Davis *et al.*, Phys. Rev. Lett. **75**, 3969 (1995).

[11] A. Fioretti, D. Comparat, A. Crubellier, O. Dulieu,F. Masnou-Seeuws, and P. Pillet, Phys. Rev. Lett. **80**, 004402 (1998).

[12] V. Letokhov, V. Minogin, and B. Pavlik, Opt. Comm. **19**, 72 (1976).

[13] A. Ashkin, Phys. Rev. Lett. **24**, 000156 (1970).

[14] T.W. Hansch and A. L. Schawlow, Opt. Comm. **13**, 68 (1975).

[15] D. J. Wineland and H. Dehmelt, Bul. Am. Phys. Soc. **20**, 637 (1975).

[16] W. D. Phillips and H. Metcalf, Phys. Rev. Lett. **48**, 596 (1982).

[17] S. Chu, L. Hollberg, J. Bjorkholm, A. Cable, and Ashkin, Phys. Rev. Lett. **55**, 48 (1985).

[18] E. L. Raab, M. Prentiss, A. Cable, S. Chu, and D. E. Pritchard, Phys. Rev. Lett. **59**, 2631 (1987).

[19] C. N. Cohen-Tannoudji, Rev. Mod. Phys. **70**, 707(1998).

[20] C. G. Aminoff *et al.*, Phys. Rev. Lett. **71**, 3083 (1993).

[21] S. Chu, J. E. Bjorkholm, A. Ashkin, and A. Cable, Phys. Rev. Lett. **57**, 314 (1986).

[22] J. D. Miller, R. A. Cline, and D. J. Heinzen, Phys. Rev. A **47**, R4567 (1993).

[23] K. L. Corwin, S. J. M. Kuppen, D. Cho, and C. E. Wieman, Phys. Rev. Lett. **83**, 1311 (1999).

[24] S. Dürr, K. W. Miller, and C. E. Wieman, Phys. Rev. A **63**, 011401(R)(2001).

[25] C. S. Adams, H. J. Lee, N. Davidson, M. Kasevich, and S. Chu, Phys. Rev. Lett. **74**, 3577 (1995).

[26] P. Ahmadi, B. P. Timmons, and G. S. Summy, Phys. Rev. A **72**, 023411 (2005).

[27] K. W. Miller, and S. Dürr, and C. E Wieman, Phys. Rev. A **66**, 023406 (2002).

[28] J. Y. Kim, J. S. Lee, J. H. Han, and D. Cho, J. of Korean Phys. Sc. **42**, 483 (2003).

[29] T. Takekoshi, J. R. Yeh, and R. J. Knize, Opt. Comm. **114**, 421 (1995).

[30] D. Boiron *et al.*, Phys. Rev. A **57**, R4106 (1998).

[31] K. M. O'Hara *et al.*, Phys. Rev. Lett. **82**, 4204 (1999).

[32] M. D. Barrett, J. A. Sauer, and M. S. Chapman, Phys. Rev. Lett, **87**, 010404 (2001).

[33] T. Weber, J. Herbig, M. Mark, H. C. Nägerl, and R. Grimm, Science **299**, 232 (2003).

[34] S. R. Granade, M. E. Gehm, K. M. O'Hara, and J. E. Thomas, Phys. Rev. Lett. **88**, 120405 (2002).

[35] T. G. M. Freegarde, J. Walz, and T. W. Hansch, Opt. Comm. **117**, 262 (1995).

[36] A. Goepfert *et al.*, Phys. Rev. A **56**, R3354 (1997).

[37] P. Ryytty and M. Kaivola, Phys. Rev. Lett. **84**, 5074 (2000).

[38] R. B. M. Clarke, T. Graf, and E. Riis, Appl. Phys. B **70**, 695 (2000).

[39] M. Shiddiq, C. E. Lucas, M. D. Havey, C. I. Sukenik, R. R. Jones, C. Y. Park, J. Y. Kim, and D. Cho, J. of. Korean. Phys. Soc. **47**, 207 (2005).

[40] H. F. Dylla and S. T. Corneliussen, *Free Electron Lasers Come of Age. Photonics Spectra*, (Laurin Publishing, August, 2005).

[41] S. J. M. Kuppens, K. L. Corwin, K. W. Miller, T. E. Chupp, and C. E. Wieman, Phys. Rev. A **62**, 013406 (2000).

[42] K. L. Corwin, Ph. D. Thesis, University of Colorado, Boulder, 1999.

[43] K. M. O' Hara, S. R. Grenade, M. E. Gehm, and J. E. Thomas , Phys. Rev. A. **63**, 043403 (2001).

[44] H. J. Metcalf and P. van der Straten, *Laser Cooling and Trapping. Graduate Texts in Contemporary Physics*, (Springer, New York, 1999).

[45] D. G. Fried *et al.*, Phys. Rev. Lett **81**, 3811 (1998).

[46] J. E. Simsarian *et al.*, Phys. Rev. Lett. **76**, 3522 (1996).

[47] J. E. Sansonetti, J. Phys. Chem. Ref. Data, **35**, No. 1 (2006).

[48] C. Savage, Aust. J. Phys. **49**, 745 (1996).

[49] D. Budker, D. F. Kimball and D. P. DeMille, *Atomic Physics, An exploration through problems and solutions*, (Oxford University Press, New York, 2004).

[50] M. Schulz, Ph. D. Dissertation, Innsbruck University, Innsbruck, 2002.

[51] W. D. Phillips, Rev. Mod. Phys. **70**, 721 (1998).

[52] R. Grimm, M. Weidemüller and Y. B. Ovchinnikov, Adv. At. Mol. Phys. **42**, 95 (2000).

[53] A. E. Siegman, *Lasers*, (University Science Books, Sausalito, CA, 1992).

[54] C. Wieman, G. Flowers, and S. Gilbert, Am. J. Phys. **63**, 317 (1995).

[55] K. B. MacAdam, A. Steinbach, and C. Wieman, Am. J. Phys. **60**, 1098 (1995).

[56] J. Weiner, V. S. Bagnato, S. Zilio, and P. S. Julienne, Rev. Mod. Phys. **71**, 1 (1999).

[57] D. Sesko, T. Walker, C. Monroe, A. Gallagher, and C. Wieman, Phys. Rev. Lett. **63**, 961 (1989).

[58] C. G. Townsend *et al.*, Phys. Rev. A **52**, 1423 (1995).

[59] C. D. Wallace, T. P. Dinneen, K. Y. N. Tan, T. T. Grove, and P. L. Gould, Phys. Rev. Lett. **69**, 897 (1992).

[60] H. C. W. Beijerinck, Phys. Rev. A **61**, 033606 (2000).

[61] S. Bali, K. M. O'Hara, M. E. Gehm, S. R. Granade, and J. E. Thomas, Phys. Rev. A **60**, R29 (1999).

[62] Thad Walker and Faul Feng, Adv. At. Mol. Phys. **34**, 125 (1994).

[63] P. S. Julinne and J. Vigué, Phys. Rev. A **44**, 4464 (1991).

[64] J. F. O'Hanion, *A User's Guide to Vacuum Technology 3rd Edition*, (John Wiley & Sons, Inc, Hoboken, NJ 2003).

[65] M. W. Hamilton, Contemporary Physics. **30**, 21 (1989).

[66] T. P. Dinneen, D. W. Wallace, and P. L. Gould, Opt. Comm. **92**, 277 (1992).

[67] L. Ricci *et al.*, Opt. Comm. **117**, 541 (1995).

[68] D. W. Preston, Am. J. Phys. **64**, 1432 (1996).

[69] K. L. Corwin, Z. -T. Lu, C. F. Hand, R. J. Epstein, and C. E. Wieman, Appl. Opt. **37**, 3295 (1998).

[70] S. E. Park, H. S. Lee, T. Y. Kwon, and H. Cho, Opt. Comm. **192**, 49 (2001).

[71] C. I. Sukenik, H. C. Busch, and M. Shiddiq, Opt. Comm. **203**, 133(2002).

[72] C. J. Myatt, N. R. Newbury, and C. W. Wieman, Opt. Lett. **18**, 649 (1993).

[73] E. A. Donley, T. P. Heavner, F. Levi, M. O. Tataw, and S. R. Jefferts, Rev. Sci. Intru. **76**, 063112 (2005).

[74] Spectra-Physics, Model 3800 CW Nd:YAG Laser System *Instruction Manual* (February 1988).

[75] R. A. Cornelussen *et al.*, Appl. Phys. B **78**, 19 (2004).

[76] National Instrument Application Note 007 *Data Acqusition Fundamentals.*

[77] J.R. Taylor, *An introduction to Error Analysis: The study of Uncertainties in Physical Measurement*, (University Science Books, 1982).

[78] Robert de Levie, *Advanced Excel for Scientific Data Analysis*, (Oxford University Press, New York, 2004).

APPENDIX A

MEASURING THE NUMBER OF ATOMS IN THE MOT

The number of atoms in the magneto-optical trap (MOT) is measured using a fluorescence measurement while the number of atoms in the FORT is calculated by multiplying the percentage of FORT loaded atoms, measured using a PMT and the LabVIEW program, with the initial number of atoms in the MOT. The number of atoms initially in the MOT can be calculated using the fact that the number of photons scattered from the MOT cloud per second is

$$\eta\,(\text{photons/s}) = N \times R. \tag{69}$$

Where N = number of atoms in the MOT and R = scattering rate (rate at which an individual atom scatters photons). The scattering rate R is defined as

$$R = \frac{(\frac{I}{I_s})\Gamma/2}{(1 + (\frac{I}{I_s}) + 4(\frac{\Delta}{\Gamma})^2)}. \tag{70}$$

With a trap laser intensity at the center of the chamber $I = 22.95$ mW/cm^2, and a saturation intensity for ^{85}Rb $I_s = 1.64$ mW/cm^2, $\Gamma = 2\pi\times6$ MHz, detuning $\Delta = -2\Gamma$, R is found to be 8.51×10^6 photons/(s.atom). By substituting the result of Eq. (70) into Eq. (69), Eq. (69) becomes

$$\eta(\text{photons/s}) = N\ (8.51 \times 10^6\ \text{photons/(s.atoms)}). \tag{71}$$

On the PMT, the measured current is related to the quantum efficiency and the gain of the PMT by the relation

$$I = N_{ph}\ Q\ e\ G, \tag{72}$$

here N_{ph} = number of photons per second hitting the photo cathode. Q = quantum efficiency (for a Hamamatsu R928 = 4% in units of electrons/photons), e = electron charge 1.6×10^{-19} Coulomb. G = PMT's gain (for Hamamatsu R928 at 500V = 10^5). Note that the PMT used is *uncalibrated*, so the quantum efficiency is just an estimate. The measured voltage on the oscilloscope is related to the measured current I by the gain (10^6), so the number of photon hitting the photocathode of the PMT can be written as

$$N_{ph} = V/(10^6\ Q\ e\ G). \tag{73}$$

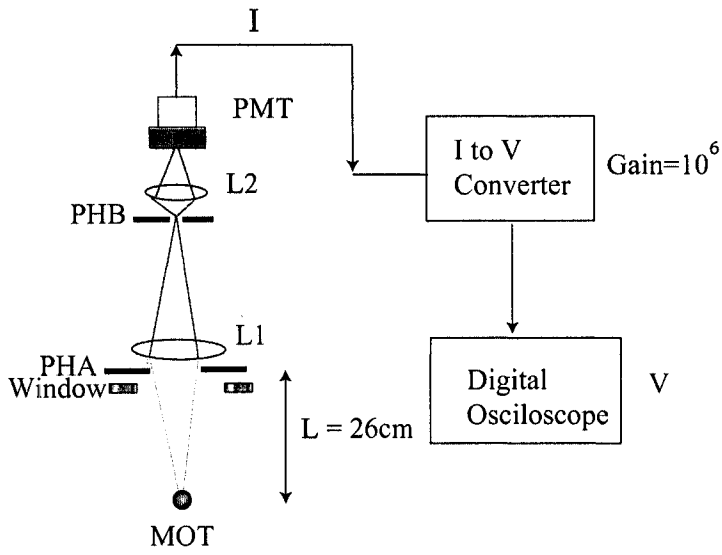

Notes:

f of L1 = 7.7 cm f of L2 = 2.55 cm PHA= Cap pinhole with d = 1.28 cm

PMT = Photomultiplier tube (Hamamatsu R928) PHB = Iris

FIG. 62: The experimental setup used to measure the number of atoms in the MOT.

However, this number of photons hitting the photocathode of the PMT in Eq. (73) above is only for the solid angle

$$\Omega = \pi r^2/4\pi R_d^2, \tag{74}$$

where r = cap pinhole radius (diameter = 1.28 cm) and R_d = distance from the MOT to the pinhole (26 cm) which is 0.00015 radian. Also, the number of photons hitting the photocathode is the number after being reduced by the uncoated chamber window reflection and the uncoated lens reflection, which gives a reduction of about 16 %.

For I getter = 2.55 A and I coils = 4.5 A, the measured voltage is 10.4 Volts. The number of photons hitting the PMT surface is then

$$N_{ph} = 10.4\,\text{Volts}/(10^6 \times 0.04 \times 1.6 \times 10^{-19} \times 10^5), \tag{75}$$

$$N_{ph} = 1.63 \times 10^{10}\ \text{photons/s}. \tag{76}$$

This number of photons measured is reduced by 16% because of the chamber windows and the lens reflection and is for a solid angle 0.00015 (assuming isotropic scattering).

The total number of scattered photons is

$$N_{ph} = 1.63 \times 10^{10}/(0.84 \times 0.00015) \text{ photons/s}, \tag{77}$$

$$N_{ph} = 1.29 \times 10^{14} \text{ photons/s}. \tag{78}$$

Equation (78) is set equal to Eq. (71) to give the number of atoms in the MOT as

$$N = 1.5 \times 10^{7} \text{ atoms}. \tag{79}$$

APPENDIX B

ERROR ANALYSIS

Experimental errors can be divided into two general categories; systematic and random error. Systematic errors are errors which tend to shift all the measurements in a systematic way so their mean value is displaced. Random error, which is known as statistical error, comes from random fluctuations in the measuring process. The difference between these two is that random errors displace measurements in an arbitrary direction while the systematic error are correlated from one measurement to the next. The sources of systematic errors come from many things such as incorrect calibration of equipment or an improper procedure in taking a measurement, whereas random errors occur for reasons such as noise in measurement electronics or the sensitivity of the equipment [77]. Once the quantity is measured, the error must be propagated correctly if that quantity is to be used in calculation.

The error bars for the experimental data in Chapter V are calculated based on statistical errors, properly propagated with the assumption that the systematic errors have been minimized. There are two things that have been done to minimize the systematic error. First, by calibrating the voltage reading of the fluorescence signal by the DAQ devices to the reading from a digital oscilloscope using offset adjustment and Gate-in width and delay, we confirmed that the input (measured) values were being recorded properly. The second effort is to take data points in random order instead of from smaller value to larger. The statistical error in this experiment emerges from measuring MOT level (voltage) and FORT level (voltage) using the LabVIEW program and DAQ devices. The propagation of errors are produced in the process of calculating the number of atoms in the MOT and FORT and in calculating the loss rates, as explained below.

Suppose that there are two measurements A and B which have independent error ΔA and ΔB respectively, the final result of measurement is defined as Z = f(A,B). If A is perturbed by ΔA then Z will be perturbed by

$$\left(\frac{\partial f}{\partial A}\right)\Delta A, \tag{80}$$

the same way as when B is perturbed by ΔB then Z will be perturbed by

$$\left(\frac{\partial f}{\partial B}\right)\Delta B. \tag{81}$$

The propagation of error for Z can be written as

$$\Delta Z = \sqrt{\left(\frac{\partial f}{\partial A}\right)^2 (\Delta A)^2 + \left(\frac{\partial f}{\partial B}\right)^2 (\Delta B)^2}. \tag{82}$$

So, the calculation error for Z = AB or Z = A/B can be written as

$$\left(\frac{\Delta Z}{Z}\right)^2 = \left(\frac{\Delta A}{A}\right)^2 + \left(\frac{\Delta B}{B}\right)^2. \tag{83}$$

.

In our experiments, we measure the MOT level and FORT level (voltage from the integrated signal from PMT). The percentage of ultracold Rb atoms loaded into the FORT is calculated by dividing the FORT level by the MOT level where the MOT level is maintained stable during data taking. A separate measurement of the number of atoms in the MOT gives the number of atoms to be (about) 1.5×10^7 atoms as discussed in Appendix A. This MOT atom number is only good to a factor ~ 2. We just use this result since we are interested only in the relative differences between the parameters of a cw FORT and a pulsed FORT. An accurate measurement is needed in the future to measure the exact number of atom in the MOT. The propagation of error for the number of atoms in the FORT can be written as

$$\Delta N = \frac{V_{FORT}}{V_{MOT}} \sqrt{\left(\frac{\Delta V_{MOT}}{V_{MOT}}\right)^2 + \left(\frac{\Delta V_{FORT}}{V_{FORT}}\right)^2}. \tag{84}$$

The ΔV_{MOT} and ΔV_{FORT} are determined by taking the standard deviation of the measurement of MOT level and FORT level, there are done by the LabVIEW program automatically as the result of running the data acquisition repeatedly. The values of this error ranges from 9% - 10%.

The loading rates and the loss rates in the FORT loading stage and the loss rates in the FORT holding stage have errors emerging from curve fittings. The curve fitting is performed using **Solver** which is part of the Analysis ToolPak attached to Microsoft Excel 2000 while the curve fitting error is calculated using a macro [78] written in TBA (The Visual Basic) language which is compatible with Microsoft Excel 2000. However this error is very small, ranging from one millionth percent to one hundredth percent, which can be neglected. We have tested the Solver and the macro using some equations that already have certain values as provided by Ref. [78]. There is also fluctuation as a result of the Solver calculation where the values of the fitting parameters (loading rates and loss rates) fluctuate around a minima. The accepted parameters are taken at the lowest minima where the sum of squares

of residuals is the lowest. So, the errors for the holding curve and loading curve are taken from these fluctuations. The amount of fluctuation (deviation) for each parameter is found by changing the value of the fit parameter around the accepted value and running the solver program until the solver gives no solution. For the holding curves, the errors range from 3% to 30% while for loading curves the errors range from 5% to 30%, depending on the loading curve shape. For example in Fig. 53 and 54, at -2Γ detuning, the curve shape is flat after the loading time reaches 100 ms, the curve fitting gives an unusually large deviation/fluctuation. In addition, before the curve fitting is performed, the differential equations for holding stage and loading stage are solved numerically by Microsoft Excel using Runge-Kutta method. The numerical solution for the holding stage is compared to the existed analytical solution as shown on Eq. (67), so that comparison of the two methods could be used to confirm the accuracy of the calculation. The written Runge-Kutta program is also tested to various equations that have an analytical solution.

VITA

Minarni Minarni
Department of Physics
Old Dominion University
Norfolk, VA 23529

Alias: Minarni Shiddiq

EDUCATION:

Ph.D. in Physics, Old Dominion University, Norfolk, VA, August 2006
M.S. in Physics, Old Dominion University, Norfolk, VA, May 2005.
M.S. in Physics, Hampton University, Hampton, VA, August 1994.
B.S. in Physics, Riau University, Pekanbaru, Indonesia, September 1989.

PROFFESIONAL EXPERIENCE:

Research Assistant, Fall 2003–present, Department of Physics, Old Dominion University, Norfolk, VA.
Teaching Assistant, Fall 2000–Spring 2003, Department of Physics, Old Dominion University, Norfolk, VA.
Lecturer, 1990–1992 and 1994–2000, Department of Physics, Riau University, Pekanbaru, Indonesia.

PUBLICATIONS:

"Direct comparison between loading of a far-off-resonance trap in continuous-wave and pulsed modes," M. Shiddiq, C. E. Lucas, M. D. Havey, C. I Sukenik, R. R. Jones, J. Y. Kim, C. Y. Park, D. Cho, Journal of the Korean Physical Society 47, 207 (2005).
"Modulation-free laser frequency stabilization and detuning," C. I. Sukenik, H. C. Busch, M. Shiddiq, Optics Comm. 203, 133 (2002).
"Comparison of pulsed and continuous-wave dipole traps for confining ultracold rubidium atoms," M. Shiddiq, C. E. Lucas, M. D. Havey, C. I Sukenik, R. R. Jones, J. Y. Kim, C. Y. Park, D. Cho, in preparation, to be submitted to Phys. Rev. A (2006).

Typeset using LaTeX.